GE Nuclear Energy

175 Curtner Avenue
San Jose, CA 95125

NEDO-32288
Revision 0
Class 1
December 1995

# Scaling of the SBWR Related Tests

R.E. Gamble
A. Hunsbedt
F.J. Moody
M.K. Parker
G. Yadigaroglu*

Reviewed: R.E. Gamble for B.S. Shiralkar

B.S. Shiralkar, Manager
TRACG Qualification
SBWR Project

Approved: R.J. Buchholz for

J.E. Quinn, Manager
SBWR Project

*Professor of Nuclear Engineering, Swiss Federal Institute of Technology (ETH), Zurich, Switzerland.

## Important Notice Regarding Contents of This Report
## Please Read Carefully

*The only undertakings of the General Electric Company (GE) respecting information in this document are contained in the contract between the customer and GE, as identified in the purchase order for this report and nothing contained in this document shall be construed as changing the contract. The use of this information by anyone other than the customer or for any purpose other than that for which it is intended, is not authorized; and with respect to any unauthorized use, GE makes no representation or warranty, and assumes no liability as to the completeness, accuracy, or usefulness of the information contained in this document.*

# Preface

This report incorporates the scaling evaluation previously contained in Appendix B of the Test & Analysis Program Description (TAPD) [59]. The basic formulations have been extended and several significant improvements have been made to the material contained in the TAPD. The momentum equation has been extended to a global formulation which emphasizes overall system behavior and the interactions between processes occurring in various components of the prototype and test facility systems. Application of the scaling formulations to the SBWR and test facilities has been done in a manner that clearly identifies the important parameters in the top-down formulations and how well they are scaled for each test facility. Scaling of additional test series, GIRAFFE/Helium and GIRAFFE/SIT have been added. In addition, supplementary bottom-up phenomena have been considered.

The report is organized into three parts. The first part is an introduction and background to provide an overview of the scaling method used and background information for the system under consideration (SBWR). The second part consists of the scaling theory divided into top-down (Section 2) and bottom-up (Section 3) sections. These are supported by appendices. The third part consists of the application of the scaling to the SBWR and related test facilities (Section 4).

# Table of Contents

# List of Tables

# List of Figures

## Acknowledgments

The authors are indebted to GE Nuclear Energy staff members P. Billig, M. Herzog, and A. Rao, for providing valuable assistance, information and comments on drafts of this report. Particular thanks are extended to J. Fitch for numerous thoughtful comments, insights, and suggestions for improvements, which have been incorporated in this report. Thanks are extended to M. Swope for editorial assistance.

The authors are also indebted to J. Healzer of S. Levy, Inc. for comments on earlier versions of this report and to PSI staff members J. Dreier, M. Huggenberger, and G. Varadi for information regarding the PANDA facility.

P. Coddington and M. Meier of PSI, in collaboration with M. Andreani (Swiss Federal Institute of Technology, ETH in Zurich), provided unpublished material regarding scaling of various phenomena and useful comments.

## Nomenclatures and Abbreviations

| Symbols | Description | Units |
|---|---|---|
| A | Surface area | $m^2$ |
| a | Cross-sectional area | $m^2$ |
| $c_p$ | Specific heat at constant pressure | J/kg K |
| $c_v$ | Specific heat at constant volume | J/kg K |
| d | Characteristic length | m |
| D | Diameter | m |
| E | Internal energy | J |
| e | Specific internal energy | J/kg |
| f | Darcy friction factor | * |
| $F_n$ | Loss coefficient for pipe segment | * |
| $F/a^2$ | Sum of loss coefficients divided by area$^2$ | $1/m^4$ |
| H | Height or submergence | m |
| h | heat transfer coefficient | $W/m^2K$ |
| h | Specific enthalpy | J/kg |
| $h_{fg}$ | Latent heat of vaporization | J/kg |
| G | Mass flux | $kg/m^2s$ |
| g | Acceleration of gravity | 9.81 $m/s^2$ |
| $i_n$ | Normalized line inertia factor | * |
| j, J | Volumetric flow rate | $m^3/s$ |
| k | Ratio of specific heats, $c_p/c_v$ | * |
| k | Thermal conductivity | W/m K |
| $k_n$ | Local loss coefficient of segment n | * |
| $k_n$ | Normalized line flow resistance factor | * |
| $\ell_n$ | Length of segment | m |
| L/a | Sum of lengths divided by areas | 1/m |
| L | Hydrostatic or gravity head | m |
| M | Mass | kg |
| | Mass flow rate | kg/s |
| p, P | Pressure | Pa |
| $\wp$ | perimeter | m |
| | Heat rate | W |
| R | Gas Constant | J/kg K |
| R | System Scale (prototype to model) | * |
| T | Temperature | K |
| t | Time | s |
| u | Velocity | m/s |

* = dimensionless

| | | |
|---|---|---|
| V | Volume | $m^3$ |
| v | Specific volume | $m^3/kg$ |
| W | Mass flow rate | kg/s |
| y | Mass fraction | * |
| z | Axial coordinate along flow path | m |
| $Bi = h\ d/k_s$ | Biot number | * |
| $F_o$ | Fourier number | * |
| $Nu = h\ d/k$ | Nussel number | * |

**Greek Letters**

| Symbols | Description | Units |
|---|---|---|
| $\alpha$ | Thermal diffusivity | $m^2/s$ |
| $\beta$ | Isobaric thermal expansivity | * |
| $\mu$ | Viscosity | kg/m s |
| $\Pi$ | Nondimensional group | * |
| $\rho$ | Density | $kg/m^3$ |
| $\sigma$ | Surface tension | $kg/s^2$ |
| $\tau$ | Time constant | s |
| $\omega$ | Characteristic frequency | $s^{-1}$ |
| $\alpha_T$ | Taylor's jet entrainment constant | * |

**Subscripts**

| | |
|---|---|
| B | Blowdown (via broken MSLB, DPVs, or GDLB) |
| $b_j$ | Free buoyant jet |
| $b_\ell$ | Wall jet |
| C | RPV to IC line |
| D | Drywell |
| d | Decay heat |
| e | Entrainment |
| EQ | Equalization line |
| G, g | Gas |
| IC | Isolation condenser |
| L | IC drain line |
| L, $\ell$ | Liquid |
| LG | Change from liquid to gas |
| LG | GDCS drain line |
| LPC | PCC drain line |

* = dimensionless

| | |
|---|---|
| o | Initial value |
| PC | PCC inlet line |
| PCC | Passive Containment Cooling Condenser |
| PCX | PCC vent line |
| R | Reactor pressure vessel, scale factor between prototype and model |
| r | Reference parameter |
| RV | RPV to WW (SRV) line |
| S | Structure |
| $s_f$ | Ambient stratified fluid |
| v | Refers to vertical distance |
| V | Main vent line |
| VB | Vacuum breaker |
| W | Wetwell |
| WS | IC vent line submergence |

Additional subscripts are defined in the text

**Superscripts**

| | |
|---|---|
| ' | Denotes derivative with respect to pressure |
| • | Denotes derivative with respect to time |
| + | Nondimensional variable |
| ° | Nondimensional parameter normalized to reference value |
| S | Specific (for a well defined geometry) |

**Abbreviations**

| | |
|---|---|
| ADS | Automatic Depressurization System |
| ALPHA | Advanced LWR Passive Heat Removal and Aerosol Program |
| BAF | Bottom of Active Fuel |
| BDLB | Bottom Drain Line Break |
| CHF | Critical Heat Flux |
| DBA | Design Basis Accident |
| DPV | Depressurization Valve |
| DW | Drywell |
| GDCS | Gravity-Driven Cooling System |
| GDLB | GDCS line break |
| GE | General Electric Company |
| GIST | GDCS Integrated Systems Test |
| H2TS | Hierarchical Two-Tier Scaling |
| h.t.c. | Heat transfer coefficient |
| IC | Isolation Condenser |
| ICS | Isolation Condenser System |

| | |
|---|---|
| LOCA | Loss-of-Coolant Accident |
| MIT | Massachusetts Institute of Technology |
| MSL | Main Steam Line |
| MSLB | Main Steam Line Break |
| NB | No-Break |
| NRC | Nuclear Regulatory Commission |
| PCC | Passive Containment Condenser |
| PCCS | Passive Containment Cooling System |
| PIRT | Phenomena Identification and Ranking Table |
| PSI | Paul Scherrer Institute |
| RPV | Reactor Pressure Vessel |
| SBWR | Simplified Boiling Water Reactor |
| SC | Pressure Suppression Chamber |
| SIT | [illegible]ns Interaction Tests |
| SP | S[illegible]ession Pool |
| SRV | Safety/Relief Valve |
| TAF | Top of Active Fuel |
| TAPD | SBWR Test and Analysis Program Description |
| UCB | University of California at Berkeley |
| WW | Wetwell |
| $\Pi$ | Refers to nondimensional group |

## Abstract

This report presents a scaling study applicable to the SBWR-related tests. The scope of the study includes:

- A description of the scaling philosophy used for the GIST, GIRAFFE, PANDA, PANTHERS, and single-tube condensation-heat-transfer tests which have been, or will be, conducted in support of the SBWR program (as described in the TAPD [55]).
- The description of a set of scaling laws which are applicable to the SBWR-related test facilities.
- An evaluation of the test facilities with respect to the scaling of the important phenomena and processes identified in the SBWR Phenomena Identification and Ranking Table (PIRT).

The study is intended to demonstrate that the experimental observations from the test programs are representative of SBWR behavior. This includes an identification of any distortions in the representation of the phenomena induced by the test facility and the manner in which these distortions can be considered when the experimental data are used for computer code qualification or the development of computer code models.

The Hierarchical Two-Tier Scaling (H2TS) methodology developed by the U.S. Nuclear Regulatory Commission (USNRC) is applied to the extent practical throughout the study. Several scaling considerations addressed by H2TS are automatically satisfied in the SBWR-related experiments where, in all cases, the fluids and their thermodynamic states are prototypical. The various scaling issues are addressed by either the top-down or bottom-up methodologies embodied in H2TS. The top-down scaling technique, as applied to generic Reactor Pressure Vessel (RPV) and containment-related processes, leads to a familiar set of scaling laws with a *system scale* for power, volume, horizontal area in volumes, and mass flow rate, and 1:1 scaling for pressure differences, elevations, and vent submergences.

The scaling of SBWR system components in relation to specific highly-ranked phenomena and processes is conducted according to the bottom-up H2TS methodology. This includes (1) void distribution and two-phase levels in the RPV; (2) consideration of thermal plumes, mixing and stratification; (3) heat and mass transfers at liquid-gas interfaces; (4) scaling of the vents; and (5) heat and mass transfer in the condensers used for decay heat removal in the SBWR design. Finally, the scaling approach followed in designing the various SBWR-related facilities is reviewed in relation to the main purpose of the tests. The data collected from these facilities are used in the qualification of the system code TRACG.

The SBWR scaling study leads to the following conclusions:

- All dominant phenomena are preserved in the experiments for various LOCA phases.
- No new phenomena are introduced by the scaled experiments.
- Scaling distortions do not exclude the essential phenomena.
- The experimental results are appropriate for TRACG qualification.

# 1.0 Introduction

The Simplified Boiling Water Reactor (SBWR) design incorporates advanced, passive safety features. A comprehensive experimental and analytical program is being carried out to demonstrate the performance of these key passive systems and components, and to provide the data necessary for validation of the TRACG Code for SBWR application.

Operation of the SBWR passive safety systems involves components with interconnecting loops and flow paths, and also involves processes such as single-phase and two-phase flow, flashing of water resulting from rapid pressure changes, components with liquid to steam/noncondensible gas interfaces, heat sources resulting from core decay heat and energy stored in structures, and steam quenching in water pools (many of these are common to BWRs). The design of meaningful experiments to obtain data to validate analytical methods requires consideration of these components and interacting processes.

The major SBWR test programs are GIST, GIRAFFE, PANTHERS and PANDA. GIST, GIRAFFE and PANDA are integral systems tests focusing on different aspects of the SBWR response to Loss-of-Coolant Accidents (LOCAs). These facilities also simulate the SBWR at different system scales (1:508 for GIST, 1:400 for GIRAFFE and 1:25 for PANDA). PANTHERS is a component test of prototypical PCC and IC modules. Details of the test programs can be found in the TAPD [55].

A scaling analysis was employed to demonstrate that the GIST, GIRAFFE, and PANDA tests are representative of the SBWR LOCA phases and, therefore, can be used to predict important behavior of the SBWR systems, and qualify specific phenomenological models in the TRACG Code. The analysis was performed by writing the global equations for mass, momentum and energy for each component or system and combining the equations in matrix form following nondimensionalization using appropriate characteristic or reference physical parameters of the system. The resulting nondimensional groups, along with the matrices when applied to the prototype and experimental systems, revealed which processes were the most important and identified scaling distortions between an experiment and the prototype. PANTHERS employs full-scale, prototypical heat exchanger modules. Thus, the scaling discussion is limited to the applicability of the data for transients.

The scaling analysis presented in this report considers overall or global systems scaling aspects referred to generally as top-down scaling in the Hierarchical Two-Tier Scaling (H2TS) methodology developed by the USNRC. More specifically, the methodology follows that presented by Wulff [53] for systems of connected loops with modifications as appropriate for the more complex SBWR and related system tests. The report also considers the detailed or fine structure behavior within regions, referred to as bottom-up scaling.

The global scaling modeling approach, along with the detailed mathematical formulations based on the principles of conservation of mass, momentum and energy, are given in Section 2 of the report. Also given in this section are the definitions of nondimensional groups and variables.

Detailed formulations of the global momentum equation are included in Appendix A. Detailed formulations of the mass, energy and state equations are included in Appendix B.

Section 3 contains the scaling development and discusses the bottom-up phenomena relevant to the SBWR and test facilities.

The numerical results and discussions of the parameters important to SBWR behavior are covered in Section 4. Section 4 also summarizes the numerical results for the test facilities and includes a discussion of how well the facilities are scaled.

The analysis and main results of level oscillation between large liquid masses connected by drain lines are given in Appendix C.

### 1.1 The SBWR and Related Tests

In case of a break in the primary system, the SBWR uses gravity or natural circulation-driven, passive safety systems to provide emergency core coolant to keep the core cooled and to remove decay heat from both the primary system and/or the containment. The main systems performing these tasks are the Gravity-Driven Cooling System (GDCS), the Isolation Condenser System (ICS), and the Passive Containment Cooling System (PCCS), ([48], [34], [45]). The performance of the SBWR System is analyzed by the TRACG Code [2].

Emergency core cooling water is provided to the core by the GDCS. This system consists of three water pools situated above the top of the core, from which makeup coolant can flow by gravity to replenish the coolant lost from the Reactor Pressure Vessel (RPV) during a LOCA. However, the GDCS can operate only after depressurization of the RPV; therefore, the SBWR is equipped with an Automatic Depressurization System (ADS) that performs this function. The depressurization of BWR primary systems is well understood, since it has been studied extensively in relation to the classical BWR designs. Indeed, the phenomena taking place during the early phase of blowdown inside the RPV have been extensively investigated by several series of tests; these constitute the basis for the corresponding qualification of the TRACG Code [3]. The containment loads during early blowdown have also been extensively investigated ([16], [32], [15]). The GDCS is, however, a relatively untested concept and requires some attention. The General Electric Company (GE) has therefore conducted the GDCS Integrated Systems Test (GIST) series of tests to investigate the behavior of the SBWR during the latter part of the depressurization phase. Proof of the technical feasibility of the GDCS concept was a major test objective. The GIST tests simulated an earlier SBWR configuration. These tests are being supplemented by the GIRAFFE/SIT tests, which represent the current SBWR configuration and also include the ICS and PCCS.

Decay heat removal from the primary system is performed by the ICS, which consists of three Isolation Condensers (ICs) located in a pool high in the reactor building. When redundant condensate return valves are opened, steam from the primary system flows into the tubes of the ICs, condenses, and returns to the RPV, removing stored energy. The behavior of the ICs is well understood, since such units have been in operation for many years in older BWRs. Heat transfer data on a prototypical module are being obtained at the PANTHERS test facility.

Decay heat is removed from the drywell (DW) by the PCCS, which employs three PCC condensers also located in the interconnected IC pool compartments. The PCC condenser tubes are permanently connected to the DW. A mixture of steam and noncondensible gases (nitrogen present in the containment during normal operation) may enter the PCC condensers. The steam will condense, while the noncondensible gases are vented to the suppression pool (SP) in the Suppression Chamber (SC) (or wetwell).

Since the DW volume is connected directly to the SP either via the main pressure suppression vents or through the PCC condensers and their vent lines, the path that the steam will follow depends on the pressure differences between the DW volume and the two possible venting points. During the long-term containment cooling period, direct opening of the main vents and condensation of the steam in the SP must be avoided, since the SP is not provided with a safety-grade cooling system; the steam must be condensed in the PCC (or IC) condensers and any noncondensibles vented to the SC. Although the operation of the condensers is understood, experimental verification of their integral, system behavior under a variety of conditions was deemed necessary. Two experimental facilities were used for this purpose. The GIRAFFE facility, operated by Toshiba in Japan,

provides extensive information about system behavior. The larger-scale PANDA facility at the Paul Scherrer Institute (PSI) in Switzerland will provide additional information and will address issues such as the effects of the operation of several condenser units in parallel, the distribution of the constituents (steam and noncondensibles) in the large DW volume, and mixing in the containment compartments. The PANDA experiments are part of the ALPHA Program (Advanced LWR Passive Heat Removal and Aerosol Program) conducted at PSI. Availability of data from integral facilities having different scales is clearly an advantage for understanding system behavior and performing code qualification [6].

The condensation of mixtures of steam and noncondensible gases in tubes under conditions expected in the PCC units has been investigated in experimental programs conducted at the Massachusetts Institute of Technology (MIT) ([41], [42], [43]) and at the University of California-Berkeley (UCB) ([46], [33], [47]). Full-scale tests of the IC and PCC units are being conducted at the PANTHERS facility at the SIET laboratory in Italy [25].

Additional references about details of the various test facilities can be found in the TAPD [55]. The design of all these experimental facilities and the conduct of the various tests was guided by consideration of the proper modeling and simulation of the various phenomena taking place.

## 1.2 General Approach for Code Qualification, Testing and Scaling

The approach adopted is similar to the one used for most LWR safety-related large-scale integral tests. System tests (such as the GIST, GIRAFFE and PANDA tests) do *not* have to provide exact system simulations of the prototype. However, system tests are expected to provide *data* covering all essential phenomena and system behavior under a variety of conditions, which are used to qualify a system code (in this particular case, the TRACG Code used for safety analysis by GE).

To obtain data in the proper range of system conditions, the relative importance of the phenomena and processes present in the tests should not differ significantly from what is expected to take place in the SBWR. Similarly, the overall behavior of the test facility should not diverge significantly from that of the SBWR; in particular, one should not observe bifurcations in system behavior leading to quite different intermediate or end states. Finally, the tests should provide sufficiently detailed information, obtained under controlled conditions, to provide an adequate and sufficient database for qualifying the system code, TRACG.

Following current practice [7], a Phenomena Identification and Ranking Table (PIRT) was prepared for the SBWR post-LOCA (Loss-of-Coolant Accident) containment phenomena (TAPD, Section 2) [55]. A PIRT identifies the phenomena and processes that are of particular importance during the various phases of a postulated accident or class of accidents. These phenomena receive, then, particular attention during code qualification. The SBWR PIRT was used to identify the phenomena of importance in relation to scaling of the experimental facilities. These phenomena are listed in Section 4 of the TAPD [55], and have been reproduced in Tables 3.2-1 and 3.2-2, where the scaling of specific phenomena is addressed.

## 1.3 Scope and Objectives of the Scaling Study

The scope of the scaling study reported here was to:

- Describe the scaling philosophy and strategy used in designing the various tests.
- Provide the applicable scaling laws.
- Show that the test facilities properly "scale" the important phenomena and processes identified in the SBWR PIRT and/or provide assurance that the experimental observations from the test programs are representative of SBWR behavior.
- Identify scaling distortions and discuss their importance; in particular, identify the ways by which scaling distortions should be considered when the experimental data are used for code qualification.
- Provide the basis for showing that the experimental data are applicable for qualifying TRACG.

### 1.3.1 Accidents and Accident Phases Considered

The range of accidents considered includes the main steam line break (MSLB), as well as other breaks of the primary system, such as the GDCS line break (GDLB) and the bottom drain line break (BDLB).

The scenario for these accidents can be roughly subdivided into three phases:

- The *blowdown phase* extending from the initiation of rapid depressurization by blowdown up to the time of GDCS initiation. The blowdown phase can be further subdivided into an *early* phase extending until the time the pressure reaches a level of about 0.8 MPa, and a *late* blowdown phase thereafter.
- An intermediate *GDCS phase* during which the GDCS is delivering its stored water inventory to the primary system.
- A *long-term cooling phase* beginning when the RPV inventory starts becoming replenished by the condensate flowing down from the ICS and PCCS (i.e., when the GDCS hydrostatic head necessary to drive flow into the core is made up by the PCCS condensate). At about the same time, the ICS and PCCS condensers become the dominant decay heat removal mechanism, replacing the heat sink provided by the water inventory initially stored in the GDCS pools.

The scaling analysis performed in this report is primarily directed at scaling the reactor and containment components and phenomena which are significant during the time period starting with the late blowdown phase and extending into the long-term cooling phase. As stated in Section 1.1, phenomena associated with the early stage of depressurization of a BWR vessel are well understood and are not considered to be part of the SBWR testing program. Thus, this report deals with *post-LOCA performance* focusing on the phases of the transient following the early blowdown phase.

### 1.3.2 Important Safety Issues

The tests conducted in relation to the SBWR are aimed at answering certain safety-related issues, including:

- The possibility of core uncovery and damage — this issue is clearly related to the water inventory in the RPV resulting from the flows out of the break and from the GDCS, and to the RPV depressurization rate. This issue was addressed with the GIST tests, which demonstrated the feasibility of depressurizing the reactor to sufficiently low pressures to enable reflooding by the gravity-driven flow from an elevated pool [5]. The GIST tests are being supplemented by the GIRAFFE/SIT tests.
- Limitation of the containment pressure — this issue is related to the capability of the ICS and PCCS to remove decay heat. The distribution of phases in the various containment compartments and the temperature at the surface of the SP are significant variables.
- Effectiveness of condensation of steam injected into the SP from the PCCS vents.
- The performance of certain key containment components, such as: (1) the cyclic performance of the PCCS (in relation to venting of noncondensibles), as observed in the GIRAFFE tests; (2) the intermittent opening of the vacuum breakers; and (3) the possible opening of the main vents during long-term containment cooling.
- The heat transfer performance of the ICS and PCCS condensers — this depends on both condensation heat transfer inside the condenser tubes in the presence of noncondensibles and on heat transfer at the outside surface of the tubes in the pool, including IC pool inventory, temperature, and circulation rate. The possible degradation of the performance of the PCCS condensers due to insufficient venting and the accumulation of noncondensibles in their tubes is also of importance.
- Structural integrity of the ICS and PCCS condenser units.

The issues identified above are addressed by the GIST, GIRAFFE, PANDA, and PANTHERS tests.

## 1.4 The H2TS Scaling Methodology

The scaling methodology developed by an NRC Technical Program Group [52] was applied in this study for the purpose of evaluating the experiments and computer models in terms of how well they represent actual cooling systems and phenomena of the SBWR.

Objectives of the NRC scaling methodology are summarized as follows:

- To provide a scaling methodology that is systematic and practical, auditable, and traceable.
- To provide the scaling rationale and similarity criteria.
- To provide a procedure for conducting comprehensive reviews of facility design, of test conditions and results.
- To ensure the prototypicality of the experimental data.
- To quantify biases due to scaling distortions or due to non-prototypical conditions.

The scaling methodology embraces the behavior of integrated subsystems and components (top-down approach), and specific processes which may occur within the subsystems (bottom-up approach).

A subsystem in the SBWR is defined as a volume, such as the reactor vessel, drywell, wetwell air space, wetwell pool, the PCC condenser, and the isolation condenser. Global properties of a given subsystem include the pressure or the hydraulic head which drives mass flow rate, the bulk temperature differences which drive heat transfer, and the total mass and energy inflows, outflows, and storage rates. Furthermore, flow paths connecting the various volumes are included in the subsystem category because associated flow rates depend on global properties of connected volumes and resistance and inertia properties of the flow paths. Similarity laws for the SBWR subsystems were obtained from top-down considerations.

The state within a volume may depend on phenomena which cause spatial nonuniformity in properties, such as bubble and droplet formation, density stratification of steam and noncondensibles in the drywell, or thermal plumes and stratification in both the pools and drywell. If stratification in two well-mixed superimposed layers occurs within a volume, two distinct volumes with uniform global properties will exist for the top and bottom layer subsystems formed. If complete mixing and spatial uniformity occurs within a volume, one subsystem and one global state is appropriate. If the degree of component or phase stratification varies throughout a volume, and the properties of the mass being discharged from a given location is important, it is desirable to satisfy bottom-up similarity laws which govern the stratification. Heat transfer and condensation processes in the PCCS are determined by fine-structure, local heat and mass transfer phenomena, which involve bottom-up considerations.

The magnitude of the nondimensional ($\Pi$) groups resulting from top-down and bottom-up scaling considerations depends on the particular LOCA phase; namely, Blowdown, GDCS and PCCS. The scaling procedure yields a unique set of $\Pi$ groups for each phase, because properties at the beginning of each phase (initial states) and the dominant time responses are different.

The H2TS procedure involves writing the equations which govern the property behavior of each subsystem in the SBWR. One set of equations gives the rates of pressurization in each volume, expressed in terms of mass and energy flow rates, and current state properties. A second set of equations provides the energy rate of change in each volume. A set of momentum equations

provides the flow rate in each connecting path, ranging from transient flow when driving pressures or hydraulic heads are changing, to steady state.

The momentum equations for each flow path were combined to obtain open- and closed-loop equations from which the response times for various LOCA phases were estimated. One possible response time during a given LOCA phase consists of a volume filling or emptying time, based on initial or other reference flow rates. Another response time is associated with the transient acceleration of an open flow loop between the reactor and wetwell, the pressure source and sink. One other response time involves the vessel decompression, and is significantly different from the water mass emptying time of that vessel.

The state properties for each volume and flow path were normalized using appropriate scales so that their nondimensional magnitudes become of order 1.0, or 0(1). Care was taken to employ normalizing parameters which were either initial values or other reference values, based on parameters which could be controlled in an experiment.

When the momentum equations were arranged in matrix form, dominant $\Pi$ groups were identified, based on their relative numerical magnitude. It was observed that the flow path inertia properties had rapid response times relative to the filling or emptying time response for system volumes. Therefore, it was not necessary to accurately scale the inertia properties. However, further examination of the momentum matrix showed that the quasi-steady $\Pi$ groups containing flow resistance and driving pressure or hydraulic head should be preserved for various flow paths.

Another process for comparing relative time responses in an integrated system is provided in the H2TS, which involves both the time constant of subsystems and a corresponding transport frequency. That is, if a flow transient response occurs in a pipe between two volumes, the system response time would correspond to either the filling or emptying time of the controlling volume (e.g., the GDCS pool). The transport frequency would correspond to the number of purges per unit time of the GDCS pool drain line. The product of frequency and response time gives the number of purges during the filling or emptying process. When a high number of purges occurs, it is not necessary to preserve the acceleration time response of the flow path, but only the quasi-steady flow properties. When a small number of purges occurs, the flow path inertia would influence the system behavior, and it would be desirable to preserve the $\Pi$ groups involving inertia.

The same result is obtained by comparing the volume fill times to the transit times of the connected piping. When the fill time is much longer than the transit time, then the flow path inertia is not important. This is the approach taken in this report, as described in Section 2.4.

Application of the scaling procedure to the SBWR provided several nondimensional $\Pi$ groups which dominate the top-down system performance for the various cooling stages. Most of the $\Pi$ groups which dominate bottom-up behavior were found also to be preserved in scaled tests as a result of preserving top-down $\Pi$ groups. However, some bottom-up $\Pi$ groups could not be simultaneously satisfied with groups dominating top-down behavior. The resulting distortions are shown to be relatively insignificant to the experimental objectives.

## 1.5 Scaling Issues for the SBWR Related Tests

The experimental program supporting SBWR safety analysis includes the tests listed in Table 1-1, together with their volume scales in relation to the actual SBWR. All of these tests were (or will be) conducted under the following conditions:

- Actual fluids (water and steam, noncondensibles, with the exception of substitution of air for nitrogen in most tests and of helium for hydrogen in all tests where hydrogen presence was simulated).
- Prototypical initial thermodynamic state of the fluids or mixtures (pressure, temperature, component concentrations).
- Full height.
- Test facilities are large enough (i.e., pipe and vessel dimensions have a sufficiently large characteristic length scale) so that "microscopic" level interactions between the phases (e.g., *local* mixing of two different gases) are not expected to distort either bottom-up or top-down behavior at the various facility scales.

The geometrical "macroscopic" level configuration of the phases needs to be considered, however, and leads to the requirement of preservation of the large-scale mixing behavior of fluids in single-phase situations, and of flow regimes in two-phase flow situations. The large-scale mixing issues are addressed in subsequent sections of this report. Scaling requirements to preserve flow regimes are discussed by Schwartzbeck and Kocamustafaogullari [40]. For the SBWR-related tests considered here, the geometrical scale of the models was sufficiently large so that important flow regime distortions are not expected; in addition, most containment flows are single-phase.

Detailed consideration of mixing phenomena and flow regimes in Section 3 should remove any hierarchical concerns regarding constituents and phases. Moreover, the full-height design of the experimental facilities leads to proper simulation of the natural gravity heads that are essential for the natural circulation systems and loops considered here. The other *geometrical* scaling issues are addressed later in this report.

Additional scaling issues examined in this report include: (1) scaling of phenomena and processes; (2) multidimensionality; and (3) multi-unit, multi-element operation.

### 1.5.1 Scaling of Phenomena and Processes

The influence of spatial scale on phenomena and processes is considered in a bottom-up fashion for those ranked as important in the SBWR PIRT (e.g., stratification in pools and the development of thermal plumes).

### 1.5.2 Multidimensionality — Nonuniform Distribution Effects

This issue is related to the large differences in spatial scales between experiments like GIRAFFE and GIST and the SBWR. One must ensure that nonhomogeneities in the distribution of constituents or phases that may be occurring at a particular scale are understood (and/or "scaled" properly whenever possible). The issue is addressed (Section 3.2) by running counterpart tests in facilities having different scales (GIRAFFE and PANDA) and by examining the physical reasons that may lead to such non-homogeneities in a phenomenological, bottom-up fashion.

### 1.5.3 Multi-Unit, Multi-Element Operation

The SBWR has multiple key components such as the ICS and PCCS condensers and vent lines. Moreover, the condensers have a large number of similar elements (tubes). The exact numbers of units, or elements per unit, cannot be duplicated in the experiments, and this raises the question of possible dissimilar, non-symmetric operation of the units or elements and its effects on system performance. Again, the issue is addressed by analysis and by running tests in facilities having a range of number of tubes or units in parallel: (1) single-tube university tests; (2) three-tube GIRAFFE tests; (3) 20-tube, 4-unit PANDA tests; and (4) testing of entire full-scale modules in PANTHERS.

## 1.6 System Considered

### 1.6.1 Subdivision of the System into Subsystems and Components

For the purposes of this study, the SBWR System is divided into the subsystems or components shown on Table 1-2; the scaling by class of subsystem is considered in this report. Interactions (in this particular case, essentially transfers of mass and energy) between components are also a scaling consideration. The remaining SBWR systems or components are not relevant to this study and thus are not considered here.

### 1.6.2 Fluids and Other Materials

The *differences* between prototypical fluids and other materials that enter into consideration are:

- Air is used instead of nitrogen in the PANTHERS, GIST, and PANDA system tests and in the UCB and MIT single-tube tests.
- Helium is used to simulate hydrogen in all related tests.
- The wall materials used in the SBWR and in the various integral facilities are different. This issue is discussed in Section 3.4, which deals with the heat capacity and conduction in containment structures.

**Table 1-1. The SBWR Related Tests**

| Test | Purpose | Volume Scale |
|---|---|---|
| GIST | Integral GDCS system test | 1/508 |
| GIRAFFE/SIT | Integral GDCS system test | 1/400 |
| GIRAFFE/He | Integral long-term containment heat removal tests* | 1/400 |
| PANDA | Integral long-term containment heat removal tests | 1/25 |
| PANTHERS | Structural and heat transfer tests of the ICS and PCCS condensers | Full-scale prototypes |
| UCB MIT | Condensation in the presence of noncondensibles | Single-tube (near full-scale) |

* Performance of PCC with lighter than steam noncondensibles.

**Table 1-2. SWBR Subsystems and Components Considered**

Reactor Pressure Vessel, RPV
Main Steam Lines (MSL) and Depressurization Valves (DPV)

Drywell, DW
- Upper DW volume
- DW annular volume surrounding RPV
- Lower DW volume below RPV skirt

Suppression Chamber, SC
- Gas space
- Liquid volume in suppression pool (SP)

Main (LOCA) vents connecting DW to SP (8)
Vacuum breakers between DW and SC (3)
Leakage path between DW and SC

Gravity-Driven Cooling System (GDCS) pools (3)
- Gas space
- Liquid space

Equalization line with check valve connecting SP to RPV (3)

Isolation Condenser System (ICS) condensers (3)
Passive Containment Cooling System (PCCS) condensers (3)
Noncondensible PCCS vent lines from condensers to SP (3)
Isolation Condenser Pool with interconnected subcompartments

Other lines connecting the various subsystems listed above.

# 2.0 General Scaling Considerations — Top-Down Approach

## Introduction

The SBWR and the corresponding scaled test facilities are referred to generically and collectively as the "System" or "SBWR System" in this report. Alternatively, the SBWR and a particular test facility are referred to as the "prototype" and the "model," respectively (following common practice in scaling studies).

The *general* scaling criteria applicable to the SBWR System with its various subsystems and components and their counterparts in the related tests under consideration are derived in this section by a top-down approach. General scaling criteria have been derived by several authors ([6], [19], [21], [22]). Generally, these are not specific to the combined thermodynamic and thermal-hydraulic phenomena taking place inside containments and therefore are not directly applicable here. To arrive at general scaling criteria applicable to the SBWR System, the controlling processes in generic subsystems having the essential characteristics of *classes* of SBWR systems (e.g., containment volumes, pipes, etc.) are considered. These lead to generic governing equations for the rate of pressurization of volumes (the "pressure rate equations") and for the flow rates between volumes (the "flow rate equations"). These equations are cast in nondimensional form and various nondimensional groups controlling component or system behavior appear.

The pressure rate and flow rate equations are then specialized for the various volumes and flow paths of the system. The resulting set of equations is combined following a *global scaling methodology* [53] and presented to make the interactions between system components evident. The choice of proper global reference scales in the identification of the various nondimensional numbers, followed by a normalization using local reference scales, allows comparisons of the orders of magnitude and importance of the various terms in the equations. The numerical evaluation of the nondimensional groups is undertaken in Section 4: this makes any scaling distortions evident. Finally, by combining considerations regarding scaling distortions (based on the numerical values of the nondimensional scaling numbers) with consideration of the relative importance of the terms where these appear in the global scaling analysis, the effect of scaling distortions can be assessed. This procedure is explained in more detail below and followed in the remaining subsections of Section 2, and in Appendices A and B.

The SBWR System consists of a number of volumes (RPV, DW, SC, etc.) connected via junctions (i.e., openings, piping, vents, heat exchanging equipment such as the ICS and PCCS condensers, etc.). Mass and energy transfers take place between these volumes through their junctions. Heat may also be exchanged between volumes by conduction through the structures connecting them. These exchanges lead to changes in the thermodynamic condition of the various volumes; this, in particular leads to changes of the volume pressures. The junction flows (flows between volumes) are driven by the pressure differences between volumes. Thus, the thermodynamic behavior of the system (essentially, its pressure history) is linked to its thermal-hydraulic behavior (the flows of mass and energy between volumes). Proper global scaling of these processes is important for the SBWR-related tests considered here and the topic addressed in this section.

Global scaling is based on the mathematical formulations of the basic physical principles which govern top-down phenomena. Dependent variables like pressure, velocity, mass flow rates, and enthalpies are normalized with respect to either their initial values, or other limiting values, which

cause the normalized variables to have an order of magnitude unity; that is, O(1). Only quantities which can be controlled in an experiment are chosen for the normalizing values. The normalizing time scale for top-down phenomena is determined for each LOCA phase; namely, Blowdown, GDCS, and PCCS.

Flow path momentum equations govern the transient nature of flows between volumes. The series and parallel flow path combinations connecting two volumes such as the RPV and wetwell yield "loop" equations (actually "open loop") between a source and sink, from which a representative response time for the flow inertial effects can be determined.

The momentum equations for entire loops are normalized and presented in matrix form to display cross-coupling importance of various individual paths. Pressure rate formulations for each volume are normalized with respect to the dominant reference time determined for the particular LOCA phase to be examined.

The magnitude of the nondimensional groups appearing in the equations displays the relative importance of various parameters. This information is useful in assessing the effect of scaling distortions, and helps to ensure that (1) all important phenomena are preserved and (2) nonrepresentative effects have not been introduced.

Prototypical fluids under prototypical thermodynamic conditions were used in all the SBWR-related tests. The fact that the fluids are expected (by design and operation of the test facilities) to be in similar states in the prototype and the models, will be used to simplify the following analyses.

## 2.1 Generic Junction Flow Rate Equation

Mass transfers between containment volumes (i.e., at flow junctions) are driven by pressure differences; these could be due to differential buildup of pressure in the two volumes attached to a junction or may be hydrostatically driven. In this section the generic equation governing junction flow rates is presented.

The general cases (Figure 2.1-1) of pipes connecting two volumes at pressure $P_1$ and $P_2$ are considered. The pipe in the receiving vessel may be immersed in a pool of liquid at a submergence H; this configuration is referred to as a "vent". The case of an open vent is considered here. When the vent is closed, the column of liquid in the vent line balances the hydrostatic pressure difference between the two volumes. The case of single-phase incompressible flow is considered here, since this is the case for the majority of the junction flows in the SBWR containment system (Appendix A). The case of two-phase flows can be obtained by specifying appropriate two-phase friction multipliers.

The detailed derivation of the junction flow rate equation of length $\ell_n$ starts by considering the momentum equation for time-dependent flow in a *segment* of the piping. By adding the momentum equations in different segments constituting a *flow path*, the following equation is obtained:

$$\sum_n \frac{\ell_n}{a_n}\frac{dW}{dt} = \Delta P_{12} + \rho g \sum_n \ell_{nv} - \rho_L g H - \sum_n \frac{F_n}{a_n^2}\frac{W^2}{2\rho} \tag{2.1-1}$$

where,

$$\Delta P_{12} = P_1 - P_2 \tag{2.1-2a}$$

and

$$F_n = \frac{f_n \ell_n}{D_n} + k_n \tag{2.1-2b}$$

The various symbols are defined in Figure 2.1-1, and $k_n$ and $f_n$ are the local loss coefficient and friction factor, respectively, in segment n. Equation 2.1-1 can be symbolically written for flow path m as,

$$\left(\frac{L}{a}\right)_m \frac{dW_m}{dt} = \Delta P_m + \rho_m g L_m - \rho_L g H_m - \left(\frac{F}{a^2}\right)_m \frac{W_m^2}{2\rho_m} \tag{2.1-3}$$

where,

$$L_m = \sum_n \ell_{nv} \tag{2.1-4a}$$

$$\left(\frac{F}{a^2}\right)_m = \sum_n \frac{F_n}{a_n^2} = \sum_n \left(\frac{f_n \ell_n}{D_n} + k_n\right) \frac{1}{a_n^2} \qquad (2.1\text{-}4b)$$

and

$$\left(\frac{L}{a}\right)_m = \sum_n \frac{\ell_n}{a_n} \qquad (2.1\text{-}4c)$$

For the gas-filled line indicated schematically in Figure 2.1-1a, the gas density is very small compared to that of the liquid and the gas gravity head $\rho_m g L_m$ can be neglected. Also, the submergence head $H_m = H_{sub}$. For the liquid-filled line shown in Figure 2.1-1b, the net gravity head is $L_m = L_1 - L_2$ and the density $\rho_m$ equals that of the average liquid density $\rho_L$ for flow path m. Also, in this case $H_m$ is set equal to zero. Equation 2.1-3 will be specialized later to represent the various flow paths in the system considered.

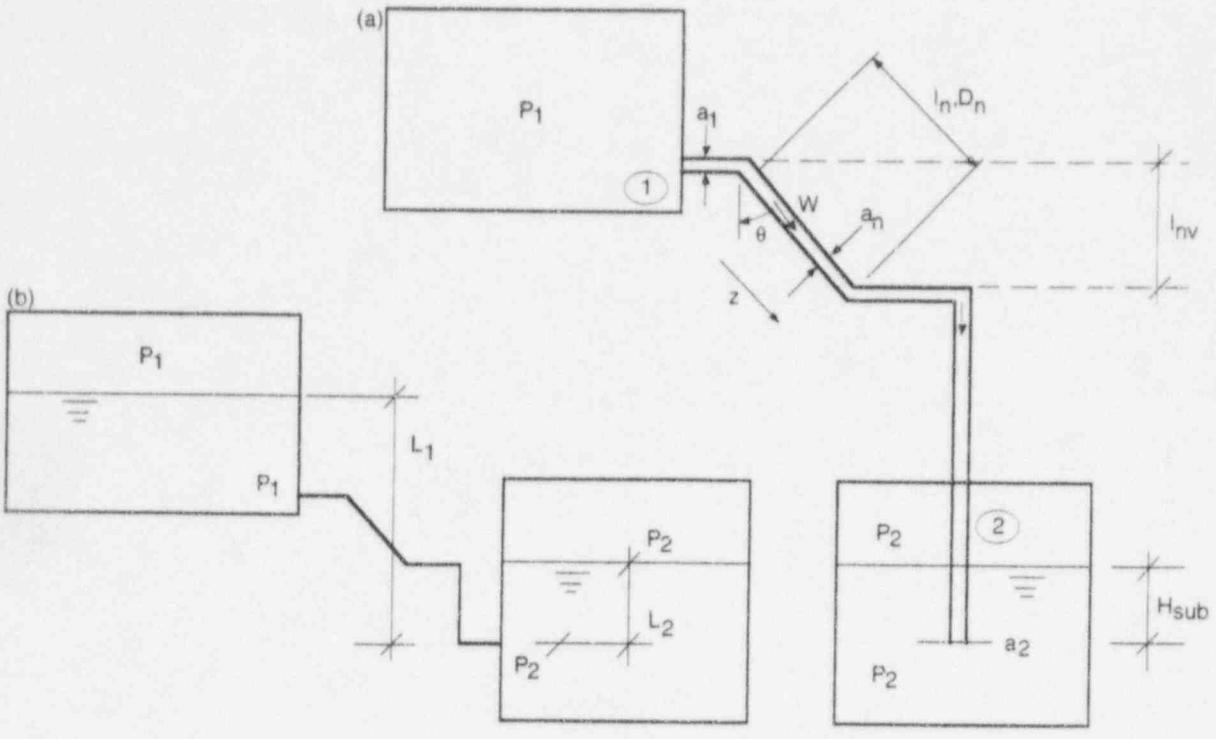


Figure 2.1-1. (a) Pipe Connecting Two Volumes and Submerged in Volume 2; in this case, $H_m = H_{sub}$ and $\rho_m g L_m \sim 0$
(b) Pipe Connecting Two Pools; in this case, $L_m = L_1 - L_2$ and $H_m = 0$

## 2.2 Vessel Pressurization Rate Equation for a Control Volume

The general equation governing the flows of mass in junctions between containment volumes was derived in Section 2.1. In this section, the equations governing the state of the fluid within a volume are derived.

Consider the control volume V of Figure 2.2-1 containing a mass M with internal energy E at a pressure P and a temperature T. The volume contains a number of constituents (noncondensible gases, steam, etc.), each denoted by the subscript j. Any changes in the kinetic and potential energy of the mass M are much smaller than changes in its intrinsic internal energy and therefore are neglected. The system is well mixed (i.e., the distributions of constituents and of the temperature are uniform), and at thermodynamic equilibrium. The conservation equations for mass and energy are used to derive an equation for the rate of pressure change in this control volume. The conservation equations and the final result are given in this section; the details of the derivation can be found in Appendix B.

The *total-mass* continuity equation for this volume is:

$$\frac{dM}{dt} - \sum_i W_i = 0 \tag{2.2-1}$$

where $W_i$ are the total (steam, noncondensibles, etc.) mass flow rates entering the volume. The mass conservation equation for *constituent j* is

$$\frac{dM_j}{dt} - \sum_i W_{i,j} = 0 \tag{2.2-2}$$

Here a constituent is either steam-water or a noncondensible gas.

The energy conservation equation is:

$$\frac{dE}{dt} = -P\frac{dV}{dt} + \dot{Q} + \sum_i W_i h_{o,i} \tag{2.2-3}$$

where $\dot{Q}$ is the heat added to the system (e.g., by conduction through the wall), and $h_{o,i}$ is the total specific enthalpy of stream i. The total enthalpy (subscript o) includes the kinetic and potential energy. The specific internal energy of the system,

$$e = \frac{E}{M} \tag{2.2-4}$$

is a function of two thermodynamic variables, namely, the pressure and the specific volume $v = V/M$; and of the mass fractions $y_j$ of the various constituents:

$$e = e(P, v, y_j) \tag{2.2-5}$$

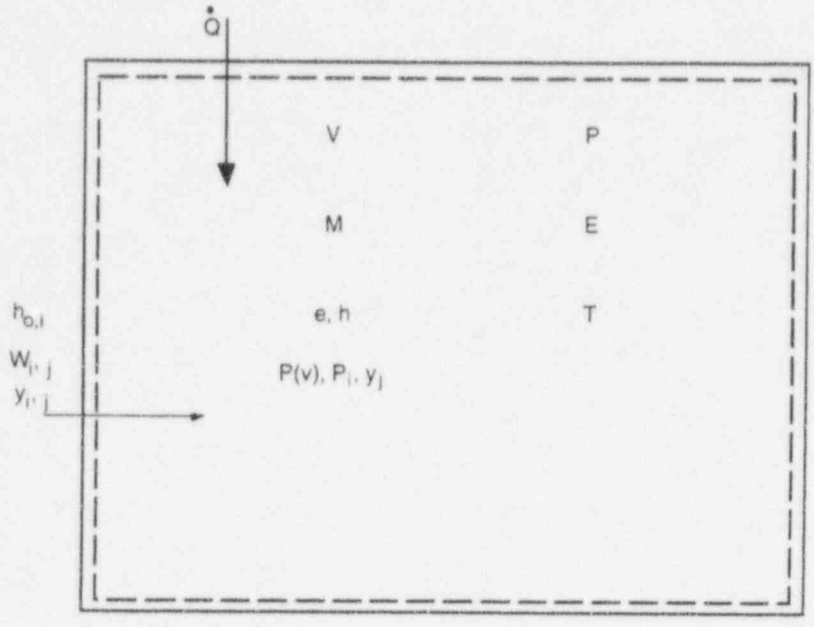


Figure 2.2-1. A Control Volume Receiving Mass Flow Rates $W_i$ With Corresponding Total Enthalpies $h_{o,i}$, and Heat the Rate $\dot{Q}$

The conservation equations and state equation listed above can be combined to derive an equation for the rate of change of the internal specific energy of the volume and an equation for the rate of pressurization, dP/dt, of a control volume. These equations are derived in Appendix B and can be written in compact form as follows:

$$M\frac{de}{dt} = -P\frac{dV}{dt} + \dot{Q} + \sum_i W_i\left(h_{o,i} - h\right) + P\Big/\rho\sum_i W_i \tag{2.2-6}$$

$$Vf_2\frac{dP}{dt} = \sum_i\left[W_i\left(h_{o,i} - h\right)\right] + \sum_i W_i P^* v + \dot{Q} - P^*\frac{dV}{dt} - V\sum_j\left[f_{l,j}\frac{dy_j}{dt}\right] \tag{2.2-7}$$

where the following short–hand notations were made:

$$P^* \equiv P + \left.\frac{\partial e}{\partial v}\right|_{P,\,y_j}$$

$$f_{1,j} \equiv \frac{1}{v}\left.\frac{\partial e}{\partial y_j}\right|_{P,\,v,\,y} \qquad \text{(units of energy per unit volume)} \tag{2.2-8}$$

$$f_2 \equiv \frac{1}{v}\left.\frac{\partial e}{\partial P}\right|_{v,\,y_j} \qquad \text{(nondimensional)}$$

where $y_j$ constant means all $y_j$ are held constant and y constant means all yj except the one in the derivative are held constant.

For containment vapor volumes, the quantities P*, $f_{i,j}$ and $f_2$ denote thermodynamic properties of the mixture, which are functions of P, v, and $y_j$. When prototypical fluids under prototypical thermodynamic conditions are used, these thermodynamic properties are identical for prototype and model.

We note that Equation 2.2-7 yields the rate of change of the pressure in terms of heat addition, mass and enthalpy fluxes into the volume, and changes of volume *composition*. The rate of change of volume dV/dt (e.g., due to phase change at the boundary) is also considered.

The system compliance in Equation 2.2-7 is a function of the vapor mass fraction in vessels containing liquid such as the RPV. The equation for the vapor fraction is obtained by combining the vapor phase continuity equation and net vapor generation equation:

$$\rho_g\frac{d\alpha}{dt} = \frac{1}{V}\sum W_g + \frac{\sum\left(h_\ell - h_f\right)W_\ell}{h_{fg}V} + \frac{\dot{Q}}{h_{fg}V} + \frac{\psi}{h_{fg}}\frac{dp}{dt} \tag{2.2-9}$$

where

$$\psi = 1 - \left(1-\alpha\right)\rho_f h_f' - \alpha\rho_g h_g' - \alpha h_{fg}\rho_g' \tag{2.2-10}$$

## 2.3 Global Model of the SBWR System

The equations governing flow rates at junctions and the pressurization rate of volumes were developed in Sections 2.1 and 2.2. They will be applied now to arrive at *a Global Model* of the SBWR system. In parts of the system, they will have to be supplemented by additional ad-hoc governing equations. A certain degree of simplification will also be used to arrive at a tractable but representative global analytical model of the system.

The purpose here is *not* to derive a model that allows simulation of detailed system behavior, but rather to gather the main equations governing this behavior with the purpose of using these to examine global system scaling.

The mass and energy continuity equations were combined in Section 2.2 to arrive at the volume pressure rate (or volume state) equation. The momentum equation was used to develop the flow rate equation for the junctions in Section 2.1. Thus, in the following analysis, instead of mass, energy and momentum conservation, flow rate equations, pressure rate (or state) equations and mass balance will be used. It is understood, of course, that the enthalpy in the various flow paths and volumes must also be calculated using again the energy equation (or a combination of a state and mass balance equation). This is not done explicitly here, but the generic form of the energy equation was nondimensionalized to ensure that it does not lead to any additional Π groups.

Having obtained a general system model, the particular behavior of the system during certain phases of certain accidents (e.g., during the Blowdown Phase of a GDLB) can then be examined by assembling specialized system models as subsets of the generic model. These specialized models (and the corresponding subset of governing equations) will form the basis of the global scaling studies that follow. The generic model equations, together with any assumptions needed to derive them, are listed below. The nomenclature and subscripts used to define various parts of the system and the corresponding variables are given in Table 2.3-1 and in the Nomenclature and Abbreviations section at the beginning of the report.

The equations are written using the symbolic forms of Equations 2.1-3 and 2.2-7. In deriving this generic model, several units working in parallel (e.g., the three PCCS condensers) are lumped together. This is indeed not a scaling issue but rather the purpose of certain experiments designed to detect any possible asymmetries in operation.

**Summary**

The following system variables and governing equations were identified:

- 11 flow rates and the corresponding flow path pressure drops governed by the 11 flow path equations.
- Five volume gas phase pressures:

$$P_R, P_D, P_W, P_{IC}, P_{PC}$$

These are governed by the three pressurization rate equations for the RPV, the drywell and the wetwell, and the two additional "imposed conditions which, together with the two mass continuity assumptions for the IC and PCC link the heat exchange rates $\dot{Q}_{IC}$ and $\dot{Q}_{PCC}$ to IC and PCCS inlet flow and, thus, indirectly to PIC and PPCC. The water levels in the IC and PCC drain lines can also be obtained from these equations.

- Three total volume masses for the RPV, the drywell and the wetwell and three corresponding mass balances.
- Two liquid inventories in the RPV and the wetwell which are derived considering the void fraction in the RPV and an energy balance for the wetwell.
- Two important liquid level differences $L_{EQ}$ and $L_{LG}$ that are obtained by considering GDCS and SP mass balances and level calculations.

**Table 2.3-1. Nomenclature for SBWR Components**

| Subscript | Flow Path in SBWR |
|---|---|
| C | IC inlet line |
| L | IC drain line |
| B | RPV to drywell (DPV, break flow) |
| PC | PCC inlet line and component |
| LPC | PCC drain line |
| PCX | PCC vent line |
| RV | RPV to wetwell (SRV line) |
| LG | GDCS line |
| V | Main vent line |
| EQ | Equalization line |
| VB | Vacuum breaker path |
| LGB | GDCS to drywell (GDCS Linebreak flow) |
| DP | RPV to DW (DPVs) |
| ADS | DPVs plus SRVs |
| BR | RPV to DW (break only) |
| **Subscript** | **Volume or Component in SBWR** |
| R | Reactor pressure vessel |
| D | Drywell |
| W | Wetwell – gas space |
| LW | Suppression pool in Wetwell |
| LG | GDCS pool |
| IC | Isolation Condenser |
| SC | Suppression Chamber |

## 2.4 General Scaling Procedure and Criteria

Scaling is performed by nondimensionalizing the equations governing a particular process or phase of an accident. This is accomplished classically by dividing the (dimensional) values by reference values or scales to make them nondimensional. The *nondimensional* variables and the various scales are then separated in two groups: (1) groups of reference scales, the so-called Π groups or Π numbers, and (2) the nondimensional variables.

If a test facility is perfectly scaled, then the values of all Π numbers for the prototype and the model should be perfectly matched. By considering a priori perfect matching of all the Π numbers for all system components, one can obtain guidance regarding *general scaling criteria*. In deriving such general scaling criteria, one does not have to worry in particular about the magnitude of the *nondimensionalized* variables, since everything should in principle be perfectly matched. This is the analysis pursued in this section. It leads to the *general* criteria that govern scaling of the models.

In practical cases, the model cannot be perfectly scaled. One then needs to evaluate the importance of scaling distortions. These appear as differences in the values of the pairs of Π groups calculated for the various components of the system (prototype and model). Since, for a given system and a specific Π number, several pairs of Π values may need to be calculated, the range of magnitudes that pairs of a *particular* Π group may take may be broad. For example, when Π groups containing the various flow rates entering into a control volume are considered, the magnitude of a component Π group will depend on the magnitude of the corresponding flow rate.

To properly evaluate the magnitude of scaling distortions, in defining the Π numbers, one should use reference scales making the magnitude of all the *nondimensional* variables of order one. The Π numbers multiplying the various nondimensional terms specify then their relative importance in the governing equation.

A further difficulty arises, however, when several Π groups of the same type appear in the governing equation (in the example cited above, the several Π groups containing the flow rates entering the control volume). Usually, one can define a variable that is of greatest importance for a particular test; for example the RPV water level or the drywell pressure. Examination of the nondimensionalized governing equation can show which term(s) dominate the behavior of this most important test variable(s) and identify the corresponding pairs of Π number(s) that should be matched. The governing equation may, however, contain many terms containing the same type of Π number. The relative magnitude of these terms will show which system components should be scaled most carefully. Again in the example cited above, the relative magnitude of the Π terms containing the various flow rates will show which component flow rates should be matched most carefully.

Thus, to make this process systematic, the following procedure is followed:

- By a proper choice of scales (described below), all the nondimensional variables (including the derivatives of variables) appearing in the nondimensionalized governing equation are to be made of order one.
- The dominant terms in the governing equations are identified by comparing the relative magnitude of the Π numbers appearing in front of the variables.

- Global system reference scales making the most important and dominant Π number(s) also of order one are used: these define the global $_P$ numbers for the particular process considered.
- This procedure brings local normalizing factors (or weights) multiplying the nondimensional term and the corresponding global P number into the equations.

The local normalizing factors will typically be the ratios of the local reference scales for a particular system component to the global reference scales. The local reference scales for a particular system component can typically be chosen as the initial or boundary values of the variable in question *for the particular component considered.*

If the scaling of a particular component is deficient (as indicated by non-matching local P numbers), the relative importance of this distortion can be assessed by looking at the importance of the local scaling or weight factor multiplying it.

The nondimensionalization and normalization procedure and the nomenclature used are defined more specifically below. Consider:

- the *local* variable zn (e.g., the particular flow rate n entering a volume)
- a local scale $z_{n,o}$:

  $z_{n,o}$ is typically an initial or boundary value or some other proper scale for that particular local variable.

- the global scale zr for all the variables z (e.g., for all flow rates):

  $z_r$ is typically the most important value of z (e.g., the blowdown flow rate when the Blowdown Phase of the accident is considered).

One then defines:

- the *locally* scaled variable,

  $$z_n^+ \equiv \frac{z_n}{z_{n,o}}$$

- the local normalizing factor or weight,

  $$z_n^o \equiv \frac{z_{n,o}}{z_r}$$

  and obtains:

  $$z_n = \left(\frac{z_n}{z_{n,o}}\right)\left(\frac{z_{n,o}}{z_r}\right)z_r = z_n^+ z_n^o z_r$$

### 2.4.1 Nondimensional Form of the Equations

The generic equations governing the flow rates between junctions (Equation 2.1-3), total and component mass conservation (Equations 2.2-1 and 2.2-2) and the pressurization rates of volumes (Equation 2.2-7) and the volume internal energy (Equation 2.2-6) were derived in Sections 2.1 and 2.2. These equations will be cast in this section in a generic nondimensional form. During this procedure, the nondimensional P groups that govern system behavior will appear.

The enthalpies ho appearing in Equations 2.2-6 and 2.2-7 were *total* specific enthalpies (i.e., the sum of the intrinsic specific enthalpy of the fluid plus its kinetic and potential energies). Consequently, the exact scaling of these would have required separate consideration of specific enthalpy, velocity and elevation scales. Since changes in kinetic and potential energy are very small or totally negligible, this complication is avoided here and the $h_o$ are replaced by h in the following.

The equations that will be nondimensionalized are repeated here for convenience:

$$\frac{dM}{dt} - \sum_i W_i = 0 \tag{2.4-1}$$

$$\frac{dM_j}{dt} - \sum_i W_{ij} = 0 \tag{2.4-2}$$

$$\left(\frac{L}{a}\right)\frac{dW}{dt} = \Delta P - \frac{1}{\rho}\left(\frac{F}{a^2}\right)\frac{W^2}{2} - \rho g H \tag{2.4-3}$$

$$V\rho\frac{de}{dt} = -P\frac{dV}{dt} + \dot{Q} + \sum_i \left(h_i - h\right)W_i + \frac{P}{\rho}\sum_i W_i \tag{2.4-4}$$

$$\frac{dP}{dt} = \frac{1}{Vf_2}\left\{\sum_i\left[W_i\left(h_i - h\right)\right] + \sum_i W_i\frac{P^*}{\rho} + \dot{Q} - P^*\frac{dV}{dt} - V\sum_j\left[f_{1j}\frac{dy_j}{dt}\right]\right\} \tag{2.4-5}$$

$$\rho_g\frac{d\alpha}{dt} = \frac{1}{V}\sum_i W_g + \frac{\sum_i \left(h_\ell - h_f\right)W_\ell}{Vh_{fg}} + \frac{\dot{Q}}{V} + \frac{\psi}{h_{fg}}\frac{dP}{dt} \tag{2.4-6}$$

These equations will be nondimensionalized using the following reference quantities (denoted by the subscript r) for use in deriving the general scaling criteria in the next subsection:

- For time: $t_r$
- For volume: $V_r$
- For mass flow rates: $W_r$
- For heat addition: $Q_r$
- For densities: $\rho_r$
- For pressure, a reference pressure difference: $\Delta P_r$
- For properties involving vapor mass function: $\psi_r$
- For enthalpies and internal energies, a reference specific enthalpy difference:

To derive the general scaling criteria, the equations will be nondimensionalized by dividing the dimensional variables z by the reference values $z_r$ above; this produces the nondimensional variables $z^+$:

$$z^+ \equiv \frac{z}{z_r}$$

In particular, note that:

$$h_{o,i} - h_o \approx h_i - h = h_i^+ \Delta h_r$$

where $h^+$ denotes a nondimensional enthalpy difference for flow i (enthalpy of stream entering $h_i$, minus average volume enthalpy, h).

Also

$$f_{1,j} = f_{1,j}^+ \frac{\rho_r \Delta h_r}{y_{j,r}}$$

and

$$f_2 = f_2^+ \rho_r \frac{\Delta h_r}{\Delta P_r}$$

### 2.4.2 Phase Changes at Interfaces

The phase changes at interfaces involve the latent heat of vaporization and the inerfacial mass flow rates and mass fluxes. The reference enthalpy scale $\Delta h_r$ used above can, in principle, be selected arbitrarily. A natural definition for $\Delta h_r$ arises, however, when phase changes at interfaces are scaled. In this case, the natural choice is the reference latent heat of vaporization.

Although it is generally difficult to scale exactly phase changes taking place by condensation on structures and walls (Section 3), it is relatively straightforward to scale phase changes at the free pool surfaces. The flow rates due to phase change at the surface of a pool are given by the product of the pool surface area $A_{LG}$ times the mass flux due to phase change $\dot{m}_{LG}$. The latter, in general, may depend on the fluid conditions on both sides of the interface (P, T, partial densities of constituents $\rho_j$) and on hydrodynamic parameters controlling mass transfer (i.e., the Reynolds and Prandtl numbers of the fluids). The hydrodynamic dependence is considered in the bottom-up analysis of Section 3. Here we derive the scaling of the surface areas.

The vapor flow rate due to vaporization

$$W_{LG} = A_{LG}\dot{m}_{LG} \tag{2.4-7}$$

must scale the same way as the other flow rates in the system. Assuming that with prototypical fluids and well scaled local conditions at the interface, the phase-change mass fluxes $\dot{m}_{LG}$ in the prototype and the model are identical, one concludes that the pool areas $A_{LG}$ must scale like the flow rates.

### 2.4.3 General Scaling Criteria

The nondimensional numbers identified above will be used now to derive general scaling criteria for the experimental facilities.

The analysis of this section considers a single individual flow path and a single volume and derives the general scaling laws applicable to these. These general criteria are applied then to each flow path and volume in the system. The resulting scaling of the entire system, any possible interactions between subsystems, and the identification of scaling distortions are considered in Section 2.5.

Although several other choices are also possible, the *system scale R* can be defined as the ratio of prototype to test facility power input:

$$R \equiv \frac{\dot{Q}_{prot}}{\dot{Q}_{mod}} = \dot{Q}_R \tag{2.4-8}$$

where the subscript R denotes the ratio between the corresponding scales of prototype and model. For a variable Z:

$$z_R \equiv \frac{z_{prot}}{z_{mod}} \tag{2.4-9}$$

Nine nondimensional groups were identified by the analysis. In addition, it was shown that the pool surface areas $A_{LG}$ must scale like the flow rates.

### 2.4.4 Scaling of the Piping

The scaling of the piping is determined by the pressure drop and reference flow rate scales.

The factor $F/a^2$ (Equation 2.1-4b) depends on both the frictional losses in the pipes (i.e., on the groups $f_n \ell_n / D_n$ and on the local losses $k_n$. The latter are generally insensitive to scale. Since the model diameters Dn are smaller, however, the $F/a^2$ factors of the models tend to be larger. Thus, conservation of $\Pi_{loss}$ leads to reduced velocities in the models. This is not important, as long as the transit times between volumes are small compared to the volume fill times $t_r$, and the velocities do not become so low as to introduce new phenomena in the models.

*In practice*, pipe scaling is performed according to the following procedure: the pipe cross-sectional areas in the scaled facilities are oversized for convenience; this leads to somewhat lower flow velocities in the pipes. Thus, considering only the *local losses* (for which the loss coefficients are only weakly dependent on flow velocity or Reynolds number), the total $\Delta p$'s in the models would be *lower* than prototypical. On the contrary, *wall friction* in the scaled facilities is *larger* (due to larger values of the $f\ell/D$ values produced by the smaller pipe diameters), as it cannot be compensated in general by the decrease in velocity. Usually (and fortunately), the total pressure drops in the piping are dominated by local losses, so that the total $\Delta P$'s in the scaled facilities end up being somewhat smaller. They can therefore be matched by introducing additional losses by local orificing.

The pipe flow areas determined in this fashion result in velocities that do not lead to matching pipe transit times. This is, however, of secondary importance, as already noted.

*In summary, matching of the total pressure drops is accomplished by using orifices in conjunction with convenient choices for pipe diameters.*

### 2.4.5 Compressibility of the Gas Flowing in Pipes

The gases flowing in pipes connecting containment volumes were treated as incompressible; this assumption is justified in this section.

We start from the continuity equation, written for the pipe segment of Figure 2.4-1,

$$\frac{dM}{dt} = W_1 - W_2 \qquad (2.4\text{-}10)$$

where $W_1$ and $W_2$ are the mass flow rates at Sections 1 and 2, respectively; in general

$$W = A_p \rho u$$

M is the mass contained in the pipe of volume $V_P = A_P L_P$ and average density $\bar{\rho}$. We nondimensionalize Equation 2.4-10 by defining

$$W^+ \equiv \frac{W}{W_r}$$

with

$$W_r = \rho_r A_p u_r$$

and

$$\rho^+ \equiv \frac{\rho}{\rho_r}$$

and a pipe transit time

$$t_{tr,r} \equiv \frac{L_p}{u_r}$$

Equation 2.4-10 takes the nondimensional form

$$t_{tr,r} \frac{d}{dt} \bar{\rho}^+ = W_1^+ - W_2^+ \qquad (2.4\text{-}11)$$

It is evident that if $t_{tr,r}$ and the rate of change of the average density are both small, the mass flow rates at the inlet and the exit of the pipe will be approximately equal, $W_1^+ \approx W_2^+$ or $W_1 \approx W_2$. Clearly, the pipe transit time $t_{tr,r}$ must be compared to the other time constants of the system; namely, the ones determining the variation of the conditions in the containment volumes (i.e., $t_r$). The same volume fill constant $t_r$ determines the rate of variation of the inlet density $\rho_I$ and, consequently, of the average density $\bar{\rho}$ in the pipe.

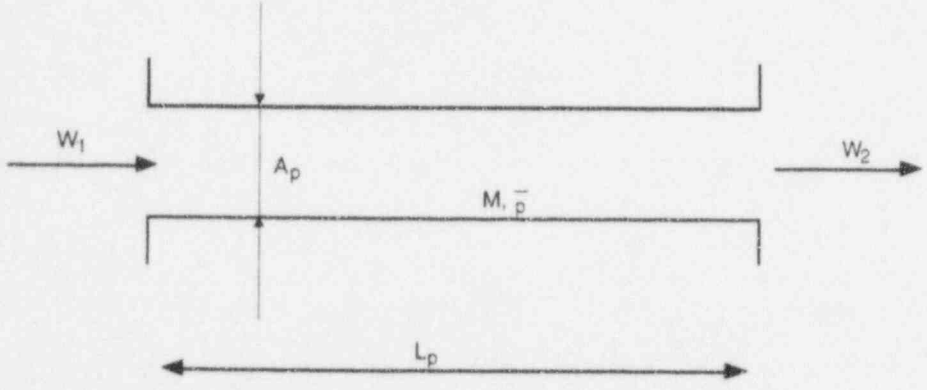


Figure 2.4-1. A Pipe Segment Connecting Two Volumes

### 2.4.6 Time Scales

### 2.4.7 Specific Frequencies of the Process

Another way of viewing the processes taking place is by considering their specific frequencies [52]. Specific frequencies are given as ratios of a transfer intensity to capacity (amount) of the receiving volume.

### 2.4.8 Summary

## 2.5 Scaling of the SBWR System

This section describes the results of nondimensionalizing the model equations derived for the SBWR System in Section 2.3. The equations were nondimensionalized, as indicated in Section 2.4. The results of numerical evaluations are reported in Section 4.

### 2.5.1 Application of the Global Momentum Scaling

This general form is specialized to the active flow paths in the SBWR during different LOCA phases. The equations for the paths active in a phase are combined to give a single matrix equation for the entire system. The resulting matrix equation is different for different phases and different conditions (e.g., vacuum breaker open or not open).

The numerical evaluation of the $\Pi$ groups and multiplying matrices is given in Section 4. The leading $\Pi$ groups are based on global reference values for the entire system. These are multiplied by the ratios in the matrices on which they operate. In this way, the variables are nondimensionalized to local reference values so that the nondimensional variables and their derivatives are approximately one. Numerical results for both the general $\Pi$ groups and the multiplying ratio matrices are given in the tables. The products of these, which indicate the values of the local $\Pi$ groups, are also given.

### 2.5.2 Application of the Pressure Rate and Vapor Fraction Equations

The nondimensional general form of the pressure rate equation is applied to the RPV, drywell and wetwell. The equation is specialized for the specific application by eliminating terms that are not used and expanding out the summations for the case of multiple sources.

The equations, as applied, are based on uniform mixing and assume a state of thermal equilibrium for the considered volume. The void fraction equation is considered for the RPV control volume. The assumptions of uniform mixing and a state of thermal equilibrium are also true for this equation.

### 2.5.3 Results

The equations are used to calculate numerical values for the nondimensional $\Pi$ groups for the SBWR, GIST, GIRAFFE/SIT, GIRAFFE/He and PANDA tests. The results for the SBWR are discussed in Section 4.1. Comparisons of the results for the test facilities with the SBWR are given in Subsections 4.2 to 4.5.

# 3.0 Scaling of Specific Phenomena — Bottom-Up Approach

The scaling of particular SBWR System components in relation to specific phenomena and processes considered important is conducted in a bottom-up fashion in this section. The discussion is limited to the spatial-scale-dependent phenomena ranked as important in the SBWR PIRT and not considered generically in Section 2.

## 3.1 Important Phenomena

The SBWR PIRT was used to identify the phenomena of safety importance for post-LOCA behavior of the SBWR. The important phenomena for each subsystem or component and for each phase of the class of accidents considered were identified. The phenomena in each of the three main phases of the class of accidents, together with the subsystems where they are expected to be of importance, were considered.

## 3.2 Thermal Plumes, Mixing, and Stratification

Thermal plumes, mixing and thermal stratification phenomena can be encountered:

- In the DW and in the gas space of the SC, for steam and noncondensible gases (nitrogen or hydrogen).
- In the suppression pool.

Combinations of single-phase/two-phase, axisymmetric/plane, and free/wall plumes for fluids emerging from vents or originating on hot or cold wall surfaces can be encountered. The various stratification, plume, and jet situations are sketched in Figure 3.2-1.

The situations involving mixing induced by plumes are discussed in this section, while the condensation phenomena from either jets or two-phase plumes are considered in Section 3.5.2.

### 3.2.1 Stratification and Mixing of the Suppression Pool

Possible stratification of the suppression pool (SP) is an important issue, since the temperature of the top layer of pool water determines the saturation pressure of the vapor in the gas space of the SC, which, together with the partial pressure of the noncondensible gas, determines the containment pressure level.

The PCC vents inject noncondensible gases and steam into the SP at temperatures somewhat in excess of the SP water. Ideally, the steam condenses near the injection point. (Other possible situations, such as partial channeling of steam to the SP gas volume, are discussed in Section 3.5.2.) The SP may become stratified during the long-term containment cooling phase, since the hot gases and the hot condensate will create plumes that rise to the surface of the pool and spread horizontally.

#### 3.2.1.1 Horizontal Spreading

Plumes created at the PCC vents rise, "impinge" on the free surface of the pool, and spread horizontally. Since their momentum must be conserved, the plume vertical rise velocity is essentially converted to a horizontal spreading velocity [54]. Plume rise velocities are of the order of 10 m/s and provide a first estimate of the horizontal spreading velocity. Consequently, the time characterizing the horizontal spreading of the hot plume on the pool surface, out to the walls, will be of the order of seconds or tens of seconds at most. This time is short compared to the time scale of containment response and *the horizontal spreading of the plume can be considered as being instantaneous*[†].

*Consequently, at any instant, the surface of the pool will have a temperature equal to the average plume temperature reaching the surface of the pool.* Thus, this temperature is particularly important; it will depend on the dilution of the initial mass injected by the rate of entrainment of liquid into the plume from the colder pool (i.e., on pool stratification and plume behavior).

[†] This statement can be verified in the PANDA test facility where the hot plume rising from a vent in one of the SC vessels can spread towards the nearest vessel wall and also cross the large pipe connecting the two SC vessels and propagate in the second vessel, traversing a much larger distance, comparable to the circumferential distance between vents in the SBWR SC.

### 3.2.1.2 Vertical Stratification

We will consider first the case of relatively *quiescent spreading* of the plume on the surface of the pool. The layers of hot water near the surface of the pool will be displaced downwards by subsequent, hotter layers spreading on the surface [44]. This process will produce a degree of pool stratification, dependent, of course, on the amount of entrainment into the plume from the surrounding pool. With sufficiently large entrainment, the liquid reaching the surface of the pool will be only slightly above the pool average temperature, and the pool will be well mixed above the injection point [54].

If the entrainment into the plume is scaled properly (i.e., if the plume reaching the surface of the pool has the correct temperature history), it is evident that correct scaling of the stratification (i.e., identity of the temperature gradients in a vertically 1:1 scaled facility or, alternatively, identical downward displacement velocity of the stratified fluid front) requires pool surface area to volumetric flow rate scaling:

$$(A_{LG})_R = J_R = Q_R = R \tag{3.2-1}$$

This condition already resulted from the top-down scaling considerations of Section 2. Plume behavior is considered in Section 3.2.3.

If the plume spreads on the surface of the pool *with significant horizontal momentum*, it will reach and impinge upon the vertical bounding walls, turn and penetrate downwards; a recirculation pattern may be created resulting in good mixing of *all* the fluid above the injection point [54]. In this case, stratification may be practically absent. The pool temperature will be scaled properly, regardless of the details of plume behavior, if the horizontal flow areas are scaled as shown above.

### 3.2.2 Natural Circulation in Wetwell Gas Space

Different temperatures on various surfaces in the wetwell (WW) will result in some amount of natural circulation of the gas space. The amount of natural circulation will be characterized by the Grashof number to the 1/3 power:

$$Gr^{1/3} = \left( \frac{g\beta L^3 \Delta T}{\nu^2} \right)^{1/3} \tag{3.2-2}$$

where

$$\beta = -\frac{1}{\rho}\left( \frac{\partial \rho}{\partial T} \right)_p \tag{3.2-3}$$

The length scale of interest depends on which wall temperatures are driving the flow. If temperature differences exist between the two vertical walls (or across a cylinder in the case of PANDA or GIRAFFE), then the appropriate length scale for calculating Gr is the distance between the inner and outer walls for SBWR, and the vessel diameters for PANDA and GIRAFFE.

In addition to temperature difference driven flow, there will be some mixing resulting from the agitation at the pool surface due to the gases from the PCCS vent escaping from the pool surface.

The unknown nature of the buoyant jet or jets resulting from the PCCS gases makes it difficult to quantitatively show what effect this has on the WW gas space in a way similar to what is done in Section 3.2.4. The bubbles coming off of the pool will entrain water droplets into the airspace and will keep the air near the surface saturated in both the prototypes and the test facilities.

### 3.2.3 Scaling of Plumes in Suppression Pool

Free plumes can be classified as laminar or turbulent. Geometrically, one distinguishes between axisymmetric round plumes and plane plumes. Thus, four different combinations exist [17]. The scaling of plumes was recently discussed in relation to the SBWR by Peterson et al. [36]. Wall plumes (i.e., plumes rising around pipes or other vertical walls) provide lesser entrainment than free plumes (ibid) and should be avoided, if good mixing is desired[†]. Simple vertical pipe vents located near the vessel wall were, however, used in the GIRAFFE facility. Such vents will create wall plumes.

The scaling of fully-developed plumes (i.e., plumes having self-similar radial distributions at various elevations) is relatively straightforward. The discussion of this section applies to such plumes. It is also assumed that the plumes do not interact with vessel walls and with neighboring plumes. This will be the case in sufficiently large-scale experiments.

### 3.2.4 Stratification and Mixing of Gases in the Drywell

A situation for plumes in the SP arises regarding hot or cold and/or steam or noncondensible gas plumes in the DW. The geometry of the DW is relatively complex and the plumes can interact with structures, walls, etc. Releases from breaks in the primary system will create hot plumes or jets of steam; vacuum breaker openings will introduce plumes or jets of gases from the SC into the DW. Differences in the temperatures of vertical surfaces in the DW can produce rising hot and descending cold wall plumes; free plumes can be created by evaporation from the surface of pools of water. In relatively simple geometries, the correct scaling of such phenomena will be possible as long as either (1) the situation can be characterized by identical plumes or segments of linear plumes formed from nozzles or jets, both in the prototype and the models, or (2) the plumes and jets from the prototype and the model both produce a well mixed volume, even though the details of the flow structures differ.

The vacuum breakers can be visualized as horizontal disks, having a diameter of the order of 0.5 m, lifting under the pressure difference between the SC and the DW. Flow through the vacuum breaker openings is discharged through openings on four arms of the vacuum breaker housing. The flow is discharged vertically downwards towards the diaphragm floor, where it impinges and is forced outwards as a horizontal plume — spreading radially towards the containment outer wall and the annulus.

[†] The PCC vents will be terminated by quenchers.

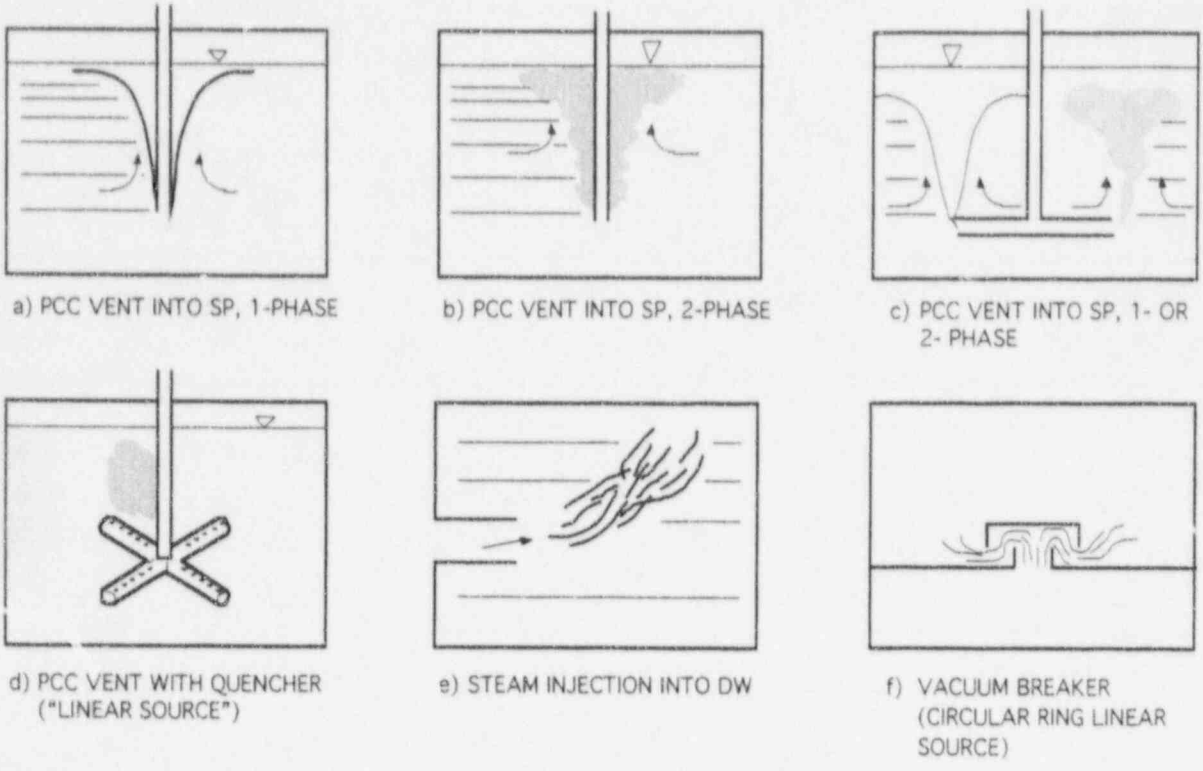


Figure 3.2-1. Thermal Plumes and Jets, and Associated Mixing and Stratification Phenomena in the SBWR. Cases a, b and f are wall plumes; Cases c to e are free plumes. (Not drawn to scale.)

### 3.3 Heat and Mass Transfers at Liquid-Gas Interfaces

Heat and mass transfers at liquid-gas interfaces (such as the surface of pools and of liquid films draining along the walls) depend on the interfacial surface area and on the variables driving the exchanges; namely, the state of the fluids at the interface and the hydrodynamic condition (i.e., the fluid velocities) near the interface.

The scaling of the **horizontal interfacial surface areas** was considered in Section 2.4.2. The horizontal interfacial areas (e.g., pool surfaces) can be made to correctly scale with the system scale: $(A_{LG})_R = R$. The fluids used in the experiments and their thermodynamic states are prototypical. Thus, regarding mass transfers at horizontal interfacial areas, the only remaining scaling issue is the effect of the hydrodynamic conditions (i.e., essentially of the fluid velocities near the interfaces). This question is examined in Section 3.3.1.

The **vertical interfacial areas** for the PCC and IC heat exchangers are scaled 1:1. The situation is different for interfacial areas such as liquid films on vertical surfaces other than the heat exchangers. Phenomena taking place on these vertical surfaces can be accurately estimated (Section 3.4) to make sure that the vertical-interface phenomena taking place in the SBWR and its models are of similar orders of magnitude in relation to the heat and mass transfer phenomena which dominate *overall* system behavior. The data obtained from the scaled experiments can then be used to qualify the system code.

#### 3.3.1 Interfacial Transfers at Horizontal Surfaces

The state of the fluids in the models being essentially prototypical, the temperature and concentration differences driving the interfacial exchanges should be very similar in the prototype and the models. The remaining question raised here is the effect of the flow conditions in the proximity of the interface on the heat and mass exchange *coefficients*.

### 3.4 Heat Capacity of Containment Structures and Heat Losses

The walls and structures of the SBWR containment are complex composite structures with very large **heat capacity**. The massive reactor pressure vessel (RPV) is an additional source of stored heat. These structures cannot be easily simulated in scaled experimental facilities typically made of relatively thin-wall vessels, and no such attempt was made. It should be noted, however, that the importance of both heat release from the RPV and of heat "soaking" into the containment structures decreases with time (as the structures come into temperature equilibrium with their surroundings and exchange less heat). Thus, for the long-term behavior of the experimental facilities considered here, heat exchanges with the RPV and the containment structures do not constitute the dominant heat sink.

The **heat losses** from the systems considered are a directly related issue. Because of its much smaller surface area-to-volume ratio, heat losses from the SBWR are relatively much smaller than from the experimental facilities. It is important to accurately measure the heat losses in the experimental facilities for application of the test data to computer code qualification.

The concerns regarding any influence (on the overall behavior of the system) of heat storage and release from the RPV and containment structures and/or of heat losses from the experimental facilities are of significance only if such influences distort system behavior and lead to states of the system in the experiments which differ significantly from the expected behavior of the prototype.

Note that the heat capacity of both the SBWR containment and of the corresponding parts of the experimental facilities, and the effects of transient heat conduction in the various structures and/or losses from the system, can be considered in computer calculations with a system code. Since conduction calculations are very well understood and can be performed with the necessary degree of spatial detail, and the thermal resistance in the test facilities is dominated by insulation with known properties, no significant uncertainty is expected in such calculations.

*In conclusion, the structure heat storage and heat loss issues for the experimental facilities can be addressed adequately via data reduction and by the system codes* for both the SBWR and the experimental facilities.

### 3.5 Scaling of the Vents

The main (LOCA) vents will operate during the blowdown phase of the accidents considered; this phase is investigated in the GIST and GIRAFFE/SIT tests. The dynamics of **main vent clearing** is not an issue for these tests, since vent flow is well established by the time the RPV pressure falls below the initial pressure of these tests. The main vents are not normally expected to open during the long-term containment cooling phase.

The PCCS vents will inject mixtures of steam and noncondensibles into the SP starting with the blowdown phase and continuing thereafter.

The important phenomena that must be considered to understand the operation and consequently to properly scale the vents are:

- Flow regime and formation of bubbles at the vent.
- Creation of single- or two-phase plumes from the vents.
- Entrainment and mixing of fluid from the pool into the rising plume.
- Residence time of the two-phase plumes in the pool.
- Condensation rate of bubbles or jets containing noncondensibles.

The second and third items were already considered in Section 3.2. The remaining points related to the creation and behavior of two-phase plumes from vents are discussed in Section 3.5.2.

#### 3.5.1 Number of Vents, Flow Area and Vent Hydraulic Diameter

The scaling of the number of vents and vent dimensions (up to the location of submergence in the SC pool) is covered by the general scaling criteria for the piping (Section 2.4.4). The geometrical configuration of the vents and their dimensions at the submergence point can clearly play an important role.

#### 3.5.2 Condensation of Steam and Noncondensible Mixtures Injected from Vents into the Suppression Pool

The effects of vent design and scaling on pool stratification were discussed in Sections 3.2.1 and 3.2.3. Moody [28] provides information useful for the scaling of discharges from vents.

#### 3.5.3 Vent Clearing, Chugging and Oscillations in the PCCS Vents

The dynamics of **main (LOCA)** vent clearing affect the peak containment pressure only during the early phases of blowdown. The main vents are not expected to open during the post-LOCA period, as already noted in Section 3.5 above. During the long-term decay heat removal period, any uncovery of the main vents will be driven by relatively *slow* increases in DW pressure and will be properly scaled by the correct submergence depths of the main vents.

The condensation of steam and noncondensible mixtures injected from the *PCCS vents* into the SP may lead to cyclic condensation phenomena. The scaling of vent geometry and dimensions and their effects on such phenomena were discussed in Section 3.5.1. Proper scaling should be guaranteed if the vents in the experiments are a segment of the actual ("line source") vents used in the SBWR.

### 3.6 Heat and Mass Transfer in the ICS and PCCS Condensers

#### 3.6.1 Overall Heat Transfer in PCC and IC Systems

The PCC and IC heat removal capability is determined by a combination of thermal resistances from convection/condensation on the inner tube surface, conduction through the wall and boiling/convection on the tube outer surface. The overall heat transfer through the PCC is governed by

$$\dot{Q}_{pcc} = N_{tubes}\ N_{units}\ \frac{A_i}{R}\left(T_{pcc} - T_{pool}\right)$$

where

$$R = R_{inner} + R_{wall} + R_{outer}$$

and

$$R_{inner} = \frac{1}{h_{inner}}$$

$$R_{wall} = \frac{D_i\ \ln\left(D_o / D_i\right)}{2k_{wall}}$$

$$R_{outer} = \frac{1}{h_{outer}} \bullet \frac{A_i}{A_{outer}}$$

#### 3.6.2 Condensation Inside the Tubes

The IC/PCC primary heat transfer is governed by a function of the film Reynolds number, $Re_f$, free stream Reynolds number, the local mass fractions, y, and the local steam quality, x.

The detailed database for low-pressure condensation heat transfer in the presence of noncondensibles inside the PCC (or the IC) tubes is provided by the MIT and UCB single-tube data. These data were used to develop the condensation heat transfer model used in TRACG [47]. The GIRAFFE, PANTHERS, and PANDA data provide mostly integral verification of the adequacy of this database. The GIRAFFE data were used to qualify the TRACG model [3]. A limited number of local tube heat flux measurements are also foreseen for the PANTHERS tests.

#### 3.6.3 Heat Transfer on the Secondary Side

The secondary side heat transfer is possibly influenced by the local void fraction and circulation in the pool. When the pool is at saturation (which will primarily be the case for SBWR conditions), the pool heat transfer is not influenced by circulation. Therefore, the local void fraction is of primary consideration in scaling.

Natural circulation within the IC pool is tested at full scale in the PANTHERS facility, which has a prototypical pool size. In the smaller-scale facilities (GIRAFFE and PANDA), natural circulation in the pool can only be approximated. Comparisons of single-tube (UCB and MIT), GIRAFFE, PANDA, and PANTHERS data will provide information regarding the importance of the natural circulation and bundle flow pattern effects.

### 3.7 Analysis of Oscillations Between Large Liquid Pools

In the SBWR, there may be situations where water drains from one pool to another via connecting drain line pipes. For example, this situation occurs when water contained in the GDCS pool drains into the RPV via one or more GDCS drain line pipes if such emergency core cooling should be required under accident conditions. The other situation may occur if the water level in the RPV drops so low following an accident that makeup water is required to drain from the Suppression Pool (SP) via one or more equalization lines.

Concerns have been expressed that large water level oscillations may occur in these situations when a disturbance occurs, for example, in the form of a pressure change above one of the water masses. The pressure change may be in the form of a step change in the pressure which could result in free, undamped oscillations in the system water levels before new, equilibrium water levels are reached. Another situation that might arise is that of a periodically varying pressure above one of the water masses with an imposed frequency close to that of the system natural frequency. Such a pressure function may excite the system such that resonance and a large magnification of the imposed pressure function may occur.

A dynamic model for these systems was developed to evaluate their fundamental characteristics. The equation of motion for the fluid systems was based on models developed for a uniform cross-section U-tube modified as required to account for wall friction and the unequal flow areas of the SBWR "U-tube" configurations. In these configurations, two large water masses, namely the RPV and GDCS or SP water masses, are coupled or connected via drain lines having much smaller cross-sectional areas than that of the RPV and the SP surface areas as indicated in Figure 3.7-1 for the RPV/GDCS pool system. The equation of motion developed was solved for two imposed pressure variations, namely: (1) a step change in the RPV pressure, and (2) an harmonic varying (sinusoidal) pressure in the RPV having an imposed period of 500s.

The equation of motion for the system depicted schematically in Figure 3.7-1 cast in a form similar to that of classical vibration theory is,

$$m\ddot{h} + c\dot{h} + kh = f(t) \tag{3.7-1}$$

Two different forcing functions f(t) were considered. In the first, a step change in RPV pressure occurring at time zero was used as described in the derivation of the equation of motion. In equation form, this forcing function is written as

$$f(t) = (P_r - P_p)\, NA' \tag{3.7-2a}$$

The second forcing function considered was a sinusoidal or harmonic function with an amplitude equal to that of the step change function above. In equation form, this is written as

$$f(t) = (P_r - P_p)\, NA' \sin \omega t \tag{3.7-2b}$$

where $\omega$ is the forcing function angular frequency in rad/s.

The solution for the step change forcing function was obtained by assuming that the damping coefficient was a constant evaluated using the average fluid velocity obtained in the drain pipe during a transient. For the displacement and velocity in the drain line, the solutions are

$$h = C_1 e^{s_1 t} + C_2 e^{s_2 t} + (P_r - P_p) NA'/k \tag{3.7-3a}$$

and for the drain line velocity,

$$\dot{h} = s_1 C_1 e^{s_1 t} + s_2 C_2 e^{s_2 t} \tag{3.7-3b}$$

where

$$C_1 = \frac{A'}{\rho g N A} (P_r - P_p) \Big/ \left( \frac{s_1}{s_2} - 1 \right) \tag{3.7-3c}$$

$$C_2 = -\frac{s_1}{s_2} C_1$$

The general behavior of the fluid displacement, when subjected to a step change, is seen to be a slow movement towards a steady-state displacement as the exponential terms approach zero at long times. There are no level oscillations in this system as long as it is overdamped.

The complete solution with the sinusoidal forcing function and overdamped system is

$$h = C_1 e^{s_1 t} + C_2 e^{s_2 t} + (P_r - P_p) NA' \sin(\omega t - \varphi) \Big/ \sqrt{(k - m\omega^2)^2 + (c\omega)^2} \tag{3.7-4a}$$

or

$$h = C_1 e^{s_2 t} + C_2 e^{s_2 t} + B \sin(\omega t - \varphi)$$

where

$$B = (P_r - P_p) NA' \Big/ \sqrt{(k - m\omega^2)^2 + (c\omega)^2} \tag{3.7-4b}$$

The corresponding velocity is

$$\dot{h} = s_1 C_1 e^{s_1 t} + s_2 C_2 e^{s_2 t} + \omega B \cos(\omega t - \varphi) \tag{3.7-4c}$$

The constants $C_1$ and $C_2$ become, when applying the zero displacement and zero velocity boundary conditions

$$C_1 = \frac{s_2 B}{s_1 - s_2}\sin(-\varphi) - \frac{\omega B}{s_1 - s_2}\cos(-\varphi) \tag{3.7-5a}$$

and

$$C_2 = -\frac{s_2 B}{s_1 - s_2}\sin(-\varphi) + \frac{\omega B}{s_1 - s_2}\cos(-\varphi) - B\sin(-\varphi) \tag{3.7-5b}$$

The exponential terms in this solution also approach zero at long times and the quasi steady-state level movement is dominated by the imposed forcing function. A summary of the results is given in Section 4.7 and more detailed results are given in Appendix C.

The equation of motion (Equation 3.7-1) was nondimensionalized using the natural cycle time and the steady-state step change displacement as normalizing parameters. The nondimensional form of the equation of motion is

$$\frac{1}{4\pi^2}\ddot{h}^+ + \Pi_D \dot{h}^+ + h^+ = 1 \tag{3.7-6}$$

where

$$\Pi_D = c/c_c\pi \tag{3.7-7a}$$

with

$$c = 8N\mu A'L/R^2 + NF\rho A'|v_a|/2 \tag{3.7-7b}$$

$$c_c = 2\sqrt{km} \tag{3.7-7c}$$

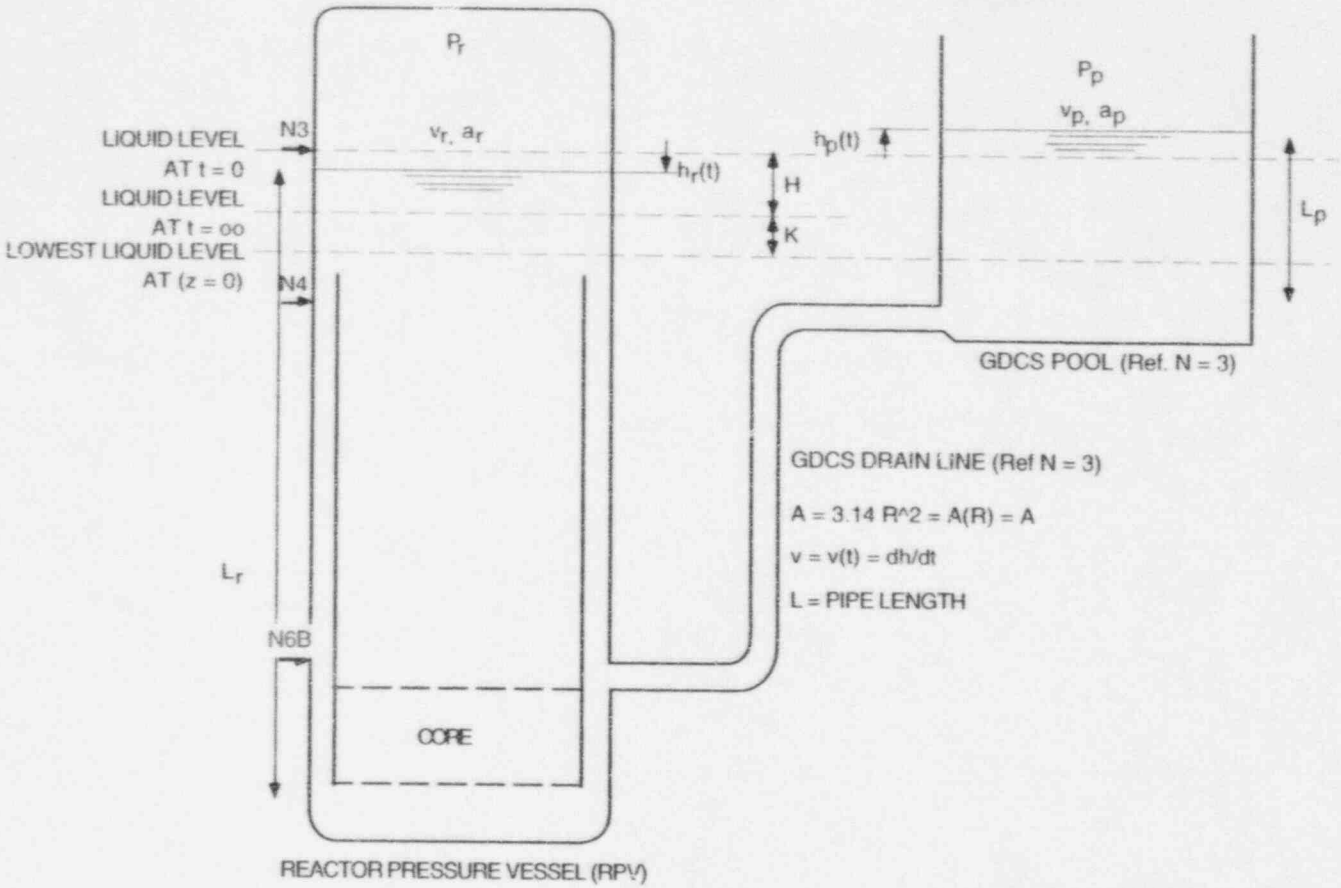


Figure 3.7-1. RPV/GDCS Pool Configuration Modeled

### 3.8 Regional Void Distribution in RPV

The regional void distribution is of importance inside the RPV, particularly in the blowdown period.

The vapor continuity equation can be written in cross-sectional area averaged form as [57]:

$$\frac{\partial\langle\alpha\rangle}{\partial t}+\frac{\partial}{\partial z}\left(\langle\alpha\rangle\left(C_o j+\overline{V}_{gj}\right)\right)=\frac{\langle\Gamma_g\rangle}{\rho_g} \tag{3.8-1}$$

where $C_o$ and $\overline{V}_{gj}$ are the conventional drift flux parameters. When the vapor transport time for the region is small compared to the depressurization time constant, the quasi-static form of Equation 3.8-1 can be used for the spatial void distribution:

$$\frac{d}{dz}\left(\langle\alpha\rangle\left(C_o j+\overline{V}_{gj}\right)\right)=\frac{\langle\Gamma_g\rangle}{\rho_g} \tag{3.8-2}$$

Integrating Equation 3.8-2,

$$\langle\alpha\rangle\left(C_o j+\overline{V}_{g_i}\right)=\int\frac{\langle\Gamma_g\rangle}{\rho_g}dz=\frac{\langle\Gamma_g\rangle z}{\rho_g} \tag{3.8-3}$$

$$\langle\alpha\rangle=\frac{\dfrac{\langle\Gamma_g\rangle z}{\rho_g}}{C_o j+\overline{V}_{g_i}} \tag{3.8-4}$$

Also, integrating the mixture continuity equation,

$$j=V_i+\frac{\Delta\rho}{\rho_f}\int_o^z\frac{\langle\Gamma_g\rangle}{\rho_g}dz=V_i+\frac{\Delta\rho}{\rho_f}\frac{\langle\Gamma_g\rangle}{\rho_g}z \tag{3.8-5}$$

where $V_i$ is the inlet velocity.

Then

$$\langle \alpha \rangle = \frac{\frac{\langle \Gamma_g \rangle Z}{\rho_g}}{C_o \frac{\Delta\rho \langle \Gamma_g \rangle Z}{\rho_f \rho_g} + C_o V_i + \overline{V}_{g_j}} \tag{3.8-6}$$

Thus, in order to match the axial void fraction distribution, we must match: $C_o$, the void distribution parameter; $\overline{V}_{gj}$, the average drift velocity; $V_i$, the fluid inlet velocity; and $\Gamma g$, the vapor generation rate.

# 4.0 Scaling Analysis Results

## Introduction and Background

This section contains the results of the scaling analysis. It is organized into five subsections that consider the SBWR and each of the five major test series used for TRACG qualification; namely, GIST, GIRAFFE/SIT, GIRAFFE/He, PANDA, and PANTHERS. In Subsection 4.1, parameters and phenomena that are important to the SBWR behavior are identified. The tables containing numerical results are located at the end of Subsection 4.1. In Subsections 4.2 through 4.5, the scaling parameters of the test facilities are compared to the SBWR to determine the ability of the facility to meet its objectives. The PANTHERS test scaling results are discussed in Subsection 4.6, while a summary of a study of level oscillation between large connected pools is given in Subsection 4.7.

System tests (such as GIST, GIRAFFE and PANDA tests) are designed to provide data covering all essential phenomena and system behavior under a range of conditions for the purpose of qualifying a system code (in this case, the TRACG Code used for analyses of systems by GE).

To obtain data in the proper range of system conditions, the relative importance of the phenomena and processes present in the tests should not differ significantly from that in the SBWR. Similarly, the overall behavior of the test facility should not diverge significantly from that of the SBWR; in particular, no bifurcations should exist in the system behavior that derive different intermediate or end states. Finally, the test should provide sufficiently detailed information, obtained under well-controlled conditions, to provide an adequate and sufficient database for qualifying a systems analysis code such as TRACG.

Apart from this qualitative discussion of how "prototypic" the scaling of the test facilities must be, it is difficult to specify a quantitative rule for determining acceptable deviations. Deviations in some parameters are more important than others and bifurcations do not occur at a specific level of distortion. Because of this, each parameter must be evaluated on an individual basis using engineering judgment to determine the acceptability of the scaling.

## 4.1 Important Phenomena in the SBWR

The nondimensional Π groups from the momentum, mass, energy, and state equations developed for the SBWR configuration are discussed in this section. The nondimensional Π groups indicate the relative importance of different phenomena to the behavior of the SBWR. The Π groups are evaluated at different times during a LOCA event. The values reported are typically the maximum values expected for a given parameter. This indicates the maximum effect that a parameter can have. It is then possible to infer that the value can range from some lower value — usually zero — up to this maximum value. The unique reference values used in the scaling analysis are selected in accordance with the guiding principles identified in Section A.3.1 of Appendix A.

Figure 4.1-1 shows a schematic of the progression of some key variables during an SBWR LOCA transient. Four points in time are of particular interest, as indicated in the figure. These points represent the three main transient phases identified for a LOCA, as well as transitions between these phases. The first point represents the Blowdown Phase and is the starting point for the GIST and GIRAFFE/SIT tests. The second point represents the time at which the reactor has depressurized to the point that flow begins from the GDCS. This point is of interest to evaluate parameters that may affect the initiation of GDCS flow. The depressurization then continues until the RPV and DW are at virtually the same pressure and the GDCS is at full flow. The third point characterizes most of the GDCS Phase. The fourth point represents the period when the PCCS is in steady operation. The results of the nondimensional analysis for each period of time are discussed below.

Global momentum scaling numerical values have been calculated for the LOCA phases referred to as the Blowdown Phase, GDCS Phase, and PCCS Phase. The global momentum scaling results are based on the formulation for the momentum balance equations described in Appendix A, as summarized in Section 2. The pressure and vapor mass scaling results are based on the formulations described in Appendix B, as summarized in Section 2. The numerical input parameter data and initial conditions for the test facilities were obtained largely from the TAPD report [59].

### 4.1.1 Blowdown Phase

#### 4.1.1.1 Initial Parameters

#### 4.1.1.2 Prototype Reference Parameters

#### 4.1.1.3 Prototype Global Momentum Results (at 1.03 MPa)

The nondimensional groups, the matrices for inertial and flow resistance and the pressure drop number matrix for the prototype, are discussed individually first. Then, the overall results are summarized by multiplying the groups with the elements appearing in each line (row) of the matrix.

#### 4.1.5.2 Scaling for Pressure and Energy

#### 4.1.5.3 Time Scales

There are many time scales in the SBWR system. Some are much more important than others and the importance of a time scale can change from phase to phase. The selection of the dominant or reference time scale is determined by the phenomena of most interest. An important point to keep in mind when selecting a time scale for a particular process is to select the reference time scale such that the derivative with respect to time of a quantity such as a flow rate, a pressure rate or a vapor mass fraction render the corresponding nondimensional time derivatives of order one, or O(1). Only with such a choice for the reference time scale will the nondimensional group multiplying a derivative have any direct meaning.

##### 4.1.5.3.1 Numerical Values of Time Scales

**Blowdown Phase**

**GDCS Phase**

**PCCS Phase**

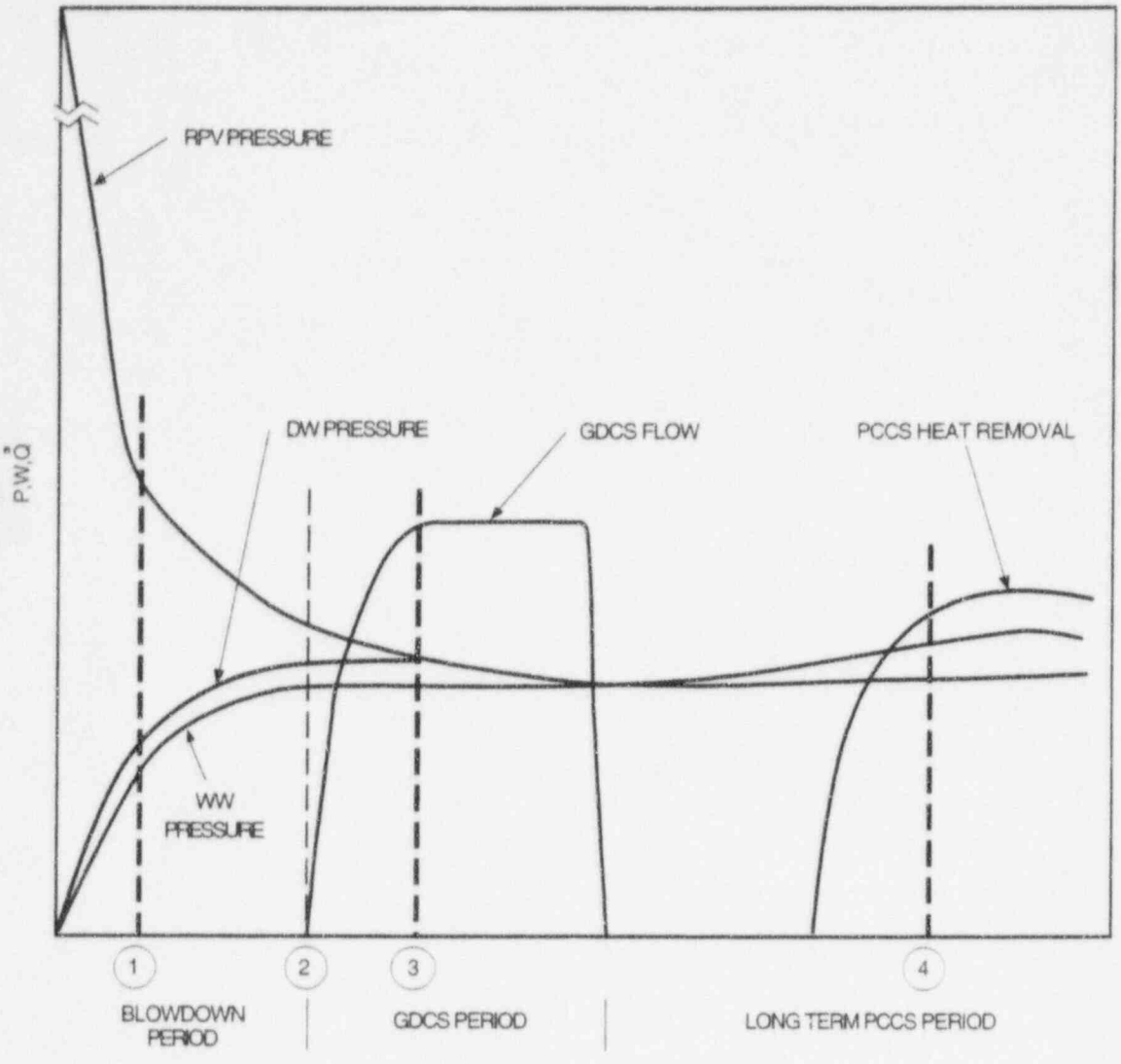


Figure 4.1-1. Key SBWR Characteristic Values During Transient Phases

## 4.2 GIST Tests

The Gravity-Driven Integrated Systems Test (GIST) was performed by GE Nuclear Energy in San Jose, California, in 1988 [27]. The GIST facility was a section-scaled simulation of the 1987 SBWR design configuration, with a 1:1 vertical scale and a 1:508 horizontal area scale of the RPV and containment volumes. Because of the 1:1 vertical scaling, the tests provided real-time response of the expected SBWR pressures and temperatures.

### 4.2.1 Facility Description

The GIST facility was built at the GE Nuclear Energy site in San Jose, California. Significant plant features which could affect the performance of the GDCS were included ([3], [30]). Since the containment pressure and the GDCS pool water level determine GDCS activation, the containment (both upper and lower DW and SC volumes) was modeled. The facility is schematically shown in Figure 4.2-1. Subsystem horizontal areas are also scaled according to the system scale of 1:508, except for the drain flow lines, as discussed in Section 4.2.3.1. Decay heat was modeled in proportion to the 1:508 system scale to provide the correct depletion of water from the RPV by boiling [5].

The scaling of the tests produced data at real time and at prototypical pressures and temperatures. Detailed descriptions of the design and operation of GIST can be found in a report by Mross [30].

The test objectives and a listing of the test conditions for the 24 tests performed can be found in the TAPD [55].

GIST has cylindrical vessels interconnected by piping simulating the various volumes of the SBWR: (1) RPV; (2) upper DW; (3) lower DW; and (4) elevated SC (filling also the role of GDCS pool). The piping includes simulation of the Automatic Depressurization System (ADS), the GDCS lines, and the conditions at the break location for all break types considered [5].

During the GIST tests, the system was first depressurized by venting to the atmosphere from its initial pressure of 1.07 MPa to 0.79 MPa. This period of the tests was thus used to create representative initial conditions in the RPV, as it entered the later stages of the depressurization transient (Figure 4.2-2). The initial conditions of importance are the decay heat generation rate and representative water levels, as well as void fraction distributions in the RPV. When the RPV reached the pressure level of 0.79 MPa, the blowdown flow rate was switched from the atmosphere to the DW for the break flow line, and to the SC for the ADS lines. Care was provided to obtain a smooth transition by not introducing changes in the blowdown flow areas.

With further depressurization of the RPV, the low pressure DPVs open. Eventually, the head of water in the SP becomes sufficient to overcome the RPV pressure and open the GDCS check valves allowing GDCS flow to enter and reflood the vessel.

### 4.2.2 General Scaling Approach

The design of the experimental facility is in agreement with the general top-down scaling criteria derived in Section 2. The feasibility of the GDCS would be demonstrated if it delivered sufficient core flooding flow during various LOCAs. The overall "global" system effects of pressure and RPV water inventory history during the LOCA had clearly to be modeled in a top-down fashion to include representative coupling effects of the GDCS flow with the RPV inventory. The GIST tests provided representative data that were used to qualify the TRACG Code [3]. The particular phenomena not scaled in detail are not expected to produce bifurcations in system behavior

invalidating the representativeness of the tests, or bringing the experimental apparatus outside the range of conditions expected in the SBWR; furthermore, the differences are captured adequately in code calculations [5].

As noted earlier, LOCA blowdown pressure history was simulated from a RPV pressure of 0.79 MPa, since the GDCS begins to function at lower pressure. The pressure-time characteristics were controlled by adjusting the flow area in the blowdown pipe for the various accident scenarios simulated.

### 4.2.3 Specific Scaling Issues for the GIST Tests

#### 4.2.3.1 Exact Scaling of the SBWR Geometry

#### 4.2.3.2 Establishment of Representative Initial Conditions

The initial test conditions for the GIST tests were determined from TRACG simulations of the early blowdown behavior of the SBWR from 7 MPa to 1.03 MPa. For the tests, the system was first depressurized to the atmosphere from this initial pressure of 1.03 MPa to 0.79 MPa. Thus, this period of the tests was used to create the representative initial conditions in the RPV as it entered the later stages of the depressurization transient (Figure 4.2-2). The pressure dropped from 1.03 to 0.79 MPa in 30 to 50 seconds [5]; this provided sufficient time for representative conditions in the RPV to develop.

The vessels representing the containment were pressurized and preheated to the TRACG calculated pressures and temperatures. The DW was purged of air with steam to simulate the effect of air carryover into the SC.

Initial pool water temperatures in the GIST tests were controlled by heating prior to system blowdown. The initial temperatures ranged from 42 to 69°C, which embraces possible initial conditions in the SBWR.

The GDCS check valves, which open only when the pressure differences across them reaches zero, were not required to provide exact opening time characteristics, because the actual opening time is rapid relative to the vessel filling time.

The heat release from the RPV metal in SBWR could not be simulated in the GIST tests; the heat stored initially in the RPV wall and its rate of release could not be scaled properly. Thus, voids could not be maintained in the lower plenum and the water level in the core dropped; this was compensated by increasing the initial RPV water level in the tests. This distortion can be considered in TRACG calculations which can simulate the situation in the tests and in the SBWR.

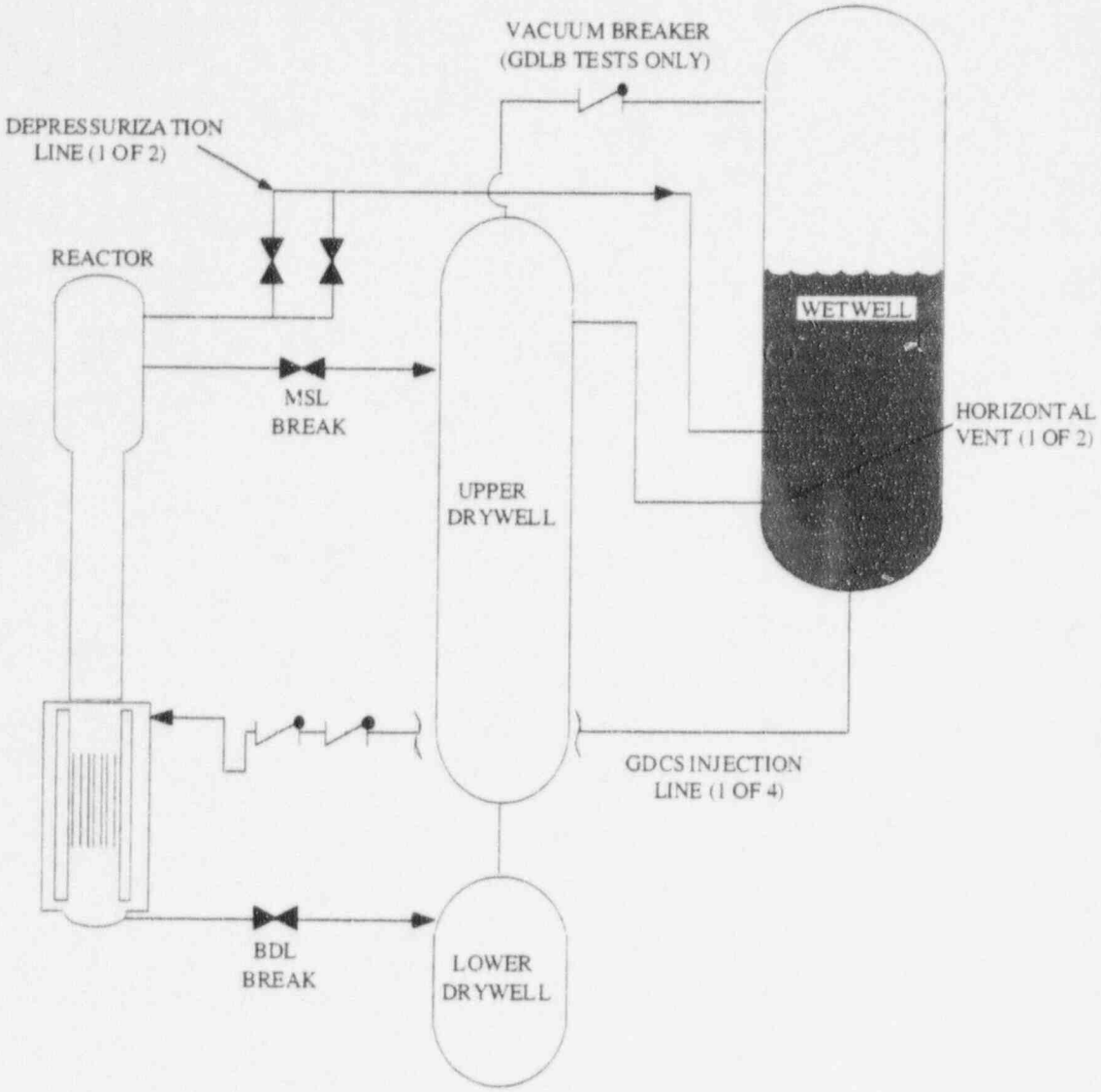


Figure 4.2-1. Main Components of the GIST Facility

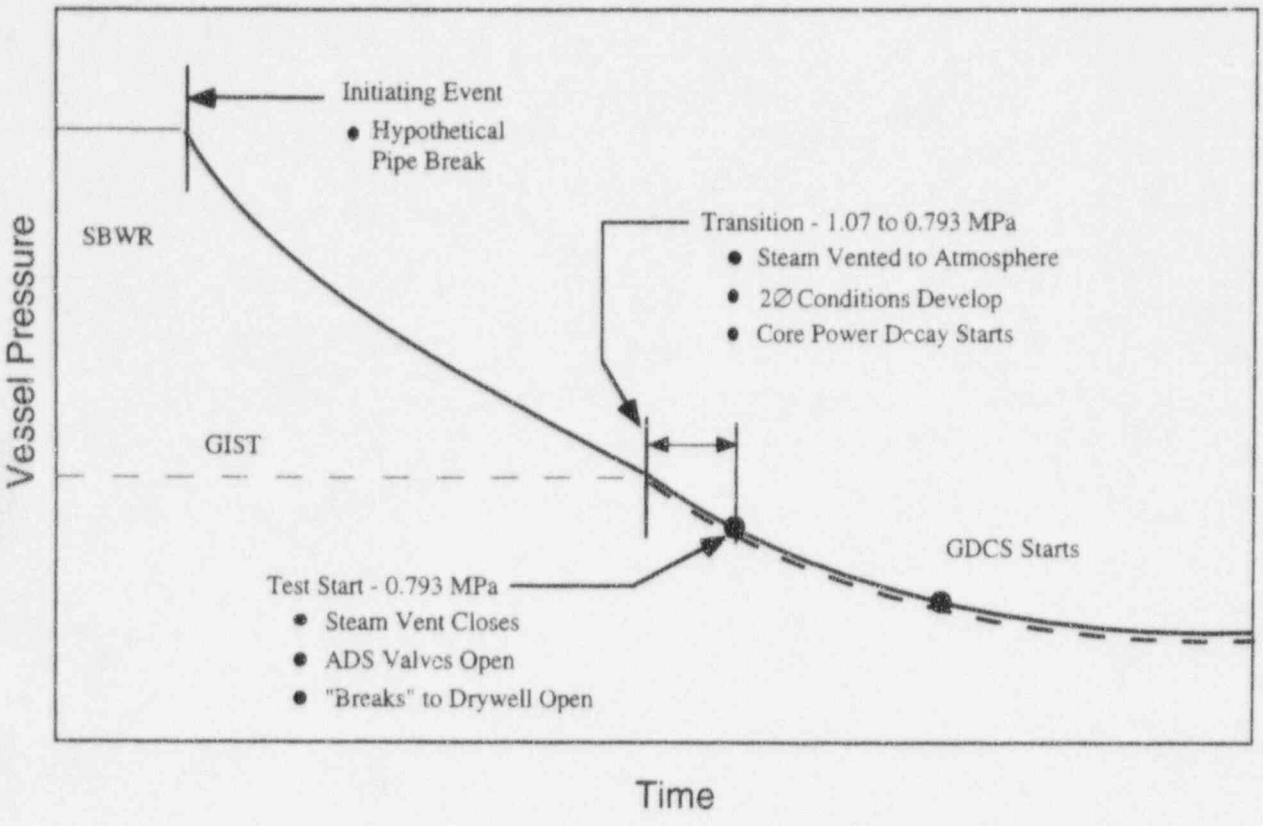


Figure 4.2-2. Vessel Pressure Coastdown During the SBWR and the GIST Depressurization Transients

## 4.3 GIRAFFE/SIT Tests

The GIRAFFE test facility ([20], [31], [51]) is a full-height, reduced volume, integral system test facility, built by Toshiba at its Kawasaki City, Japan site. Test data will be obtained for TRACG qualification during the late Blowdown/early GDCS Phase for liquid line breaks.

### 4.3.1 Facility Description

The facility consists of five major components representing the SBWR primary containment and IC pools, the PCCS and ICS condenser, and the connecting piping. Separate vessels represent the RPV, the DW, SC, GDCS pools, and ICS pools, which house the ICS and PCCS condensers. The facility scales the SBWR at a volumetric scale of 1:400. The heights and vent submergences are scaled 1:1. Pressure and temperature levels and pressure drops are preserved.

#### 4.3.1.1 GIRAFFE/SIT

A detailed description of the facility can be found in TAPD Rev. C and in the GIRAFFE System Interactions Test Specification. To comply with top-down scaling criteria, the GIRAFFE facility has been constructed on a 1:1 height scale to the SBWR design, and all essential elevation differences between the various vessels and between corresponding SBWR components have been preserved [51]. The system scale for volumes, power, horizontal areas, and mass flow rates is approximately 1:400. The RPV heater simulates decay heat following a scram.

The RPV is simulated in full height from the bottom of the core up to the MSL exit, with the RPV-to-PCC and RPV-to-GDCS pool elevation differences conserved. The volumes below and above this full-height-simulation region have been shortened, but their volumes have been included in the volume of the RPV.

The DW is also nearly full-height, with only the upper- and lower-most regions shortened. The volumes and areas are scaled down 1:400, and the cross-sectional area variation with height is preserved, so that the DW water level transient is similar to that expected in the SBWR under LOCA conditions. Although the annular shape of the SBWR DW could not be accommodated in GIRAFFE, the facility includes compartments that can be associated with the various regions of the SBWR drywell. The lower drywell volume, which represents on a 1:400 system scale the corresponding SBWR volume, can retain noncondensible gases and/or water. There is also a connection to a steam injection line, which is used to simulate evaporation from accumulated water. The narrowest region, representing the annular DW space around the RPV in the SBWR, has a correctly-scaled cross-sectional area, thus, water level changes in the DW occur at prototypical rates in this region. A vacuum breaker line connects the upper DW to the SC gas space. Connections to the main steam line, main LOCA vent line, GDCS air space, DPV line, and PCC steam supply line correspond to those in the SBWR.

The full height of the SC has been preserved, while the gas and water volumes have been again scaled down 1:400. The LOCA vent line is at its actual SBWR elevation. The vertical section of the main LOCA vent is a close-ended pipe extending from the upper DW almost to the SC floor; each of the three holes in the pipe wall representing the main vents has the proper size and elevation. Three alternative PCC vents, each with a different submergence depth, were installed in the SP to allow the study of submergence effects. These vents are vertical pipes with open ends, installed near the vessel wall.

The GDCS pool has exactly scaled height and volume.

The GIRAFFE condenser is a scaled representation of the three SBWR PCCS condensers; it has three tubes. The tube wall thickness is 2.5 mm, compared to the 1.65 mm wall thickness of the SBWR PCC units. The three GIRAFFE condenser tubes are spaced so as to maintain correct secondary-side cross-sectional flow area.

The IC pools house the PCC and IC units, which are placed within a chimney separating the region where the water is in contact with the PCC and IC tubes from the outer pool region; this provides for simulation of the circulation in the IC pool. The total heat transfer rate from the condenser tubes is relatively insensitive to the circulation pattern on the secondary side.

All lines are sized and orificed so as to allow for prototypical pressure drops at scaled mass flow rates; the pipes are somewhat oversized with respect to the system scale. This reduces the frictional pressure drops, and the total resistance of each line is adjusted by inserting an orifice plate representing the appropriate loss coefficient. The adequacy of this scaling was discussed in Section 2.4.3.

Since these tests will be performed in an existing test facility, many of the parameters affecting scaling are established already. The purpose of this section is to characterize the distortions that may occur as a result of the fixed parameters, and to determine how to best scale the remaining parameters to provide the best fidelity with the SBWR design. The facility heights, volumes, general piping configuration, and heat loss characteristics are set by the existing facility. The initial and boundary conditions, together with the piping orifices, will be adjusted to provide the best fidelity possible with this facility.

### 4.3.2 Particular Phenomena of Relevance to the GIRAFFE/SIT Tests

The parameters of primary interest for the GIRAFFE/SIT tests are associated with the RPV blowdown, water level and any possible systems interactions related to these phenomena. Systems of primary interest for this purpose are the IC, GDCS and Depressurization systems.

### 4.3.3 Scaling of GIRAFFE Facility for Systems Interaction Tests (SIT)

GIRAFFE is scaled in agreement with the general top-down inertia derived in Section 2. Global momentum scaling numerical values for the GIRAFFE facility have been calculated for the operating phases referred to as the Blowdown Phase and the GDCS Phase. The global scaling results are based on the formulation for the momentum balance equations given in Appendix A, as summarized in Section 2. The pressure rate in vapor mass scaling numerical values were calculated for the Blowdown Phase, beginning of GDCS injection and the GDCS phase as indicated by points 1, 2 and 3 in Figure 4.1-1. The numerical input parameter data and initial conditions, etc. were obtained largely from the TAPD report [55].

#### 4.3.3.1 Blowdown Phase

##### 4.3.3.1.1 Global Momentum Results

###### 4.3.3.1.1.1 Comparison of Nondimensional Groups — Prototype vs. GIRAFFE

###### 4.3.3.1.1.2 Comparison of Inertia Matrices — Prototype vs. GIRAFFE

###### 4.3.3.1.1.3 Comparison of Resistance Matrices — Prototype vs. GIRAFFE

###### 4.3.3.1.1.4 Comparison of Pressure Drop Number Matrices — Prototype vs. GIRAFFE

#### 4.3.3.1.1.5 Overall Comparison of Terms

#### 4.3.3.1.2 Mass Continuity and Pressure Rate Scaling

#### 4.3.3.2 GDCS Phase

#### 4.3.3.2.1 Global Momentum Results

#### 4.3.3.2.1.1 Comparison of Nondimensional Groups — Prototype vs. GIRAFFE, VB Closed

#### 4.3.3.2.1.2 Comparison of Nondimensional Groups — Prototype vs. GIRAFFE, VB Open

#### 4.3.3.2.1.3 Comparison of Inertia Matrices — Prototype vs. GIRAFFE, VB Closed

#### 4.3.3.2.1.4 Comparison of Resistance Matrices — Prototype vs. GIRAFFE, VB Closed

#### 4.3.3.2.2 Mass Continuity and Pressure Rate Scaling

### 4.3.4 Summary of Results for GIRAFFE/SIT

From previous discussions, it is concluded that based on top-down scaling, GIRAFFE will provide a good simulation of vessel depressurization, GDCS flow initiation time, and GDCS flow rate for TRACG qualification. It will also provide proof-of-concept for GDCS ECCS injection and interactions between the SC, PCC and GDCS systems.

The GIRAFFE/SIT tests cover the period of late blowdown through the GDCS Phase to the PCC initiation in a postulated LOCA event. The facility was scaled well to provide integrated system data for code qualification in the areas of GDCS initiation time and GDCS flow rate, RPV water level and system interactions between the PCCS, ICS and GDCS.

## 4.4 GIRAFFE/He Tests

The GIRAFFE/Helium tests are being performed by the Toshiba Corporation at their Nuclear Engineering Laboratory in Kawasaki City, Japan. The purpose of these tests is to demonstrate the operation of the Passive Containment Cooling System (PCCS) in post-accident containment environments with the presence of a lighter-than-steam noncondensible gas as well as a heavier-than-steam noncondensible gas. These tests will demonstrate SBWR containment thermal-hydraulic performance, heat removal capability, and systems interactions. Also, they will provide additional data for the qualification of containment response predictions in the presence of lighter-than-steam noncondensible gases by the TRACG computer program.

### 4.4.1 GIRAFFE/He Facility Description

The facility configuration is described in Reference [55]. The primary facility changes from the earlier Phase 2 configuration include shortening the PCC tube length (to 1.8 meters) and modifying the piping orifices to yield flow resistances which more closely model the current SBWR values. Additionally, provision has been made for the continuous addition of helium to the drywell during a test. Details are provided in the GIRAFFE/Helium Test Specification.

### 4.4.2 Specific Scaling Issues for the GIRAFFE/He Tests

#### 4.4.2.1 Specific Differences in the GIRAFFE/He Tests

### 4.4.3 Scaling Results for the GIRAFFE/He Tests

#### 4.4.3.1 PCCS Phase

##### 4.4.3.1.1 Global Momentum Results

###### 4.4.3.1.1.1 Comparison of Nondimensional Groups — Prototype vs. GIRAFFE, VB Closed

###### 4.4.3.1.1.2 Comparison of Inertia Matrices — Prototype vs. GIRAFFE, VB Closed

###### 4.4.3.1.1.3 Comparison of Resistance Matrices — Prototype vs. GIRAFFE, VB Closed

##### 4.4.3.1.2 Mass Continuity and Pressure Rate

##### 4.4.3.1.3 Bottom-Up Scaling

### 4.4.4 Summary of Results for GIRAFFE

The GIRAFFE/He test series provides data for the performance of the PCC in the presence of lighter than steam and heavier than steam noncondensibles. The overall top-down scaling of the GIRAFFE facility shows very good simulation of the SBWR facility. The global momentum scaling indicates that all of the important parameters are scaled very well to the SBWR values. The continuity and pressure rate scaling indicates some distortions due to several differences between the GIRAFFE facility and SBWR design. The impact of these distortions was found to be acceptable from both top-down and bottom-up evaluations. The range of nondimensional parameters in the GIRAFFE tests is sufficient to provide an adequate range of data for TRACG qualification in this area.

### 4.5 PANDA Tests

The PANDA test facility is used to conduct integral system tests, as part of the ALPHA program at the Paul Scherrer Institute (PSI) in Switzerland. It demonstrates PCCS performance on a larger scale than GIRAFFE. The facility has a full 1:1 vertical scale, and 1:25 "system" scale (volume, power, etc.). It is primarily intended to examine system response during the long-term containment cooling period. Detailed discussions of the PANDA test objectives and facility description and test matrix are contained in Appendix A of Reference 55.

#### 4.5.1 Facility Design

Early during the conceptual design phase of the facility, it was recognized that it is neither possible nor desirable to preserve exact geometrical similarity between the SBWR containment volumes and the experimental facility. On the other hand, multidimensional containment phenomena such as mixing of gases and natural circulation between compartments may depend on the particular geometry of the containment building. The general philosophy followed in designing the experimental facility was to allow such multidimensional effects to take place by dividing the main containment compartments in two and by providing a variety of well-controlled boundary conditions (e.g., imbalances) during the experiments, so that the various phenomena could be studied under well-established conditions, and a behavior envelope of the system established. Carefully conducted parametric experiments will also provide more valuable data for code qualification, rather than attempts to simulate geometrically, but to a necessarily limited degree, the rather complex reactor system. Boundary conditions and the behavior of the interconnections between containment volumes can be controlled to study various system scenarios and alternative accident paths.

Thus, the RPV and the GDCS pools are represented each by a vessel. The DW and SC are both represented by two separate, interconnected vessels (Figure 4.5-1). The RPV contains a 1.5 MW electrical heat source. There is a total of three PCCS condensers representing the corresponding three units in the SBWR and a single ICS condenser representing two of the three SBWR units. The condensers are connected to the two DW vessels, as shown in Figure 4.5-2. The fact that there are three PCC units and only two DW volumes will allow some degree of asymmetric behavior or create flows between the two DWs, even with equal flow areas from the RPV to the two DW volumes.

The details of the system and its scaling rationale are described by Coddington et al [11]. Figure 4.5-2 shows details of the piping interconnecting the various volumes. The facility is heavily instrumented with some 560 sensors for temperature, pressure, pressure difference, level or void fraction, flow rate, gas concentration, electrical power, and conductivity (presence of phase) measurements.

#### 4.5.2 Scaling of the PANDA Facility

The scaling of the facility conforms to the top-down and bottom-up criteria developed in Sections 2 and 3 of this report. Full vertical heights and submergences are preserved to correctly represent the various gravity heads; volumes are represented at the system scale. The exceptions to these are noted below. The experiments will be conducted under reactor pressure and temperature conditions which are prototypical for the phase of the accident under consideration.

#### 4.5.2.1 Volumes

Figure 4.5-3 shows the geometrical arrangement of PANDA in comparison to the SBWR and the relative elevations of the two systems. All the SBWR heights are represented except those below the Top of Active Fuel (TAF) in the core. The top of the PANDA RPV electric heaters is placed at the TAF location; however, the heaters are about 1/2 the height of the SBWR core.

In the RPV, the liquid inventory above the Bottom of Active Fuel (BAF) is scaled according to the system scale of 1:25. The *liquid inventory below BAF in the RPV* was eliminated (Figure 4.5-3), since it remains saturated or only slightly subcooled and essentially inactive during the post-LOCA phase of the accidents considered, and is not required for the correct simulation of gravity heads. However, the *liquid volume between mid-core and BAF* is included in the scaled PANDA RPV volume by a small adjustment of the vessel diameter. The lowest SBWR line simulated in PANDA is the equalization line, which enters the RPV at one meter above TAF. Thus, eliminating and redistributing the water volume below mid-core and modifying the length of the heater elements will not significantly influence any natural circulation paths.

The PANDA RPV includes a downcomer and a riser above the heater rods which represent the reactor core. The flow areas in the downcomer, the riser, and the core are scaled according to the top-down criteria of Section 2 (areas proportional to the system scale). The PANDA riser has no vertical partitions; its diameter is close to the hydraulic diameter of one partition of the SBWR riser. There is no representation of the steam separators and dryers, because liquid entrainment and RPV to DW pressure drop are insignificant for the portion of the post-LOCA transients simulated by PANDA.

The *lower part of the water inventory in the SP* was eliminated to reduce vessel size; this water will not participate in the system thermal-hydraulic transient during the long-term cooling phase of the accidents considered. Indeed, the important phenomena will take place above the submergence depth of the PCCS vents. The PANDA PCCS vent lines are submerged in the SP with at least 2m clearance above the bottom of the SC vessel, so that the reduced depth of this vessel will not influence venting of the noncondensibles. Effects such as the convection of water to the bottom of the vessel by cold plumes running down the walls [36] are of minor importance.

The water is approximately 1.6m deep below the main vent submergence in PANDA, which is sufficient to accommodate any mixing during the accident phase simulated in this facility. The effect of deeper mixing *during blowdown* in the SBWR is simulated by proper adjustment of the test initial conditions.

The *lower part of the annular DW volume* surrounding the RPV was not included in the *height* of the PANDA DW volume, since it was felt that possible natural circulation phenomena taking place in this annular volume (heated on one side by the RPV) could not be adequately simulated. The volume of this annular space was, however, added to the PANDA DW *volume*.

The *lowest part of the SBWR DW volume* (the region below the RPV support skirt and pedestal) is not included or added to the PANDA DW volume. Indeed, the lower DW volume provides only a "repository" for noncondensible gas or water. The water inventory in the lowest part of the DW is significant only from the standpoint of producing long-term evaporation which could carry noncondensible gas to the upper DW and counteract the tendency of the noncondensibles to sink to the bottom of the DW.

The GDCS compartment volume scale (1:64) is smaller than the system scale (1:25). This volume does not play an important role in the dynamics of the system; in the transients considered, it simply provides a return path for the condensate to the RPV. The GDCS volume is sufficient for containing the water inventory one hour after the LOCA. The scale of the horizontal surface area of the GDCS pool is also smaller (1:64) than the system scale. Thus, while any tendency of the steam to condense on the surface of the GDCS pool water will be reduced, this will also lead to a slower heatup of the GDCS water. In terms of overall energy removal, the net effect should not be significant.

Finally, *the volume of the ICS pools* is smaller than in the SBWR; these are scaled for 24 hours of decay heat capacity, rather than three days, as in the SBWR. However, water can be added at a required flow rate and temperature by the facility conditioning system to compensate for the lesser initial inventory.

#### 4.5.2.2 Scaled Models of the PCC and IC Condensers

A critical factor that led to the choice of 1:25 for the PANDA system scale was the desire that the condenser unit secondary side behavior be representative of the prototype condensers. The PANDA condensers are "sliced" from the prototypes (Figure 4.5-4). Thus, the circulation of the secondary coolant in a plane perpendicular to the axis of the cylindrical headers can be made very similar to that in the actual SBWR ICS pools. The units are provided with baffles, preventing entry of the flow into the bundle in the direction of the header axis. A sufficient number of tubes was provided to have at least a couple of tubes completely surrounded by other tubes. This led to five rows of tubes, twenty tubes in total, and to the 1:25 system scale. In PANDA, condenser tubes are in all respects (height, pitch, diameter, and wall thickness) prototypical.

#### 4.5.2.3 Design of the Piping and Other Connections

All piping is scaled according to the criteria developed in Sections 2.3 and 2.4. The pipe diameters were calculated to match the frictional and form losses of the SBWR; the resulting pipe diameters were rounded to the next larger normalized diameter. The actual pressure drops are usually dominated by form losses which depend weakly on flow velocity (or Reynolds number) and can thus be matched very well. All lines are provided with interchangeable orifice plates that can be used to further adjust the pressure losses in the system.

The total flow area of the PANDA main steam lines (one to each DW) is the sum of the SBWR MSLs *and* the DPVs. To investigate asymmetric DW conditions, all of the steam flow can be directed through one of the PANDA steam lines to one DW.

The vacuum breakers, which provide the flow path for potential redistribution of noncondensible gas between the SC and the DW, are simulated by programmable control valves which can reproduce the characteristics of the corresponding SBWR components. The scaling of the flows emerging from the vacuum breakers in relation to stratification in the DW was discussed in Section 3.2.3.

Finally, the vents are designed according to the criteria developed in Section 3.5. In PANDA, the vertical-pipe sections of the main vents have a cross-sectional area smaller than the one dictated by the system scale. However, they are not expected to open during the experiments. The gas velocities in the main vents are, in both the prototype and the model, low enough to eliminate worries about dynamic effects modifying system behavior, if the vents were to open.

#### 4.5.2.4 Heat Capacity and Heat Losses

The simulation of the heat capacity of the various SBWR structures was contemplated during the design phase of the PANDA facility. The PANDA vessels have thin walls and therefore very limited heat capacity. One could have inserted "heat capacity slabs" *in* the vessels to match the heat capacity of the SBWR structures. Use of appropriate layers of different materials could have provided the necessary time response. The idea was not implemented, however, since heat soaking in the SBWR structures during the long-term containment cooling period of interest is estimated to be of the same order of magnitude as the heat losses from the experiment. The heat capacity and heat loss aspects of the facility will be addressed by computation and use of calibration results during data reduction and analysis.

The PANDA vessels are very well insulated and the heat losses were conservatively estimated (for a 0.3 MPa saturated systen.) to be less than 4% of the decay heat level one hour after shutdown and less than 9% of the 24-hr-after-shutdown level. More recent and more accurate estimates show that the actual losses will be significantly lower [4].

The vessel internal and external wall temperatures are measured at 42 points [13], which allows accurate calculations of both the heat stored in the vessel walls and of the heat losses. Heat loss calibration tests will be performed during commissioning of the facility. The information from these tests will be used to construct a heat-loss model of the facility. The data from the wall thermocouples will be used as inputs to the model to calculate the heat stored in the vessel walls and the heat losses during the tests; both are relatively small and both will be known with good accuracy. The heat-loss model of the facility will also be used for the code assessment analyses using the experimental data.

### 4.5.3 Establishment of the Proper Initial Conditions for the Tests

The PANDA facility is equipped with auxiliary air and water supply systems for preconditioning the contents of the various system components; these are also shown in Figure 4.5-2. In particular, all vessels are provided with both top and bottom filling ports and drains or vents. Thus, the possibility of establishing stratified initial conditions in the water space of the vessels at the beginning of the tests is assured.

There is also the ability to vary the submergence depth of the vents and of the initial water level in the SP. In particular, this water level can be positioned below, at, or above the location of the large pipe connecting the two SP in the SC vessels.

#### 4.5.4 Scaling Results for the PANDA Facility

##### 4.5.4.1 PCCS Phase

###### 4.5.4.1.1 Momentum Scaling

####### 4.5.4.1.1.1 Comparison of Nondimensional Groups — Prototype vs. PANDA, VB Closed

####### 4.5.4.1.1.2 Comparison of Inertia Matrices — Prototype vs. PANDA, VB Closed

####### 4.5.4.1.1.3 Comparison of Resistance Matrices — Prototype vs. PANDA, VB Closed

###### 4.5.4.1.2 Pressure and Energy Scaling

###### 4.5.4.1.3 Bottom-Up Scaling

#### 4.5.5 Summary of Results for PANDA

The PANDA test series provides data for the containment performance during the long-term PCCS Phase. The overall top-down scaling of the PANDA facility shows very good simulation of the SBWR facility. The global momentum scaling indicates that all of the important parameters are scaled very well to the SBWR values. The continuity and pressure rate scaling indicates no important differences between the PANDA facility and SBWR design. The larger facility scale of 1:25 results in better simulation of the drywell mixing phenomena than the smaller GIRAFFE facility. The data from these tests provide a sufficient database for qualification of TRACG for long-term containment performance.

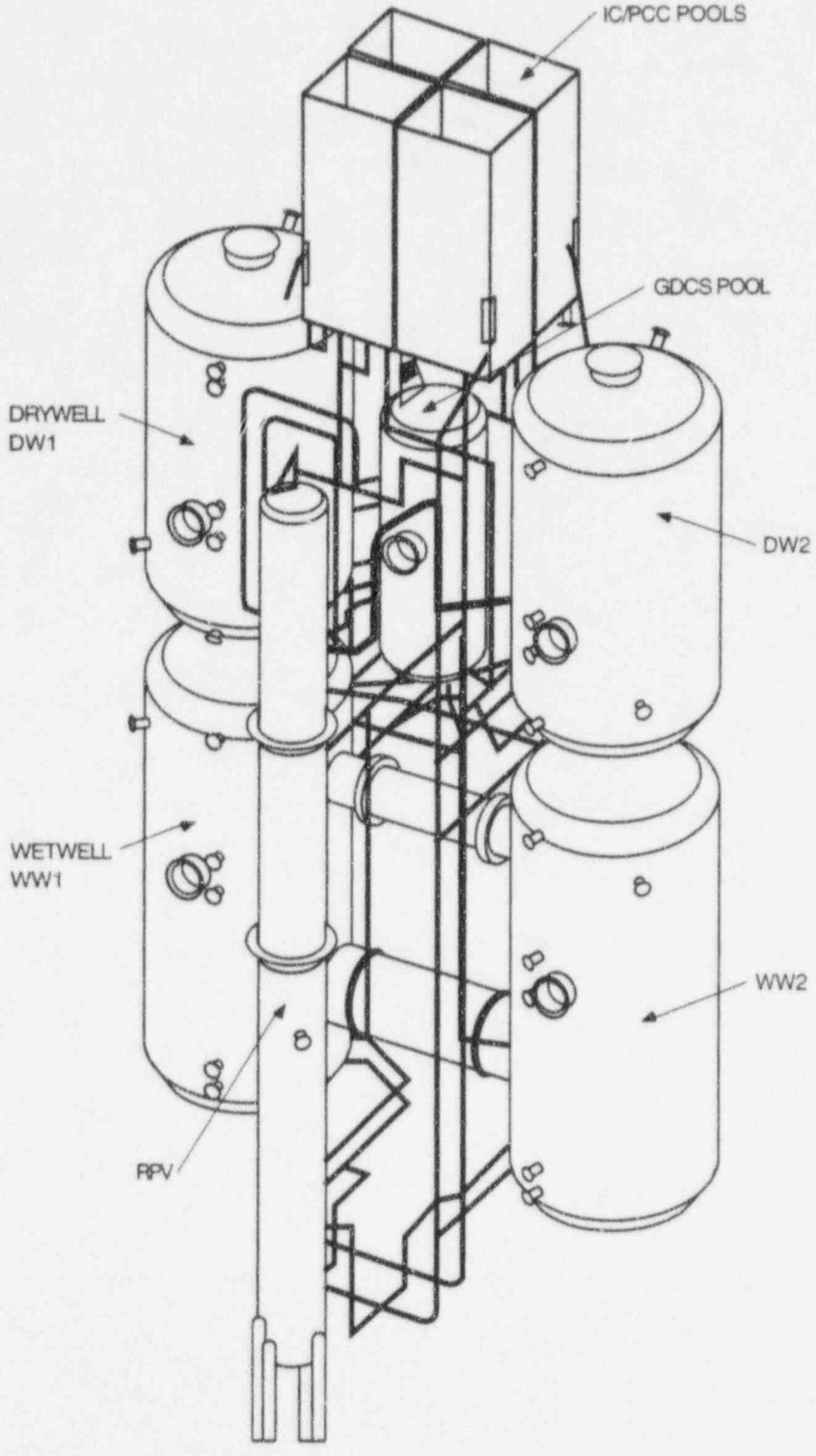


Figure 4.5-1. Isometric View of the PANDA Facility

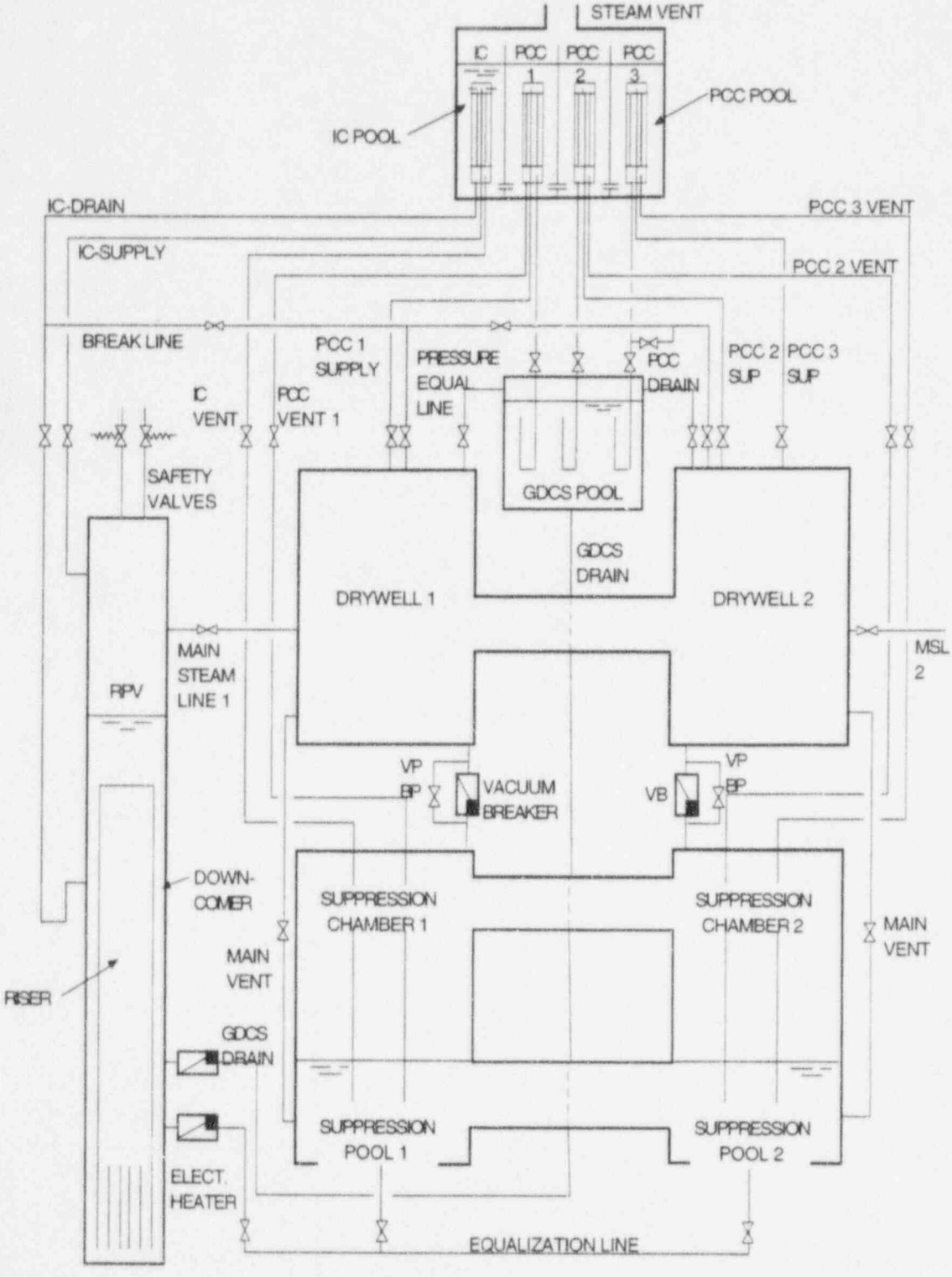


Figure 4.5-2. Piping Connections and Process Lines of the PANDA Facility

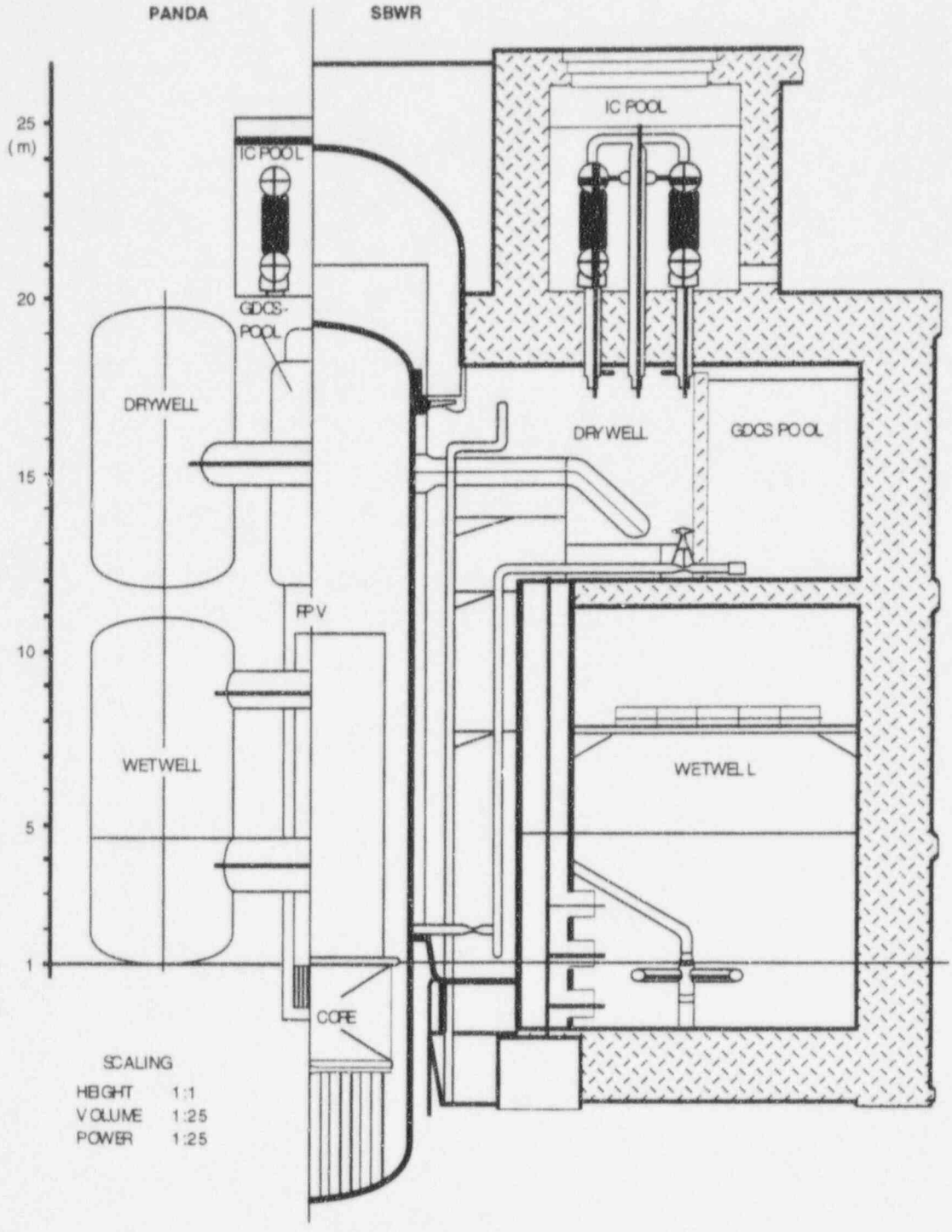


Figure 4.5-3. Comparison of the PANDA Elevations with the SBWR

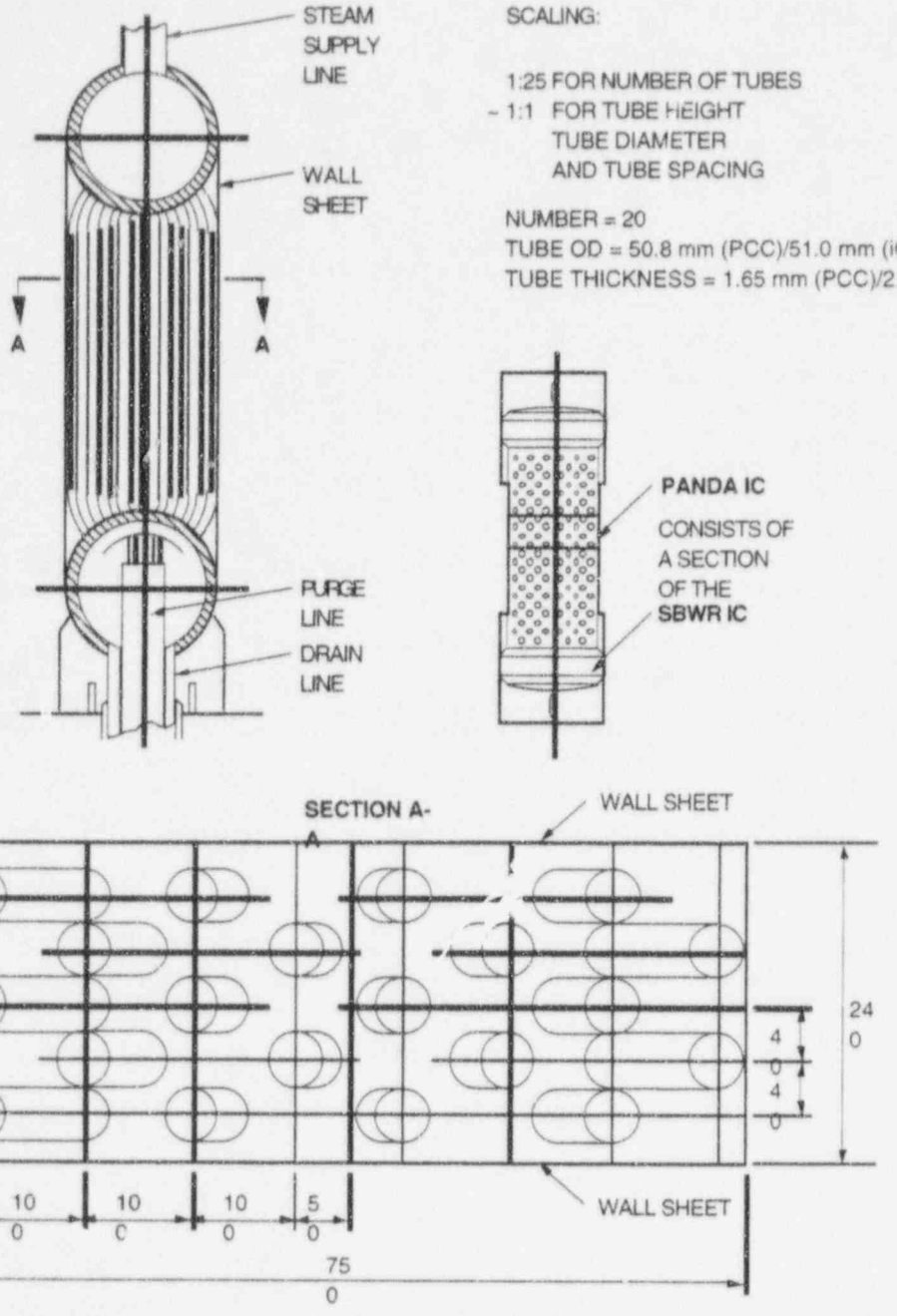


Figure 4.5-4. The PANDA PCCS and ICS Condenser Units

## 4.6 PANTHERS Tests

PANTHERS is a full-scale test under prototypical flow, pressure, temperature, and noncondensible fraction conditions of a prototypical single module of an IC condenser (half unit) and of a full PCC condenser. The PANTHERS test facility and the planned tests are described in the TAPD [55].

The purpose of the tests is to qualify the proposed condenser designs regarding structural integrity and steady-state thermal-hydraulic performance. Figure 4.6-1 shows the schematic of the PANTHERS test facility, for both types of tests. The test objectives are given in the TAPD [55].

The operation of the PCCS as part of the SBWR can be described as a slow transient. Under certain conditions, its operation may become cyclical, but the period of the cycles will be long in comparison to the response time of the PCCS. The characteristic response time of the PCC condenser unit is mainly determined by the transit time of the fluid in the tubes (which is of the order of seconds), and to some extent by the time constant of the tube wall; since these walls are thin, this time constant is also of the order of a few seconds. Thus, the response of the PCC condenser units to changes in inlet conditions is much faster than the response of the large SBWR containment volumes. In terms of the discussion of Section 2.4.1, this can be expressed as $t^{o} \gg t^{o}_{tr,\,tubes}$. Thus, the *steady state* PANTHERS tests provide adequate data to characterize the operation of the PCCS condenser units.

Some local heat flux data are also obtained from these multi-tube units. Special care was used [25] in installing thermocouples on both sides of the tube wall to reduce the relatively large error inherent in such measurements.

Since the PANTHERS tests are conducted with full-scale components (i.e., a prototypical PCC unit and a symmetric one-half of an IC unit), there are no scaling distortions to be addressed. There is no expected effect of testing only one half of the IC unit (one module), except possibly some influence on circulation in the pool.

The PCC condensers are installed in pools having the same dimensions as the SBWR IC pools. For the IC tests, the pool volume is reduced to maintain the same volume per module. Although this partly affects the boundary conditions regarding natural circulation in the pool (introduces a wall instead of a symmetry condition on one side of the unit), the effect should be minimal. In any case, small changes in the circulation patterns on the secondary side are not expected to have much influence on overall heat transfer, as discussed in Section 3.6.2.

The IC pools are well mixed by natural circulation. The condensers are located at prototypical elevations in the pools. Furthermore, since the lower parts of the condenser units are located slightly above the bottom of the pools, the entire pool water inventory participates in the mixing process. No stratification was detected by the PANTHERS pool thermocouples.

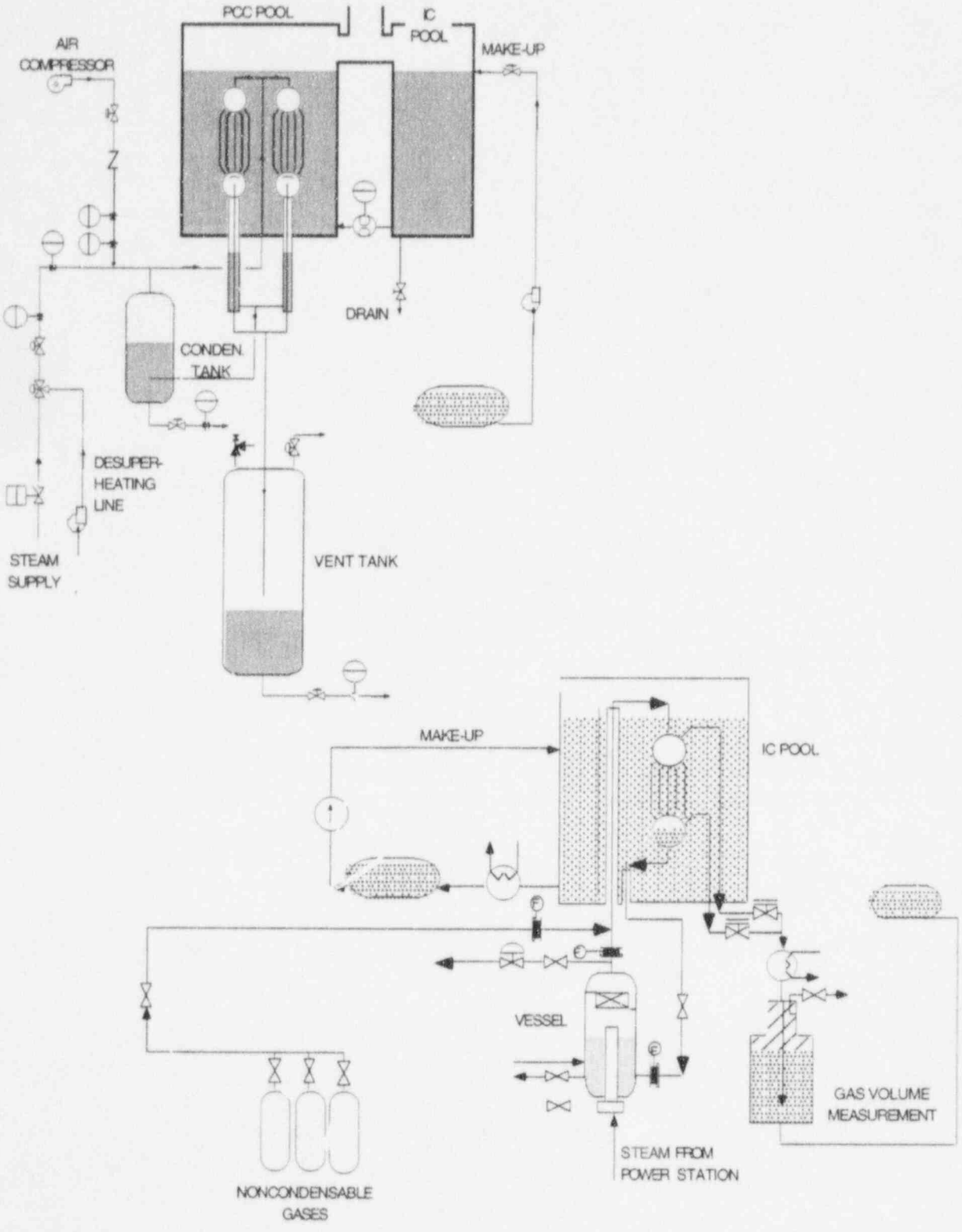


Figure 4.6-1. Schematics of the PANTHERS Test Facility
[Top: PCC Tests; Bottom: IC Tests]

### 4.7 Analysis of Oscillation Between Large Liquid Pools

The key result of the study, as reported more fully in Appendix C, is that the drain lines with relatively small cross-sectional flow areas tend to damp out level oscillations between the large water masses because of the high impedance or flow resistance of the connecting drain lines. For the specific SBWR configurations considered, it was found that these systems are overdamped whenever the pressure step change or harmonic input magnitude was greater than about 0.5m head pressure equivalent. For pressure changes of less than 0.3m head equivalent, the system may be underdamped and small amplitude, low frequency oscillations may occur. The larger the pressure change, the more overdamped and stable the systems are, because wall friction and the damping coefficient increase with the flow velocity in the connecting pipes and larger pressure changes produce larger flow velocities.

The long natural cycle time calculated for the system is caused by the relatively small diameter drain lines connecting the large liquid masses. The flow resistance in the lines provides resistance or impedance to moving the fluid from pool to the other. One factor that affects the natural cycle time is the pool radius to line ratio Rr/R and the number of drain lines in operation.

Natural cycle times for the basic systems considered and configuration variations considered to evaluate alternative operating modes and parameter uncertainties, varied by a factor of less than three. The liquid level amplitude resulting from an harmonic forcing function input was less than that of the input function corresponding to the zero frequency or step change input function because the magnification factor was less the unity for the overdamped system. This was the case even when the imposed forcing function frequency was equal to that of the natural system frequency.

The equation of motion was nondimensionalized using the system natural cycle time period as the normalizing time scale, and the imposed pressure difference as the normalizing displacement. The results showed that only one important nondimensional group appears in the equation. This group contained the damping ratio (i.e., the actual damping coefficient divided by the critical damping coefficient) as a variable. The damping ratio must be greater than unity to assure that level oscillations do not occur. The criteria and methodology developed here can be applied to evaluate the stability of other, similar systems.

## 5.0 References

[1] *TRACG Prediction of Gravity-Driven Cooling System Response in the SBWR/GIST Facility LOCA Tests*, Alamgir, Md., Andersen, J.G.M., Yang, A.I., and Shiralkar, B., *Trans. ANS*, 62, 665-668.

[2] *TRACG Model Description*, Andersen, J.G.M. et al., Licensing Topical Report, NEDO-32176, Class 1, February 1993.

[3] *TRACG Qualification*, Andersen, J.G.M. et al., Licensing Topical Report, NEDO-32177, Class 1, February 1993.

[4] Personal communication, Paul Scherrer Institute, Aubert, C.

[5] *Simplified Boiling Water Reactor (SBWR) Program Gravity-Driven Cooling System (GDCS) Integrated Systems Test — Final Report*, Billig, P.F., GE Nuclear Energy Report GEFR-00850 (Class II), DRF A00-02917, October 1989.

[6] *Scaling Issues for a Thermal-Hydraulic Integral Test Facility*, Boucher, T.J., diMarzo, M., and Shotkin, L.M., 19th Water Reactor Safety Information Meeting, Washington, DC, October 30, 1991.

[7] *Quantifying Reactor Safety Margins — Application of Code Scaling, Applicability, and Uncertainty Evaluation Methodology for a Large-Break, Loss-of-Coolant Accident*, Boyack, B. et al., Nuclear Regulatory Commission Report NUREG/CR-5249, EGG-2552, 1989.

[8] *Bubbling Regimes at the Wellhead of a Subsea Oilwell Blowout*, Bugg, J.D. and Rowe, R.D., pp. 571-576 in *Proc. of the 11th Int. Conf. on Offshore Mechanics and Arctic Engineering — 1992*, 1992 – OMAE, S.K. Chakrabarti et al. (editors), Vol. 1, Part B, ASME.

[9] *Vertical Turbulent Buoyant Jets, A Review of Experimental Data*, Chen, C.J. and Rodi, W., HMT, The Science and Applications of Heat and Mass Transfer, Vol. 4, Pergamon Press, Oxford, 1980.

[10] *Bubbles, Drops and Particles*, Clift, R., Grace, J.R., and Weber, M.E., Academic Press, New York, 1978.

[11] *ALPHA — The LongoTerm Passive Decay Heat Removal and Aerosol Retention Program*, Coddington, P., Huggenberger, H., Güntay, S., Dreier, J., Fischer, O., Varadi, G., and Yadigaroglu, G., pp. 203-211 in *Proc. of the Fifth Int. Topical Meeting on Reactor Thermal Hydraulics, NURETH-5*, (American Nuclear Society), 21-24 September 1992, Salt Lake City, Utah.

[12] *Fluidised Particles*, Davidson, J.K. and Harrison, D. , Cambridge University Press, London, 1963.

[13] Personal communication, Paul Scherrer Institute, Dreier, J.

[14] *Hydrodynamics of Underwater Blowouts*, Fannelop, T.K. and Sjoen, K., AIAA 8th Aerospace Sciences Meeting, 14-16 January 1980, Pasadena, CA, AIAA paper 80-0219.

[15] *Containment Horizontal Vent Confirmatory Test*, Part I, General Electric Company Report NEDC-31393, March 1987.

[16] General Electric Company BWR/6 Nuclear Island Design, Docket No. STN 50-447, March 1980, Amendments 1 through 21.

[17] *Buoyancy-Induced Flows and Transport*, Gebhardt, B., Jaluria, Y., Mahajan, R.L., and Sammakia, B., Hemisphere Publ. Corp., Cambridge, 1988.

[18] *Proceedings American Nuclear Society Meeting on FissionoProduct Behavior and Source Term Research*, Huebner, M.F. (editor), 15-19 July 1984, Snowbird, Utah; EPRI Report NP-4113-SR, July 1985.

[19] *Similarity Analysis and Scaling Criteria for LWR's Under Single-Phase and Two-Phase Natural Circulation*, Ishii, M. and Kataoka, I., NUREG/CR-3267, ANL-83-32, 1983.

[20] *Joint Study Report, Feature Technology of Simplified BWR (Phase I), 2nd Half of 1990, Final Report*, JAPC et al., Report by the Japan Atomic Power Company and partners, November 1990.

[21] *Scaling Criteria for Nuclear Reactor Thermal Hydraulics*, Kiang, R.L., Nucl. Sci. and Eng., 89, 207-216, 1985.

[22] *Scaling Criteria for Two-Phase Flow Loops and their Application to Conceptual 2x4 Simulation Loop Design*, Kocamustafaogullari G. and Ishii, M., Nucl. Tech., 65, 146-160, 1984.

[23] *Turbulent Jets and Plumes*, List, E.J., Ann. Rev. Fluid Mech., 14, 189-212, 1982.

[24] *Letter from P.W. Marriott to R. Borchardt, Standardization Project Directorate*, May 7, 1993, MFN No. 071-93, Docket STN 52-004.

[25] *Confirmatory Tests of FulloScale Condensers for the SBWR*, Masoni, P., Botti, S., and Fitzsimmons, G.W., pp. 735-744, Vol. 1, in Proc. 2nd ASME-JSME Nuclear Engineering Joint Conf., 21-24 March 1993, San Francisco, CA.

[26] *Computer Model of a Passive Containment Cooling Condenser Tube*, Meier, M., Semester Project, Nuclear Engineering Laboratory, Swiss Federal Institute of Technology, 1992.

[27] *Mean Flow in Round Bubble Plumes*, Milgram, J.H., J. Fluid Mech., 133, 345-376, 1983.

[28] *Dynamic and Thermal Behavior of Hot Gas Bubbles Discharged into Water*, Moody, F.J., *Nuclear Eng. and Design*, 95, 47-54, 1986.

[29] *Introduction to Unsteady Thermofluid Mechanics*, Moody, F.J., John Wiley & Sons, New York, 1990.

[30] *Final Test Report: Testing of the Gravity-Driven Cooling System for the Boiling Water Reactor*, Mross, J.M., GE Nuclear Energy Report NEDO-31680, July 1989.

[31] *Heat Removal Tests of Isolation Condenser Applied to a Passive Containment Cooling System*, Nagasaka, H., Yamada, K., Katoh, M., and Yokobori, S., pp. 257-263, paper b.1, in *Proc. 1st JSME-ASME Int. Conf. on Nuclear Engineering, ICONE-1*, Tokyo, 1991.

[32] *Mark III LOCA-Related Hydrodynamic Load Definition*, Nuclear Regulatory Commission Report NUREG-0978, August 1984.

[33] *Vertical Downflow Condensation Heat Transfer in Gas-Steam Mixtures*, Ogg, D.G., M.Sc. thesis, University of California at Berkeley, 1991.

[34] *SBWR Loss-of-Coolant Accident Analysis*, Paradiso, F.M., Yang, A.I., and Sawyer, C.D., Vol. 1, pp 313-318, *Proc. 2nd ASME-JSME Nuclear Engineering Joint Conf.*, 21-24 March 1993, San Francisco, CA.

[35] *Radionuclide Scrubbing in Water Pools — Gas-Liquid Hydrodynamics*, Paul, D.D. et al., *Proceedings: American Nuclear Society Meeting on Fission-Product Behavior and Source Term Research*, 15-19 July 1984, Snowbird, Utah, EPRI Report NP-4113-SR, July 1985.

[36] *Scaling for Integral Simulation of Mixing in Large, Stratified Volumes*, Peterson, P.F., Schrock, V.E., and Greif, R., NURETH 6, *Proc. Sixth Int. Topical Meeting on Nuclear Reactor Thermal Hydraulics*, 5-8 Oct. 1993, Grenoble, France, Vol. 1, pp. 202-211.

[37] *An Experimental Investigation of the Thermally Induced Flow Oscillations in Two-Phase Systems*, Saha, P., Ishii, M., and Zuber, N., J. Heat Transfer, 98, 616-622, 1976.

[38] *Condensation Inside Tubes with Noncondensable Gas Present*, Schrock, V.E., USNRC-GE meeting on SBWR Passive Containment, Rockville, MD, May 29, 1992.

[39] Personal communication, Schrock, V.E., 1993.

[40] *Two-Phase Flow-Pattern Transition Scaling Studies*, Schwartzbeck, R.K. and Kocamustafaogullari, G., ANS Proceedings, *1988 National Heat Transfer Conference*, 24-27 July 1988, Houston, Texas, pp. 387-398.

[41] *The Effects on Noncondensable Gases on Steam Condensation Under Forced Convection Conditions*, Siddique, M., Ph.D. thesis, Dept. of Nuclear Engineering, Massachusetts Institute of Technology.

[42] *The Effect of Hydrogen on Forced Convection Steam Condensation*, Siddique, M., Golay, M.W., and Kazimi, M.S., AIChE Symp. Ser., 85 (No. 269) 211, 1989.

[43] *Local Heat Transfer Coefficients for Forced-Convection of Steam in a Vertical Tube in the Presence of a Noncondensable Gas*, Siddique, M., Golay, M.W., and Kazimi, M.S., *Nucl. Technology*, 102, 386-402, 1993.

[44] *Analysis of Single-Phase Mixing Experiments in Open Pools*, Smith, B., Dury, T.V., Huggenberger, M., and Nöthiger, H., pp. 101-109 in *Proc. ASME Winter Annual Meeting*, Anaheim, CA, 1992.

[45] *Simplified Boiling Water Reactor Passive Safety Features*, Upton, H.A., Cooke, F.E., Sawabe, J.K., pp. 705-712, Vol. 1, in *Proc. 2nd ASME-JSME Nuclear Engineering Joint Conf.*, P.F. Peterson (ed.), 1993.

[46] *Behavior of Steam-Air Systems Condensing in Cocurrent Vertical Downflow*, Vierow, K.M., M.Sc. thesis, University of California at Berkeley, 1990.

[47] *Condensation in a Natural Circulation Loop with Noncondensable Gases. Part I — Heat Transfer*, Vierow, K.M. and Schrock, V.E., *Proc. of the Int. Conf. on Multiphase Flows*, 24-27 September 1991, Tsukuba, Japan, Vol. 1, pp. 183-190.

[48] *Analysis of SBWR Passive Containment Cooling Following a LOCA*, Vierow, K.M., Fitch, J.R. and Cooke F.E., *Proc. Int. Conf. on the Design and Safety of Advanced Nuclear Power Plants*, 25-29 October 1992, Tokyo, Japan, Vol. III, pp. 31.2.1-7.

[49] *One-Dimensional Two-Phase Flow*, Wallis, G.B., McGraw-Hill Book Co, New York, 1969.

[50] *Fundamental and Higher-Mode Density-Wave Oscillations in Two-Phase Flow*, Yadigaroglu, G. and Bergles, A.E., J. Heat Transfer, 94, 189-195, 1972.

[51] *System Response Test of Isolation Condenser Applied as a Passive Containment Cooling System*, Yokobori, S., Nagasaka, H., Tobimatsu, T., pp. 265-271, paper b.2, in *Proc. 1st JSME-ASME Int. Conf. on Nuclear Engineering, ICONE-1*, Tokyo, 1991.

[52] *Hierarchical, Two-Tiered Scaling Analysis Appendix D to An Integrated Structure and Scaling Methodology for Severe Accident Technical Issue Resolution*, Zuber, N., Nuclear Regulatory Commission Report NUREG/CR-5809, EGG-2659, November 1991.

[53] Personal communication , Wulff, W., 1995.

[54] *SBWR PCCS Vent Phenomena and Suppression Pool Mixing*, Coddington, P. and Andreani, M., Seventh International Topical Meeting on Nuclear Reactor Thermal Hydraulics — NURETH 7, September 10-15, 1995, NY, USA.

[55] *SBWR Test and Analysis Program Description*, General Electric Company Report NEDC-32391 Rev. C, August 1995.

[56] *Single Tube Condensation Test Program*, Usry, W.R., GE Report NEDC-32301, March 1994.

[57] *Variation of the Vapor Volumetric Fraction During Flow and Power Transients*, Shiralkar, B.S., Schnebly, L.E., and Lahey Jr., R.T., Nuclear Eng. and Design, 25, 350-368, 1973.

[58] *Scaling and Analysis of Mixing in Large Stratified Volumes*, Peterson, P.F., Int. J. Heat Mass Trans., 37, 97-106, 1994.

[59] SBWR Test and Analysis Program Description, General Electric Company Report NEDC-32391, Rev. B, 1995.

# Appendix A — Global Momentum Scaling Formulations

## Table of Contents

## List of Figures

## A.1 Background

This appendix first gives descriptions of the flow paths which describe the global momentum equation formulation presented in Subsection A.3. The resulting equations are also summarized in Section 2. In the global formulation, emphasis is on overall system behavior and interaction between processes occurring in various parts of the prototype and the corresponding test facilities. This approach allows direct comparisons of the prototype system behavior with each of the test facility systems that might reveal differences or scaling distortions in the systems. In the general scaling section given in Section 2, the processes occurring in individual components and flow paths are examined and described in terms of the applicable conservation equations.

## A.2 Description of Flow Paths

Brief descriptions of the prototype SBWR systems and each of the major supporting test facilities (GIST, GIRAFFE, and PANDA) are given in this section. The major features of the systems and components and their operation, as required to understand the basic simplifying assumptions made in the global scaling analysis, are emphasized. More detailed system and component descriptions are given by Vierow, et al [1]* , Paradiso, et al [2], and by Upton, et al [3] and in Sections 1 and 4 of this report.

### A.2.1 Prototype SBWR System

All of the flow paths of the prototype SBWR may not be operational at any one time. The main vent flow path from the DW to the SP with a submerged vent line exit and a vacuum breaker (VB) flow path connecting the SP with the DW are present. The vacuum breaker flow path is only activated if the DW pressure falls below a certain value relative to the SC pressure. Opening of the VBs allows primarily noncondensible gases contained in the SP gas space to escape to the DW, thus equalizing pressures in the DW and SC. Furthermore, an equalization line exists which allows water contained in the SP to enter the RPV if the RPV water level should fall below predetermined level setpoints, and a adequate gravity head is available for the SP water to drain into the RPV.

There are five water masses with water/steam/gas interfaces. The major water volume is that of the SP followed by the RPV water mass. The size of the water mass contained in the lower portion of the DW depends on the accident scenario assumed and, for the GDLB scenario, could be a considerable fraction of the original RPV mass. Smaller water masses are normally present in the ICs and PCCs. A large water mass, referred to as the IC pool in which the ICs and PCCs are submerged, is also present outside the containment, but this mass is not involved directly in the global momentum scaling analysis. Flashing of water into steam or condensation of steam may take place at the liquid/steam/gas interfaces identified above, depending on local system conditions experienced during the postulated accident.

Heat sources and sinks are present in the overall system. The major heat source is the core decay heat, while heat transfer from the RPV vessel wall and from internal steel structures may become heat sources, particularly during rapid pressure changes such as those which occur during the Blowdown Phase. The major heat sink is the heat transferred to the IC pool via the ICs and the PCCs. During the later phases of the transient, these heat sinks together are approximately of the same magnitude as the core decay heat. The heavy steel-lined, reinforced containment structure

* References for Appendix A are listed in Section A.4.

acts mostly as a heat sink during a postulated accident because its temperature changes slowly from the original near-room temperature condition existing at the start of the transient.

Several flow paths can be activated for rapid blowdown of the RPV should this become necessary following a line break accident. The line break accident scenarios most often considered are: (1) break of one of the two Main Steam Lines (MSLs); (2) break of one of the six GDCS lines (GDL) next to the RPV; and (3) break of the Bottom Drain Line (BDL). The various flow paths involved in the blowdown process are indicated schematically in Figure A.2.1-1. There are three lines leading from three of the four stub tubes to the ICs that are activated by a depressurization valve (DPV) in each line. The total flow in all three lines is denoted by $W_{IC}$ and the state of the fluid entering the line at the DPVs is considered to be saturated steam, since the elevation of the stub tubes is far above the RPV water level.

There are six DPVs, one on each of the four stub tubes and one on each of the MSLs, that release primarily saturated, or slightly superheated, steam directly into the upper DW when the DPVs are open. However, in case of a MSL break, steam flow can occur through five of the DPVs. Additionally, there is steam flow through the broken MSL at a location indicated schematically in Figure A.2.1-1. The total steam blowdown flow from all these sources is denoted by $W_B$ in the MSL break scenario. In case of a GDL break or a BDL break, steam can be released from five of the six DPVs to the upper DW (one DPV failure is assumed), and a steam/water mixture is released into the lower DW, since these lines are normally located at elevations below the RPV water level. Therefore, for the GDL and BDL break scenarios, the total blowdown flow $W_B$ is the total for five DPVs and either of the broken lines, assuming that all DPVs open. In the GDL break scenarios, there is also discharge of water into the DW from the GDCS pool via the broken drain line.

A third blowdown flow path is also activated and the total flow in this flow path is denoted by $W_{RV}$. This flow path leads from the steam space above the RPV water level into the SP, where the steam is discharged via submerged spargers and quenched. There are four safety/relief valve (SRV) lines mounted on each MSL with SRVs (Figure A.2.1-1). In the MSL break scenario, the total SRV blowdown flow $W_{RV}$ is the total of four SRV line flows located on the intact MSL; whereas, in the BD and GDL break scenarios, a total of eight SRV lines would be activated, discharging steam into the SP.

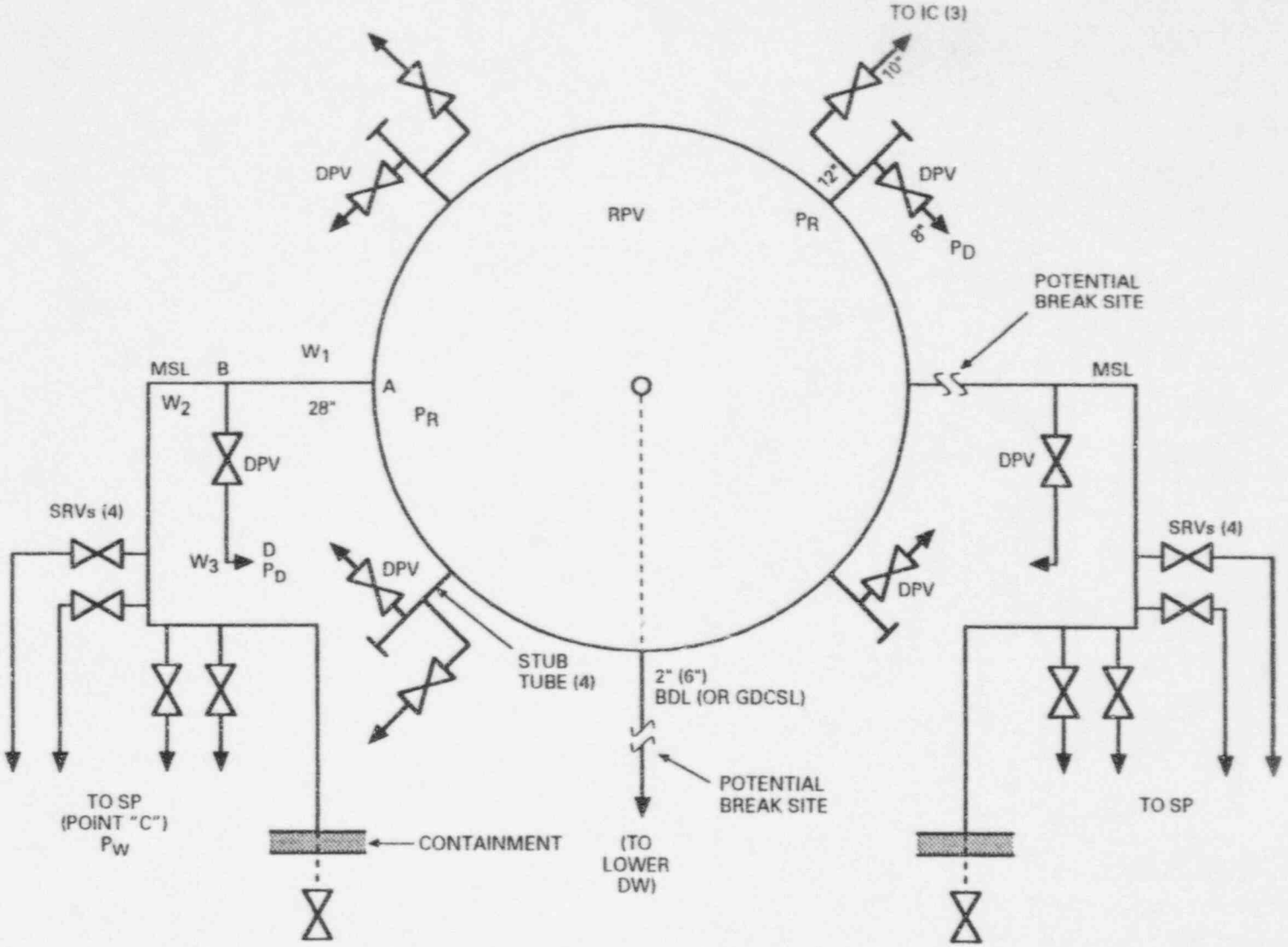


Figure A.2.1-1. Schemaitic of SBWR Blowdown Flow Paths with GDL Break

### A.2.2 GIST Facility System

A schematic diagram of the GIST test facility is given in Figure A.2.2-1. The facility incorporates the main components and flow paths to simulate a number of features of the SBWR design as it existed at the time of facility construction. The major difference between the 1987 and current SBWR designs is that, in the earlier version, a single pool was used to provide both containment pressure suppression and the source of the GDCS water (Figure A.2.2-1). In the final SBWR design, the water inventories for GDCS and pressure suppression are separated. The suppression pool is on the SC and the GDCS water inventory is equally divided among three pools located on the diaphragm floor within the DW.

A second difference is the six DPVs discharging directly to the DW in the SBWR prototype, which are not present in the GIST facility. A third major difference between the current SBWR and the GIST facility is that the test facility has neither an IC nor a PCC. Thus, five flow paths present in the prototype are not present in the GIST test facility. These flow paths for the IC are: (1) the IC inlet flow path having total flow denoted by $W_C$ and (2) the IC drain flow path with flow $W_L$. The corresponding flow paths in the PCC having flows $W_{PC}$, $W_{LPC}$, and the PCC vent flow line having a flow rate $WP_{CX}$ are also not present in the GIST facility.

On the other hand, the blowdown flow paths in GIST are essentially equivalent to those in the prototype with a couple of exceptions. The SRV flow path in the prototype (i.e., the direct flow from the RPV to the SP) is represented by the ADP flow path in GIST and is essentially equivalent in the prototype and in GIST. However, the only direct flow path from the RPV to the upper DW in GIST is the MSL break flow path, which is only activated for the MSL break scenario (there are no DPVs in GIST). Thus, for the MSL break scenario, the total blowdown flow to the DW is that denoted by $W_{B1}$ in Figures A.2.2-1 and A.2.2-2.

For the BDL and GDL break scenarios, flow paths are available from the RPV to the lower DW (Figures A.2.2-1 and A.2.2-2). The total blowdown flow is represented by either $W_{B2}$ or $W_{B3}$, depending on the accident scenario. The main vent and the vacuum breaker flow paths in GIST are entirely equivalent to that in the prototype. The GDCS drain line is also equivalent except that, in GIST, its source of water is the SP instead of the GDCS pool in the prototype.

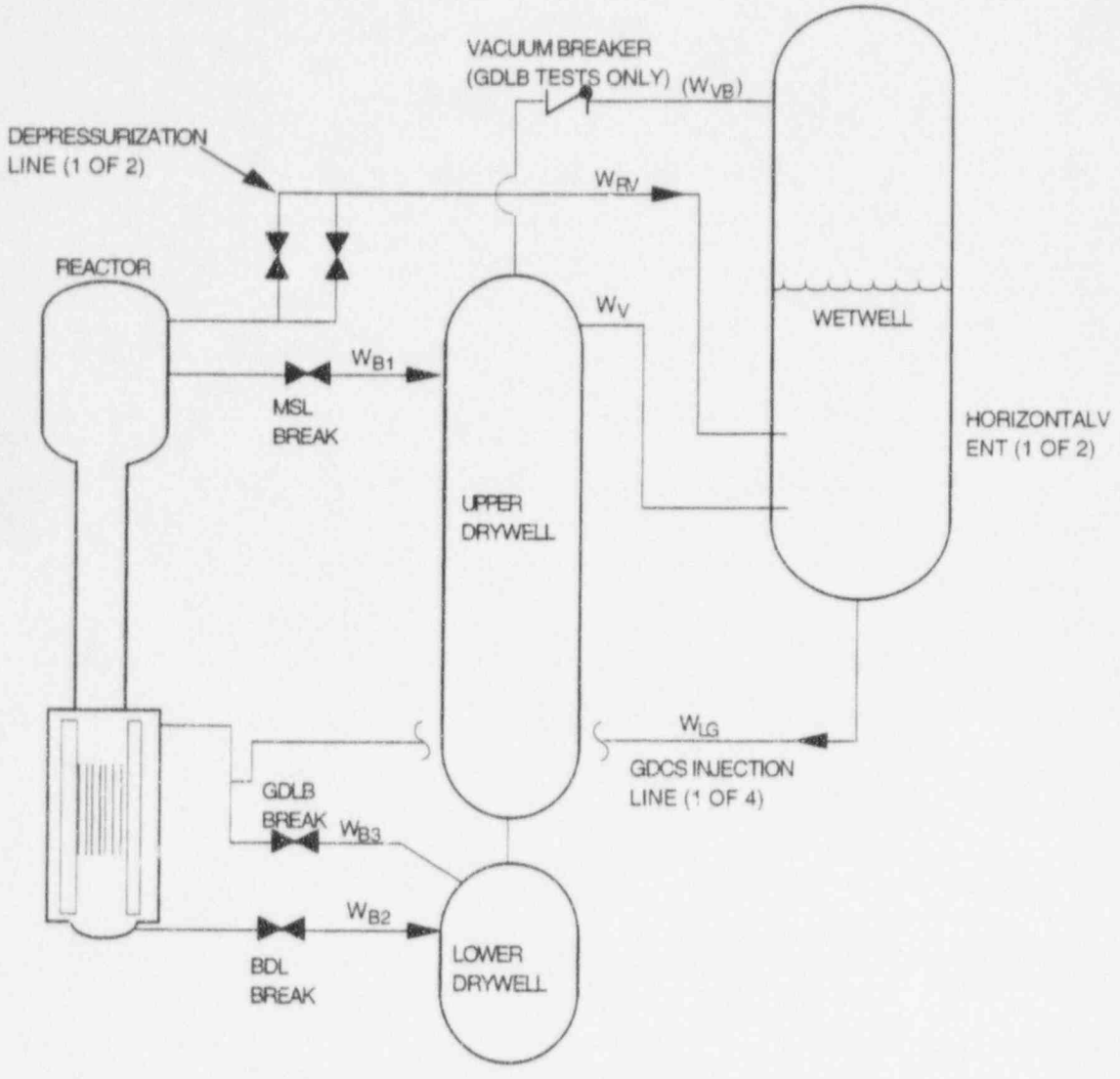


Figure A.2.2-1. GIST Facility Piping Arrangement

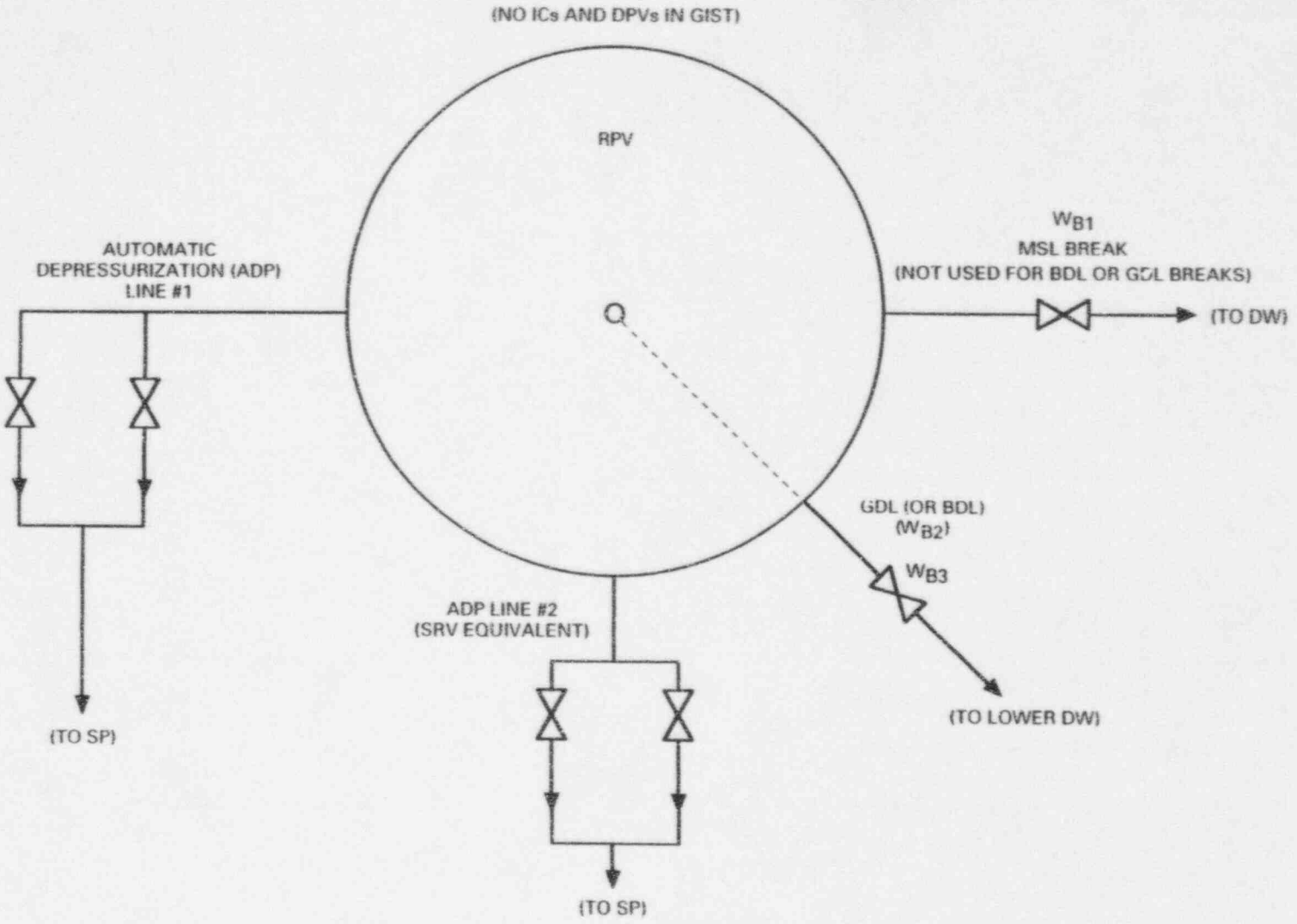


Figure A.2.2-2. Schemaitc of GIST Blowdown Flow Paths with GDL Break

### A.2.3 GIRAFFE Facility System

This facility incorporates the main components and flow paths to simulate most features of the SBWR. The flow paths in the GIRAFFE facility are essentially equivalent to those in the prototype for the GIRAFFE/SIT tests. There is no equivalent blowdown directly from the RPV to the SC (i.e., SRVs). Rather, all blowdown from the RPV is via two lines referred to as the MSB and the DPV lines to the upper DW. The MSB line is opened only if a MSL break is simulated. If not, blowdown to the DW is via the DPV line only. From the DW, steam flows into the SC via the main vent lines. There is also blowdown of a steam/water mixture from the RPV via the BD or GDCS lines, depending on which of these simulates a break. The test configuration for the GIRAFFE/He tests is similar to that for the GIRAFFE/SIT tests except that there is no IC; therefore, its two associated flow paths are not present.

### A.2.4 PANDA Facility System

A schematic diagram of the PANDA facility is given in Figure A.2.4-1. PANDA experiments will be conducted under reactor pressure and temperature conditions which are prototypical of the phase of the accident under consideration. The flow paths in PANDA are essentially equivalent to those on the prototype. The exception is that there are no SRVs in PANDA. However, flow via this flow path is expected to be small or non-existent in the long-term cooling phase tests.

The pipe line sizes were selected such that the frictional and form losses of the SBWR were matched. The actual line pressure drops are usually dominated by form losses which depend weakly on the Reynolds number and can thus be matched very well. All lines are provided with interchangeable orifice plates that can be used to adjust the pressure losses in the system.

The flow area for blowdown to the DW in the PANDA main steam lines is the scaled equivalent of the sum of the MSLs and the DPVs in the SBWR. Control valves are installed in each line (one to each DW) to simulate the different break geometries. The vacuum breaker flow path for potential redistribution of noncondensible gas between the SC and the DW is simulated in PANDA. The vertical pipe sections of the main vent flow paths have cross-sectional areas smaller than the one dictated by the system scale. However, they are not expected to open during the longer term PCCS cooling phase simulated in these experiments.

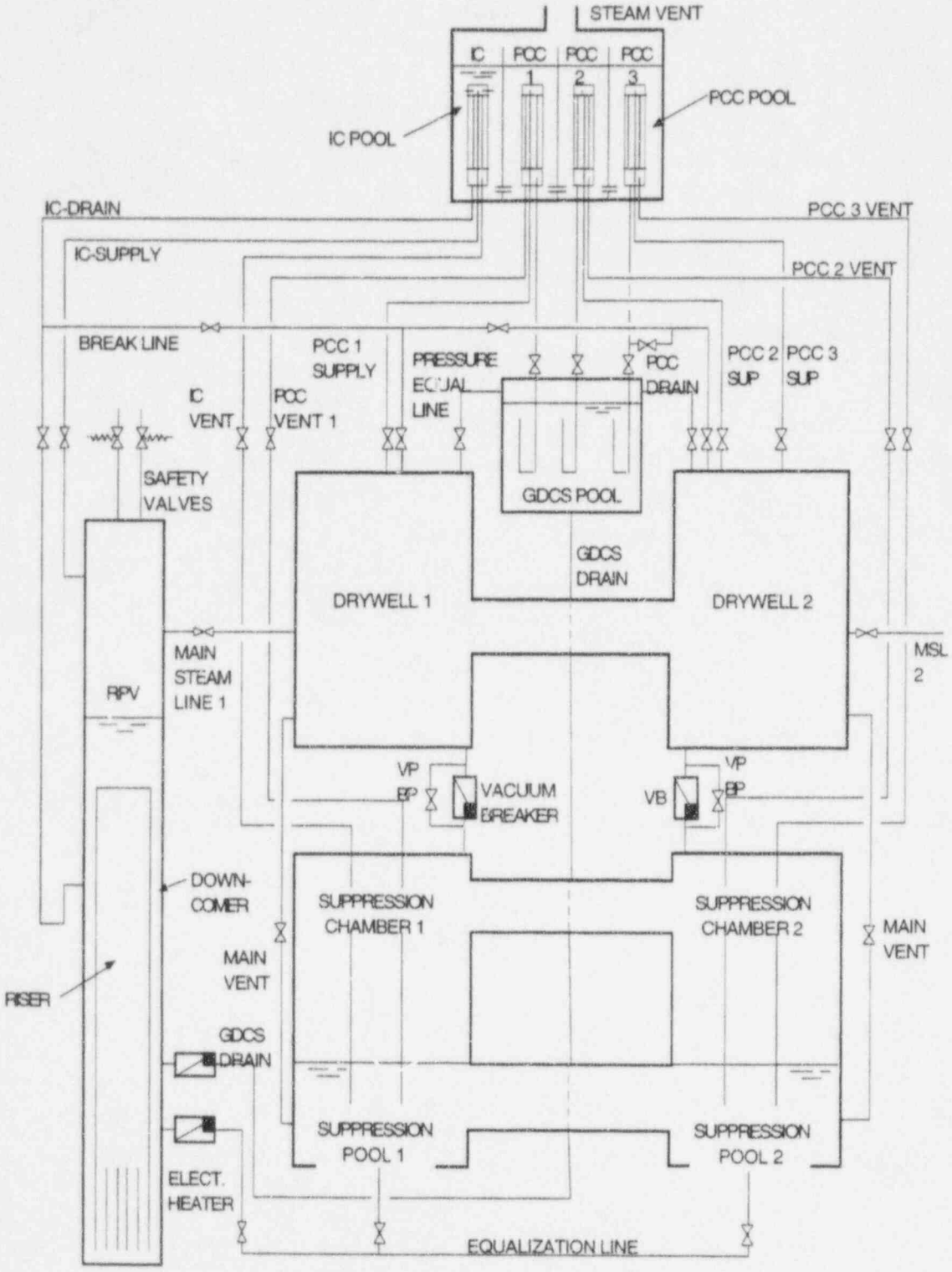


Figure A.2.4-1. PANDA Facility Schematic

## A.3 Global Scaling Formulations

Derivation of equations governing the essential characteristics of the SBWR System based on the principles of conservation of mass and momentum, along with simplifying assumptions and the approach used in the analysis, is documented in this section.

### A.3.1 Scaling Analysis Approach

The general approach followed in this analysis is similar to that developed by W. Wulff [4] with modifications as required to account for the complexity involved in the current systems. The approach is summarized in the following:

- Write momentum conservation equation for each flow loop segment or line in the system in terms of its driving pressures.
- Develop global formulation by combining equations for individual loop segments to eliminate intermediate pressures.
- Derive "closed" or "open" loop momentum equations in terms of pressure differences, hydraulic heads and submergences and specialize for each of the operating phases.
- Use mass continuity at branch points to eliminate some flow variables.
- Arrange equations in matrix form for global system.
- Non-dimensionalize variables and parameters using unique reference parameters according to the "Guidelines and Principles" outlined below.

Specialize nondimensional groups and variables by selecting specific reference parameters for each operating phase (i.e., blowdown, GDCS and PCCS phases).

Compute numerical values for global scaling groups and matrix elements for SBWR and the test facilities.

#### A.3.1.1 Guidelines and Principles

Unique reference parameters are selected to make dimensionless variables and their space and time derivatives of order one, O(1). To maintain this throughout the analysis, separate reference parameters are used for each major phase of the transients under consideration (i.e., Blowdown, GDCS and PCCS Phases). The local parameter values are scaled with the system reference parameter to indicate the dominant parameters for the system. The parameters used for reference values are limited to:

- Geometric parameters
- Parameters representing operating conditions imposed by the experimenter
- Constitutive parameters such as friction factors
- Thermophysical properties at initial conditions

Scaling of constitutive parameters such as friction factors is then scaled using bottom-up analysis to obtain proper scaling of numbers such as the Reynolds number. Initial parameters such as a velocity would only appear if it is an experimentally controlled parameter (e.g., velocity controlled by a valve).

Code calculations are not used to determine values used as reference parameters with one exception. Since these tests start at various times during a transient, TRACG analysis results are used to determine the state at which the SBWR would be in at the time the test is begun. These conditions are then used as initial conditions for the test. The test initial conditions of temperature and pressure are used as reference parameters where necessary. They are used because they are the test initial conditions, not as a direct attempt to calculate reference parameters with an unvalidated code.

Specific quantities used as reference parameters are indicated in more detail in the sections describing the scaling of equations and application to the individual test facilities and operating phases.

### A.3.2 Conservation of Momentum

The global momentum equations are derived first in terms of the driving pressure differences between various volumes as well as hydraulic heads and submergences if such terms exist. A total of five sets of momentum equations are also derived where the equations have been specialized to the Blowdown Phase (1 set), to the GDCS Phase with or without VB flow (2 sets) and to the PCCS Phase also with and without VB flow (2 sets). This specialization accounts for closed flow paths (lines) and the flow mode (i.e., critical flow or normal flow) in the system.

The flow paths and interconnected volumes are treated mathematically like a complex electrical network consisting of resistances, junctions and capacitances in which individual line currents can be obtained by a formulation in terms of loop currents. The electrical loops may or may not close on themselves, but provide a sufficient number of coupled equations to solve simultaneously for the current in each line. Similarly, the flow loops (or paths) defined for the prototype SBWR provide coupled formulations for all the flow rates. This approach provides a sufficient number of equations to include the 11 flow rates. It was necessary to utilize conservation of mass at junctions to eliminate flow rates, eventually resulting in a smaller number of loop equations.

#### A.3.2.1 Momentum Equations in General Form

#### A.3.2.2 Specialization for Blowdown Phase

#### A.3.2.3 Specialization for GDCS Phase

#### A.3.2.4 Specialization for PCCS Phase

#### A.3.2.5 Nondimensional Parameters

Nondimensional parameters and variables are defined below. The subscripts and superscripts used to denote a nondimensional quantity are, in general, defined as follows:

| | |
|---|---|
| $( )_o$ | Denotes an initial value. |
| $( )^+$ | Denotes a quantity normalized to its initial value or a reference quantity in some cases. Used for variables. |
| $( )_r$ | Denotes a unique reference parameter. |
| $( )_o$ | Denotes an initial value normalized to a reference quantity. Used to normalize variables and parameters to account for large variation in their initial magnitude. |

There are exceptions to these general rules as noted below. Each term in the momentum equations is normalized in the following:

### A.3.2.6 Nondimensional Momentum Equations

The three sets of momentum equations can be normalized and nondimensionalized and written in matrix form.

### A.3.2.7 Specialization of Groups

Appropriate values for reference parameters (i.e., those parameters having the subscript "r") have to be selected for each operating phase (e.g., the Blowdown Phase, the GDCS Phase and PCCS Phase). Also, initial values (i.e., those with subscript "o") need to be selected in principle such that the variables and thei: derivations are of the order of one or 0(1). The reference values are selected and substituted in the nondimensional groups.

## A.4 References

[1] *Analysis of SBWR Passive Containment Cooling Following a LOCA*, Viewrow, K.M., Fitch, J.R., and Cooke F.E., Proc. Int. Conf. on the Design and Safety of Advanced Nuclear Power Plans, 25-29 October 1992, Tokyo, Japan, Vol. III, pp 31.2.1-7.

[2] *SBWR Loss-of-Coolant Accident Analysis*, Paradiso, F.M, Yang, A.I., and Sawyer, C.D., Proc. 2nd ASME-JSME Nuclear Engineering Joint Conference, 21-24 March 1993, San Francisco, CA, Vol. 1, pp. 313-318.

[3] *Simplified Boiling Water Reactor Passive Safety Features*, Upton, H.A., Cooke, F.E., Sawabe, J.K., Proc. 2nd ASME-JSME Nuclear Engineering Joint Conference, 21-24 March 1993, San Francisco, CA, Vol. 1, pp. 705-712.

[4] Personal Communication, Wulff, W., 1995.

# Appendix B — Mass Energy and State Formulations

## Table of Contents

## List of Figures

## B.1 Introduction

This appendix contains the detailed formulations for the mass, energy, state (or pressure rate), two-phase level and vapor fraction in control volumes. The resulting dimensional and nondimensional equations are summarized in Section 2. The results of applying these equations to the various systems (SBWR, GIST, GIRAFFE and PANDA) are discussed in Section 4 along with the results of the momentum equations developed in Appendix A and the bottom-up formulations developed in Section 3.

## B.2 Formulations

Consider the control volume V of Figure B.2-1 containing a mass M with internal energy E at a pressure p and a temperature T. The volume contains a number of constituents (noncondensible gases, steam-water, etc.). Any changes in the kinetic and potential energy of the mass M are much smaller than changes in its intrinsic internal energy and therefore are neglected. The system is well mixed (i.e., the distributions of constituents and of the temperature are uniform, and at thermodynamic equilibrium).

### B.2.1 Mass Continuity Equation

The *total-mass* continuity equation for this volume is:

$$\frac{dM}{dt} - \sum_i W_i = 0 \qquad \text{(B.2.1-1)}$$

where $W_i$ represents the total (steam-water, noncondensibles, etc.) mass flow rates entering the volume.

A containment volume may contain a mixture of steam, water and noncondensibles. To simplify the following analysis, a saturated mixture of steam and water and a noncondensible gas will be considered as the two constituents (subscript j). This avoids the difficulty of having to consider phase changes between steam and water at this point. With this definition of constituents, the mass conservation equation for *constituent j* is

$$\frac{dM_j}{dt} - \sum_i W_{i,j} = 0 \qquad \text{(B.2.1-2)}$$

or

$$\frac{d}{dt}(V\rho_j) - \sum_i W_i y_{i,j} = 0 \qquad \text{(B.2.1-3)}$$

In these equations, $M_j$ is the mass of constituent j in the volume considered,

$$M_j = V\rho_j \qquad \text{(B.2.1-4)}$$

with

$$\rho_j = \rho y_j \tag{B.2.1-5}$$

where $\rho_j$ is the partial density, and $y_j$ the mass fraction of constituent j, with

$$\sum y_j = 1 \tag{B.2.1-6}$$

Similarly, $W_{i,j}$ is the mass flow rate of constituent j in the stream i:

$$W_{i,j} = W_i y_{i,j} \tag{B.2.1-7}$$

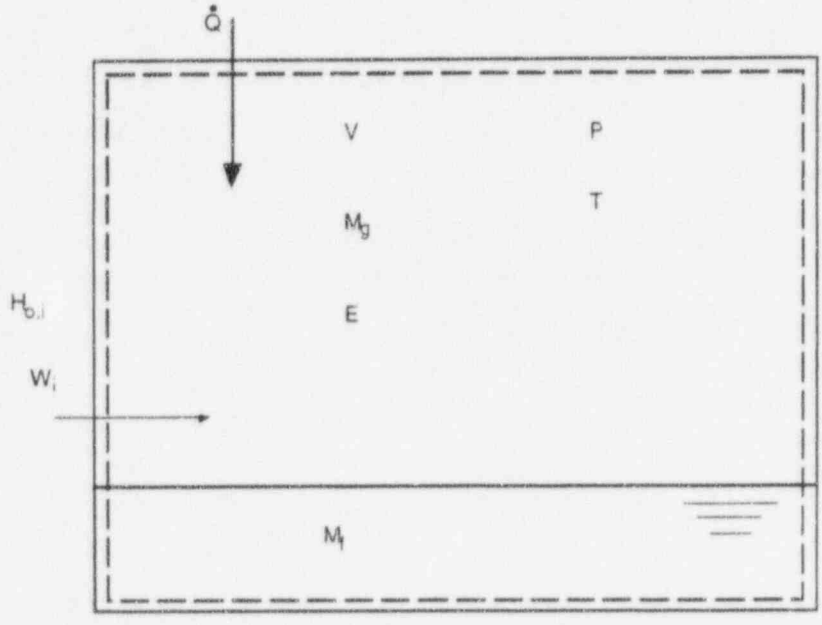


Figure B.2-1. A Containment Volume Receiving Mass Flow Rates $W_i$ with Corresponding Total Emphalpies $H_{0,j}$, and Heat at the Rate $\dot{Q}$

### B.2.2 Energy Equation

The energy conservation equation is:

$$\frac{dE}{dt} = -p\frac{dV}{dt} + \dot{Q} + \sum W_i h_{o,i} \qquad \text{(B.2.2-1)}$$

where $\dot{Q}$ is the heat added to the system (e.g., by conduction through the wall), and $h_{o,j}$ is the total specific enthalpy of stream i. The total enthalpy (subscript o) includes the kinetic and potential energy. For cases where the control volume does not include the liquid region, *phase changes* taking place at interfaces bounding the control volume are considered in the $\sum W_i$ and $\sum W_i h_{o,i}$ terms, since these bring flows of mass and enthalpy into the control volume.

The purpose here is to derive the equation relating the rate of change of the volume pressure dp/dt to the mass, enthalpy and heat additions (see, e.g., Section 2.14 of [1]*). The specific internal energy of the system,

$$e = \frac{E}{M} \qquad \text{(B.2.2-2)}$$

is a function of two thermodynamic variables, chosen here to be the pressure and the specific volume v = V/M, and of the mass fractions $y_j$ of the various constituents:

$$e = e(p,v,y_j) \qquad \text{(B.2.2-3)}$$

The differential of e can be calculated as:

$$de = \left.\frac{\partial e}{\partial p}\right|_{v,y_j} dp + \left.\frac{\partial e}{\partial v}\right|_{p,y_j} dv + \sum \left.\frac{\partial e}{\partial y_j}\right|_{p,v,y} dy_j \qquad \text{(B.2.2-4)}$$

where the subscript $y_j$ means that all $y_j$ are kept constant, while the subscript y denotes that all $y_j$ except the one appearing in the partial derivative are kept fixed. We note also that

$$E = Me \text{ and } V = Mv$$

and therefore

$$\frac{dE}{dt} = \frac{d}{dt}(Me) = M\frac{de}{dt} + e\frac{dM}{dt} \qquad \text{(B.2.2-5)}$$

$$\frac{dV}{dt} = M\frac{dv}{dt} + v\frac{dM}{dt} \qquad \text{(B.2.2-6)}$$

* References for Appendix B are in Section B.6.

Combining Equations B.2.1-1 and B.2.2-1 through B.2.2-6:

$$\frac{dE}{dt} = M\frac{\partial e}{\partial p}\bigg|_{v,y_j}\frac{dp}{dt} + M\frac{\partial e}{\partial v}\bigg|_{p,y_j}\frac{dv}{dt} + M\sum_j \frac{\partial e}{\partial y_j}\bigg|_{p,v,y}\frac{dy_j}{dt} + e\sum_i W_i$$
$$= -p\frac{dV}{dt} + \dot{Q} + \sum_i W_i h_{o,i} \qquad \text{(B.2.2-7)}$$

Also, combining Equations B.2.1-1, B.2.2-1 and B.2.2-5, we get an equation for the specific energy

$$M\frac{de}{dt} = -p\frac{dV}{dt} + \dot{Q} + \sum W_i h_{o,i} - e\sum W_i \qquad \text{(B.2.2-8)}$$

Using the relationship, h = e+pv, we get the alternate form

$$M\frac{de}{dt} = -p\frac{dV}{dt} + \dot{Q} + \sum W_i\left(h_{o,i} - h_o\right) + {}^{p}\!/\!_{\rho}\sum W_i \qquad \text{(B.2.2-9)}$$

### B.2.3 Pressurization Rate or State Equation

Solving Equation B.2.2-7 for dp/dt and using again Equations B.2.2-6 and B.2.1-1:

$$\frac{V}{v}\frac{\partial e}{\partial p}\bigg|_{v,y_j}\frac{dp}{dt} = \sum_i\left[W_i\left(h_{o,i} - e + v\frac{\partial e}{\partial v}\bigg|_{p,y_j}\right)\right] + \dot{Q} - \left[p + \frac{\partial e}{\partial v}\bigg|_{p,y_j}\right]\frac{dV}{dt} - \frac{V}{v}\sum_j\left[\frac{\partial e}{\partial y_j}\bigg|_{p,v,y}\frac{dy_j}{dt}\right] \qquad \text{(B.2.3-1)}$$

This can also be written as,

$$\frac{V}{v}\frac{\partial e}{\partial p}\bigg|_{v,y_j}\frac{dp}{dt} = \sum_i W_i\left(h_{o,i} - h\right) + \sum_i W_i\left(pv + v\frac{\partial e}{\partial v}\bigg|_{p,y_j}\right) + \dot{Q} - \left[p + \frac{\partial e}{\partial v}\bigg|_{p,y_j}\right]\frac{dV}{dt} - \frac{V}{v}\sum_j\left[\frac{\partial e}{\partial y_j}\bigg|_{p,v,y}\frac{dy_j}{dt}\right] \qquad \text{(B.2.3-2)}$$

We note that this equation yields the rate of change of the pressure in terms of heat addition, mass and enthalpy fluxes into the volume, and changes of volume composition. The rate of change of the volume dV/dt (e.g., due to phase change if the equation is applied to the gas space above a liquid level) is also considered. The partial derivatives of e with respect to v, p and the mass fractions $y_j$, as well as their combinations with other thermodynamic variables, are *thermodynamic properties* of the particular mixture contained in the volume. Thus, the following short-hand notations for certain quantities appearing in Equation B.2.3-2,

$$p^* \equiv p + \left.\frac{\partial e}{\partial v}\right|_{p, y_j}$$

(B.2.3-3)

$$f_{1,j} \equiv \frac{1}{v}\left.\frac{\partial e}{\partial y_j}\right|_{p, v, y} \quad \text{(units of energy per unit volume)}$$

$$f_2 \equiv \frac{1}{v}\left.\frac{\partial e}{\partial p}\right|_{v, y_j} \quad \text{(non-dimensional "system compliance")}$$

denote thermodynamic properties of the mixture, which are functions of p, v, and the $y_j$ (these could also be defined as functions of p and $\alpha$ in the case of a saturated mixture).

Thus, Equation B.2.3-2 takes the simpler form,

(B.2.3-4)

$$V f_2 \frac{dp}{dt} = \sum_i \left[ W_i \left( h_{o,i} - h_o \right) \right] + \sum_i W_i p^* / \rho + \dot{Q} - p^* \frac{dV}{dt} - V \sum_j \left[ f_{1,j} \frac{dy_j}{dt} \right]$$

The enthalpies $h_o$ appearing in the energy conservation and state equations (Equations B.2.2-9 or B.2.3-4) are total specific enthalpies (i.e., the sum of the intrinsic specific enthalpy of the fluid plus its kinetic and potential energies). Consequently, the exact scaling of these would have required separate consideration of specific enthalpy, velocity, and elevation scales. Since changes in kinetic and potential energy are very small or totally negligible, this complication can be avoided by neglecting the kinetic and potential energy terms. Thus, in the following, the $h_{o,i}$ are replaced by $h_i$.

### B.2.4 Vapor Mass Fraction Equations

When the control volume under consideration contains a saturated steam-water mixture, the thermodynamic properties in the energy and pressurization rate equations are dependent on the ratio of liquid to vapor mass. The equation for the vapor mass fraction is developed here for that purpose.

From the vapor phase mass balance

(B.2.4-1)

$$\frac{dM_g}{dt} = \sum_i W_{g,i} + \dot{M}_{fg}$$

Since $M_g = \alpha \rho_g V$, this can be written (for a fixed volume) as:

(B.2.4-2)

$$\frac{d(\alpha \rho_g)}{dt} = \frac{1}{V} \sum_i W_{g,i} + \Gamma$$

where $\Gamma$ is the volumetric net vapor generation

(B.2.4-3)

$$\Gamma = \frac{\dot{M}_{f_g}}{V}$$

We can expand Equation B.2.4-2 to:

(B.2.4-4)

$$\rho_g \frac{d\alpha}{dt} = \frac{1}{V} \sum_i W_{g,i} + \Gamma - \alpha \frac{d\rho_g}{dp} \frac{dp}{dt}$$

where $\frac{d\rho g}{dt}$ has been replaced by $\frac{d\rho_g}{dp} \frac{dp}{dt}$ .

To use this equation, some representation of the net vapor generation is needed. The energy and continuity equations can be combined to obtain the net vapor generation in the form [5]:

$$\dot{M}_{f_g} = \frac{1}{h_{fg}} \dot{Q} + \frac{1}{h_{fg}} \sum_i (h_{\ell,i} - h_f)\ W_{\ell,i} + \frac{1}{h_{fg}} \frac{dp}{dt} \left[ V - \left( M_f \frac{dh_f}{dp} + M_g \frac{dh_g}{dp} \right) \right] \quad \text{(B.2.4-5)}$$

or

$$\Gamma = \frac{\dot{Q}}{h_{fg} V} + \frac{1}{h_{fg}} \frac{1}{V} \sum_i \left( h_{\ell,i} - h_f \right) W_{\ell,i} + \frac{1}{h_{fg}} \frac{dp}{dt} \left[ 1 - \frac{M_f}{V} \frac{dh_f}{dp} + \frac{M_g}{V} \frac{dh_g}{dp} \right] \quad \text{(B.2.4-6)}$$

Using Equation B.2.4-6 above for the vapor generation term, Equation B.2.4-4 becomes:

$$\rho_g \frac{d\alpha}{dt} = \frac{1}{V} \sum_i W_{g,i} + \frac{\dot{Q}}{h_{fg} V} + \frac{\sum_i \left( h_{\ell,i} - h_f \right)\ W_\ell}{h_{fg} V}$$

(B.2.4-7)

$$+ \frac{1}{h_{fg}} \frac{dp}{dt} \left[ 1 - \frac{M_f}{V} \frac{dh_f}{dp} - \frac{M_g}{V} \frac{dh_g}{dp} \right] - \alpha \frac{d\rho_g}{dp} \frac{dp}{dt}$$

Rearranging and writing the liquid and vapor mass in terms of $\alpha$ yields:

$$\rho_g \frac{d\alpha}{dt} = \frac{1}{V}\sum_i W_{g,i} + \frac{\sum_i \left(h_{\ell,i} - h_f\right) W_{\ell,i}}{h_{fg}V} + \frac{\dot{Q}}{h_{fg}V}$$

$$+ \frac{1}{h_{fg}} \frac{dp}{dt}\left[1-(1-\alpha)\,\rho_f h_f' - \alpha\rho_g h_g' - \alpha h_{fg}\rho_g'\right] \quad \text{(B.2.4-8)}$$

where the notation $x' = \frac{dx}{dp}$ has been used. To simplify write as:

$$\rho_g \frac{d\alpha}{dt} = \frac{1}{V}\sum_i W_{g,i} + \frac{\sum_i \left(h_{\ell,i} - h_f\right) W_{\ell,i}}{h_{fg}V} + \frac{\dot{Q}}{h_{fg}V} + \frac{\psi}{h_{fg}}\frac{dp}{dt} \quad \text{(B.2.4-9)}$$

where

$$\psi = 1-(1-\alpha)\,\rho_f h_f' - \alpha\rho_g h_g' - \alpha h_{fg}\rho_g' \quad \text{(B.2.4-10)}$$

## B.3 Nondimensionalization

We will now nondimensionalize Equations B.2.1-1, B.2.1-2, B.2.2-9, B.2.3-4 and B.2.4-9 using the following reference quantities (denoted by the subscript r):

- For time: $t_r$
- For volume: $V_r$
- For flow rates: $W_r$
- For heat addition: $\dot{Q}_r$
- For densities: $\rho_r$
- For pressure, a reference pressure difference: $\Delta\rho_r$
- For enthalpies, a reference specific enthalpy difference: $\Delta h_r$

The minimal set of scales needed and defined above will be supplemented by an additional number of scales for

- Mass: $M_r$ or $\Delta M_r$

- Volume changes: $\Delta V_r$
- Absolute pressure: $P_r$
- Internal energy change: $\Delta e_r$
- The f2 parameter: $f_{2,r}$
- The f1,j parameter: $f_{1,j,r}$
- The corrected pressure p*: $p^*_r$
- The y parameter: $\psi_r$ (Equation B.2.4-10)
- Concentration of constituent j: $y_{j,r}$
- For changes in concentration of constituent j: $\Delta y_{j,r}$

The purpose of defining additional scales will become apparent when the nondimensional variables are *locally* further normalized using ratios of scales to arrive at *nondimensional* terms of order one.

The equations will be nondimensionalized by dividing the dimensional variables z by the reference values $z_r$ above; this produces the nondimensional variables $z^+$:

$$z^+ \equiv \frac{z}{z_r} \tag{B.3-1}$$

In particular, note that

$$h_f - h_\ell = h_{sub} = h_{sub,r}\ h^+_{sub}$$

$$h_i - h = h^+ \Delta h_r$$

$$p^* = p^* + \Delta p_r$$

$$f_{l,j} = f^+_{l,j}\ \Delta h_r \rho_r$$

$$f_2 = f_2^+\ \frac{\rho_r \Delta h_r}{\Delta p_r} \tag{B.3-2}$$

$$y_j = y_j^+\ \ y_{j,r}$$

$$dy_j = dy_j^{\dagger} \Delta y_{j,r}$$

In summary, the preceding analysis reveals the presence of five independent nondimensional numbers and a natural time scale for the system, $t_r$. Identical values for these nondimensional numbers should be maintained in the prototype and model.

## B.4 Case of a Perfect Gas

In the case of a pool that is not in thermal equilibrium with the gas space, the control volume can be taken as the gas space only. The pool then becomes an additional source of mass and energy. Also, changes in the pool level result in changes in the control volume size.

## B.5 Phase Changes at Interfaces

The phase changes at interfaces involve the latent heat of vaporization and the interfacial mass flow rates and mass fluxes. These are considered in this section.

### B.5.1 Latent Heat of Vaporization

Time scale for enthalpy changes will be obtained by considering mass continuity in a volume where phase change and mass transfers are taking place. Figure B.5-1 shows such a volume consisting of the gas space with a mass M:

$$M = V \sum_i \rho_j \qquad \text{(B.5-1)}$$

where $\rho_j$ are the partial densities of the constituents. For simplicity, consider a saturated mass of liquid vaporized by a heater providing power at the rate $\dot{Q}$. A mass flow rate $W_{ex}$ leaves the vapor space of the system. Mass continuity for the vapor space results in:

$$\frac{dM}{dt} = W_{LG} - W_{ex} \qquad \text{(B.5-2)}$$

where $W_{LG}$ is the mass transfer rate by boiling given by

$$W_{LG} = \frac{\dot{Q}}{h_{fg}} \qquad \text{(B.5-3)}$$

### B.5.2 Rates of Phase Change

In the SBWR containment volumes, phase changes typically take place at the free surface of pools and on the walls. Condensation on structures and walls is limited by conduction within the structure and, therefore, depends strongly on the conduction characteristics of the walls. As already noted, conduction in the SBWR structures cannot easily be simulated by the experimental facilities. It is left as an experimental parameter that must be addressed by measurement and detailed numerical calculations during data reduction.

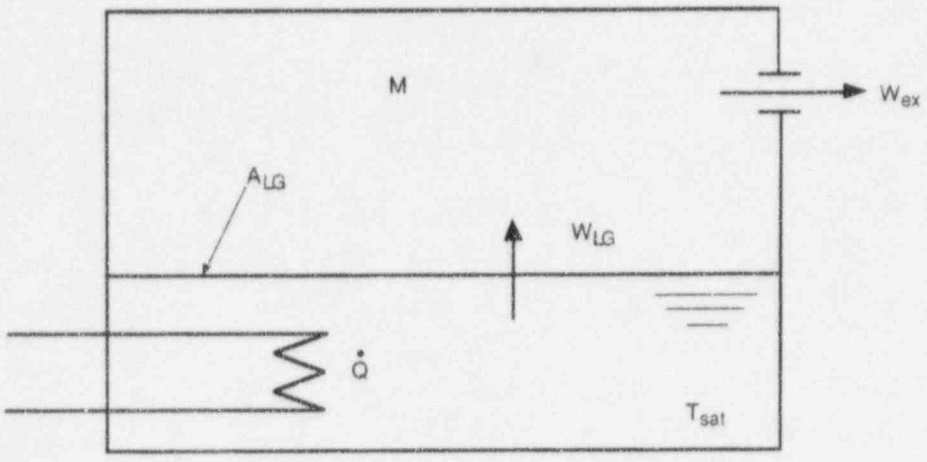


Figure B.5-1. A Volume Containing a Pool of Boiling Water

## B.6 References

[1] *Introduction to Unsteady Thermofluid Mechanics*, Moody, F.J., John Wiley & Sons, New York, 1990.

[2] *Hierarchical, Two-Tiered Scaling Analysis Appendix D to An Integrated Structure and Scaling Methodology for Severe Accident Technical Issue Resolution*, Zuber, N., Nuclear Regulatory Commission Report NUREG/CR-5809, EGG-2659, November 1991.

[3] *Fundamental and Higher-Mode Density-Wave Oscillations in Two-Phase Flow*, Yadigaroglu, G. and Bergles, A.E., J. Heat Transfer, 94, 189-195, 1972.

[4] *An Experimental Investigation of the Thermally Induced Flow Oscillations in Two-Phase Systems*, Saha, P., Ishii, M., and Zuber, N., J. Heat Transfer, 98, 616-622, 1976.

[5] *The Thermal Hydraulics of a Boiling Water Nuclear Reactor*, Lahey, R.T., Moody, F.J., American Nuclear Society, Second Edition, 1993.

[6] *Variation of the Vapor Volumetric Fraction During Flow and Power Transients*, Shiralkar, B.S., Schnebly, L.E., and Lahey Jr., R.T., Nuclear Eng. and Design, 25, 350-368, 1973.

# Appendix C— Analysis of Liquid Level Movements in the SBWR

## Table of Contents

## List of Figures

## Nomenclatures and Abbreviations

| Symbols | Description | Units |
|---|---|---|
| a | Cross-sectional area of drain line | $m^2$ |
| $A_r$ | Surface area of RPV | $m^2$ |
| $A_p$ | Surface of water pools | $m^2$ |
| $A'$ | Free surface parameter (Eq. C.4-10) | $m^2$ |
| $C_1C_2$ | Constants in homogeneous solution (Eq. C.4-36c) | m |
| c | Damping coefficient in equation of motion (Eq. C.4-23) | kg/s |
| E | Friction loss term | J |
| f | Fanning friction factor | * |
| F | Sum of loss coefficients (Eq. C.4-17) | * |
| H | Final Static defection | m |
| h | Drain line displacement | m |
| $h_r$ | RPV level displacement | m |
| $h_p$ | Pool level displacement | m |
| g | Acceleration of gravity | 9.81 $m/s^2$ |
| k | Coefficient in equation of motion (Eq. C.4-22) | $kg/s^2$ |
| k | Form loss coefficient | * |
| l | Length variable | m |
| $L_r$ | Height of RPV water column | m |
| $L_p$ | Height of pool water column | m |
| L | Length of drain line | m |
| m | Coefficient in equation of motion (Eq. C.4-22) | kg |
| N | Number of drain lines | * |
| $P_r$ | RPV Pressure | $N/m^2$ |
| $P_p$ | Pool pressure | $N/m^2$ |
| R | Drain line pipe radius | m |
| $R_r$ | RPV radius | m |
| $R_p$ | Pool radius | m |
| t | Time | s |
| S1, S2 | Homogeneous equation roots (Eq. C.4-25) | l/s |
| S | Shape factor (Eq. C.4-4) | * |
| V | Drain line velocity | m/s |
| $v_r$ | RPV surface movement velocity | m/s |
| $v_p$ | Pool surface movement velocity | m/s |
| V | Volume | $m^3$ |
| W | Mechanical work term | J |
| z | General displacement variable | m |

**Greek Letters**

| Symbols | Description | Units |
|---|---|---|
| $\xi = c/c_c$ | Damping ratio | * |
| $\kappa_{tot}$ | Fluid kinetic energy | J |
| $\Phi_{tot}$ | Fluid potential energy | J |
| $\varphi$ | Phase angle (Eq. C.4-34b) | rad. |
| $\mu$ | Viscosity | kg/m s |
| $\Pi$ | Nondimensional group | * |
| $\rho$ | Density | $kg/m^3$ |
| $\omega$ | Imposed angular frequency | rad/s |
| $\omega_n$ | Natural angular frequency | rad/s |
| $\tau$ | Imposed cycle time period | s |

**Subscripts**

| | |
|---|---|
| p | Pool |
| r | RPV |
| c | Critical |
| n | natural |

Additional subscripts are defined in the text

**Superscripts**

| | |
|---|---|
| . | Denotes derivative with respect to time |
| + | Nondimensional variable |

**Abbreviations**

| | |
|---|---|
| GDCS | Gravity-Driven Cooling System |
| LOCA | Loss-of-Coolant Accident |
| PCC | Passive Containment Condenser |
| RPV | Reactor Pressure Vessel |
| SBWR | Simplified Boiling Water Reactor |
| SP | Suppression Pool |

## C.1 Introduction

In the Simplified Boiling Water Reactor (SBWR), there may be situations where water drains from one pool to another via connecting drain line pipes. For example, this situation occurs when water contained in the Gravity-Driven Cooling System (GDCS) pool drains into the Reactor Pressure Vessel (RPV) via one or more GDCS drain line pipes if such emergency core cooling should be required for a Loss-of-Coolant Accident (LOCA) or other line break accidents. The other situation may occur if the water level in the RPV drops so low that makeup water is required to drain from the Suppression Pool (SP) via one or more equalization drain pipes.

Concerns have been expressed that water level oscillations may occur in these situations when a disturbance in the form of a pressure change occurs above one of the water masses. The pressure change may be in the form of a step change in the pressure which could result in free, undamped oscillations in the system water levels that might persist for a time before eventually dying out and new equilibrium water levels are reached. The other situation that might arise is that of a periodically varying pressure above one of the water pools that may excite the system at a resonance such that large magnification of the imposed pressure function may occur.

A dynamic model for such a system was developed to evaluate its fundamental characteristics. This report presents the results of the study. More specifically, the two physical systems considered are described briefly in Section C.3 and the basis for the model development and the derivations, along with definitions and analytic solutions, are given in Section C.4. The analysis results and interpolation thereof are given in Section C.5. The key parameter governing system behavior is derived in Section C.6 by nondimensionalizing the equation of motion for the system.

## C.2 Summary

The key result of the study is that the drain lines with relatively small cross-sectional flow areas tend to damp-out level oscillations between the large water masses because of the high impedance or hydraulic resistance of the connecting drain lines. For the specific SBWR configurations considered, it was found that these systems are overdamped wherever the pressure step change or harmonic input magnitude was greater than about 0.5m head pressure equivalent. For pressure changes of less than 0.3m head equivalent, the systems may be underdamped and small amplitude, low frequency oscillations may occur. The larger the pressure change, the more overdamped and stable the systems are. This is because larger pressure changes produce larger flow velocities and the wall friction and the damping coefficient increase with the flow velocity in the connecting pipes.

Natural cycle times for the basic systems considered and configuration variations considered to evaluate alternative operating modes and parameter uncertainties, varied by a factor of about three. The liquid level amplitude resulting from an harmonic forcing function input was less than that of the input function corresponding to the zero frequency or step change input function because the magnification factor was less than unity for the overdamped system. This was the case even when the imposed forcing function frequency was equal to that of the natural system frequency.

The equation of motion was nondimensionalized using the system natural time period as the normalizing time interval, and the imposed pressure difference as the normalizing displacement. The results showed that only one important nondimensional group appears in the equation. This group contained the damping ratio (i.e., the actual damping coefficient divided by the critical damping coefficient, as a variable). The damping ratio must be greater than unity to assure that

level oscillations do not occur. The criteria and methodology developed here can be applied to evaluate the stability of other, similar systems.

## C.3 Description of Systems

The two situations identified in the SBWR where water level oscillations might occur are pictured schematically in Figures C.3-1 and C.3-2. Brief descriptions of these situations and associated components are made for each in the following.

### C.3.1 RPV/GDCS Pool System

This system consists of the RPV, three GDCS pools and three GDCS drain lines connecting each of the GDCS pools with the RPV. Each of the GDCS pools may consist of several individual connected pools considered as a common pool. Each of the drain lines consists of a relatively long 9-inch (0.229m) diameter pipe section which branches into two shorter 6-inch (0.152m) diameter sections before entering the RPV. The drain line is treated as a 9-inch line in the analysis with appropriate hydraulic effects of the branching accounted for in the line loss coefficient. All drain lines contain check valves that limit reverse flow from the RPV to the GDCS pool. However, the presence of the check valves is conservatively ignored in this analysis except when the forward flow resistance is calculated. The analysis considers the possibility that not all drain lines are activated at the same time. Rather, one, two or three lines may be activated.

The drain lines enter the RPV above the top of core level, as indicated schematically in Figure C.3-1. The liquid within the RPV is assumed to move as one mass because the core pressure drop is very small with the low velocities in the vessel compared to that in the drain line. Thus, the effective water column in the RPV initially has a height of $L_r$ and a diameter of $A_r$, as indicated in Figure C.3-1*.

The liquid levels in both the RPV and GDCS pools are shown to be at the same level initially (t=0). A disturbance in the RPV pressure, $P_r$ (e.g., in the form of a step increase), will displace the level downward a distance H+K, as indicated in Figure C.3-1. The lowest liquid level reached is taken as z=0 in the analysis. The distance H is the permanent displacement in the liquid level resulting from a step change in RPV pressure equivalent to that of H. The liquid surface areas of the RPV and GDCS pools are generally different and are much greater than the flow areas of the GDCS drain line pipes. Accordingly, the magnitude of the displacements in each of these can be quite different from each other from mass continuity considerations.

### C.3.2 RPV/SP System

The RPV/SP system considered is shown schematically in Figure C.3-2. The RPV configuration is the same as that of the RPV/GDCS pool system except that the water level is much lower. The SP is one single pool of water with a very large surface area compared to that of the RPV. The equalization drain lines consist of three 6-inch (0.152m) diameter pipes with appropriate flow control valves. The drain lines are only about one half the length of the corresponding GDCS drain lines. The liquid levels in the RPV and in the SP are pictured as being equal just prior to initiation of a transient.

* Refer to the Nomenclature and Abbreviation Section for explanation of symbols.

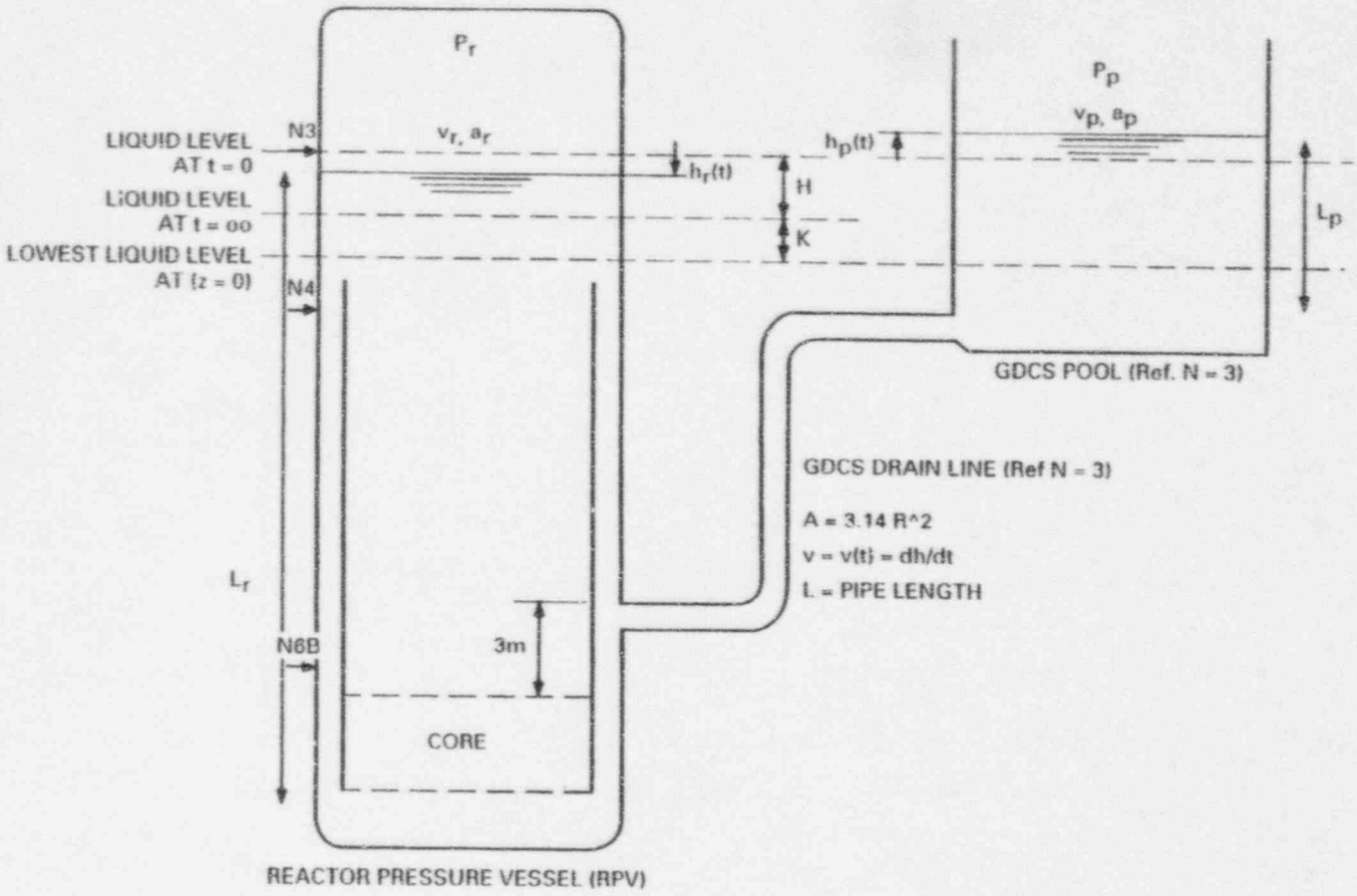


Figure C.3-1. RPV/GDCS Pool Configuration Modeled

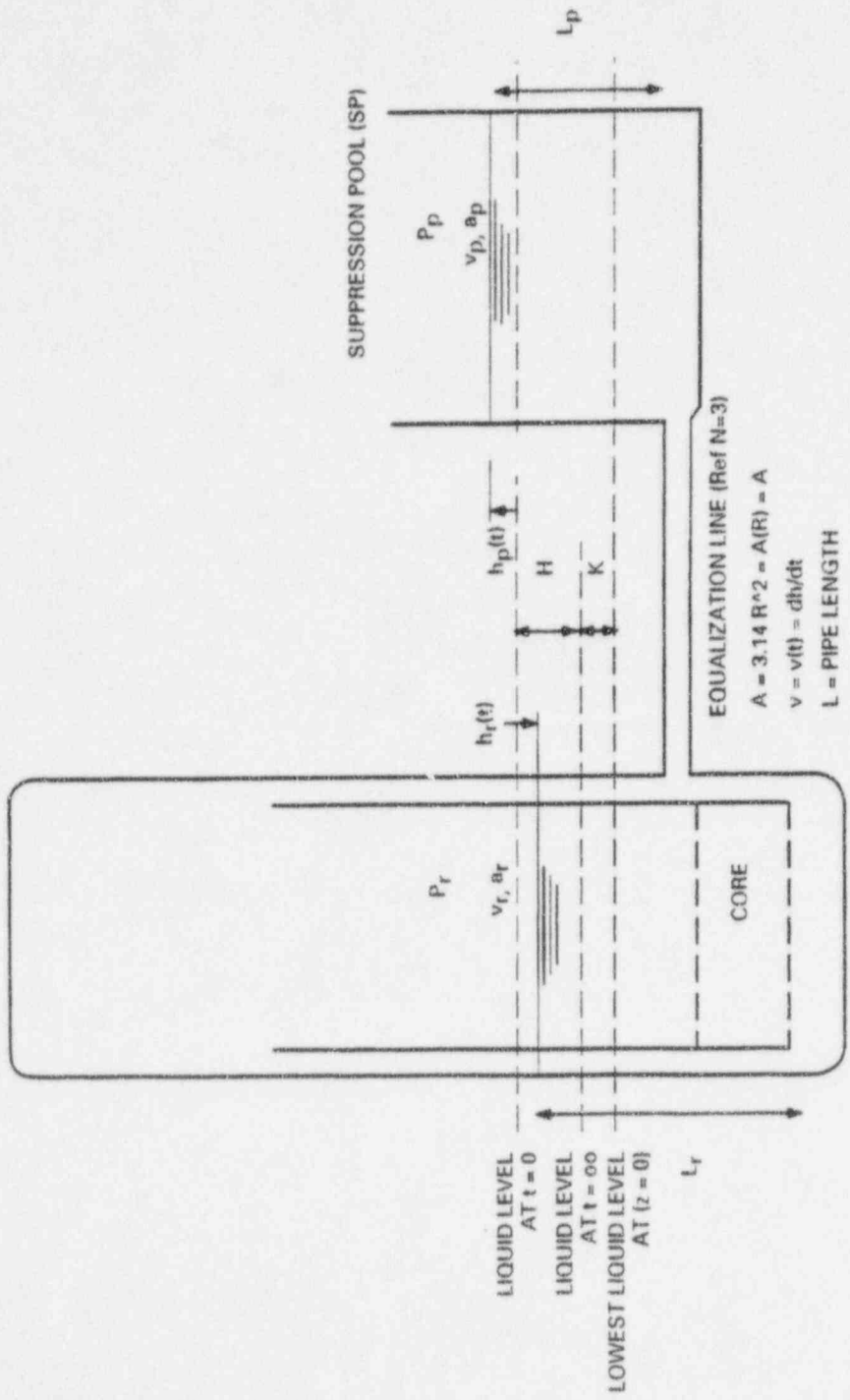


Figure C.3-2. RPV/Suppression Pool Configurtaion Modeled

## C.4 Equation of Motion

In this section the general equation of motion for level movements in two connected water pools is derived. The analysis approach and the major analysis assumptions are stated. The general solutions for the various boundary conditions are given.

### C.4.1 Major Analysis Assumptions

The equation of motion for the liquid contained in a frictionless U-tube of uniform cross-section was derived and described in the classical textbook on mechanical vibration by Thomson [1].[1] A similar problem was treated by Bird, Stewart, and Lightfoot [2] as a fluid mechanics problem and these authors included viscous dissipation within the fluid but no wall friction. The general approach followed in the present analysis is that given by Bird et al. [2], but the present analysis includes both viscous dissipation within the fluid and wall friction in the connecting line, and the "U-tube" considered here has greatly unequal flow areas on each free surface.

In the analysis it was necessary to make a number of major simplifying assumptions to reveal the essential characteristics of the system in a simple form. The validity of most of these assumptions has been checked out by supplementary analysis and found to be acceptable, as explained in Section C.5. The major assumptions made in the analysis are as follows:

- Pressure perturbations in RPV or DW initiate level movements.
- Fluid particles within each component (e.g., RPV, GDCS drain line, GDCS pools) move at the same speed in that component.
- Identical GDCS drain lines and pools act in parallel in order to maximize displacements.
- Constant water properties throughout the system.
- Each drain line has constant cross-sectional area (i.e., slight area change resulting from branching of each GDCS drain line into two near the RPV is ignored).
- Fluid at rest initially.
- Ignore friction and other losses in RPV and GDCS pools (i.e., line friction losses are dominant due to relatively higher velocities).
- Pipe friction and form loss factors are proportional to the square of velocity.
- Pipe and form loss factor summation from TAPD is used for loops and assumed to be constant as velocity changes.
- Damping coefficient in a GDCS loop is calculated using average fluid velocity for transient.
- No heat generation or losses.

[1] References cited in is appendix are listed in Section C.8.

### C.4.2 Derivation of Equation of Motion

The problem considered in the analysis and most of the symbols used are shown in Figure C.3-1. Other symbols are given in the Nomenclature at the beginning of this appendix, or they are defined in the text. The problem considered assumes for simplicity that the liquid levels in each connected pool are the same initially and the fluid in all regions is at rest initially. Unequal levels and non-zero initial flow velocities can be introduced via the initial conditions as explained later.

Derivation of the equation of motion follows the energy approach used by Bird et al. ([2], pp. 229-231) with modifications. The simplified energy equation for the system fluid is written as,

$$\frac{d}{dt}\left(\kappa_{tot} + \phi_{tot}\right) = -W - E \qquad \text{(C.4-1)}$$

where

| | | |
|---|---|---|
| $\kappa_{tot}$ | = | total kinetic energy of the fluid |
| $\phi_{tot}$ | = | total potential energy of the fluid |
| W | = | rate at which the fluid system performs mechanical work on its surroundings |
| E | = | "friction loss" (i.e., rate at which mechanical energy is converted to thermal energy) |

Each of the terms in Equation C.4-1 is evaluated in the following.

**Kinetic Energy**

The fluid system shown in Figure C.3-1 is visualized to be set in motion by a pressure perturbation in the RPV. The resulting displacement for the case of a sudden increase in the RPV pressure $P_r$ is indicated by the symbol $h_r(t)$ in Figure C.3-1 along with the corresponding displacements and velocities in the other components (i.e., the GDCS drain line and pool). The kinetic energy for the fluid is given by

$$\kappa_{tot} = \int_0^{V_r} \frac{1}{2}\rho v_r^2 dV + N\int_0^{V} \frac{1}{2}\rho v^2 dV + N\int_0^{V_p} \frac{1}{2}\rho v_p^2 dV \qquad \text{(C.4-2a)}$$

where N is the number of GDCS pools and drain lines activated (i.e., N=1, 2, or 3). Note that symbols without subscripts (e.g., v, V, L and A) apply to the connecting drain line. The integrals in Equation C.4-2a can be evaluated and written as,

$$\kappa_{tot} = \frac{1}{2}\rho\left(v_r^2 A_r L_r + v^2 NAL + v_p^2 NA_p L_p\right) \qquad \text{(C.4-2b)}$$

From mass continuity, vr and vp can be expressed in terms of the drain line velocity v, since

$$\dot{m} = \rho v_p N A_p = \rho v N = \rho v_r A_r \tag{C.4-3a}$$

and,

$$v_p = v\frac{NA}{NA_p} = v\frac{A}{A_p} \tag{C.4-3b}$$

$$v_r = v\frac{NA}{A_r} \tag{C.4-3c}$$

Substituting these into Equation C.4-2b gives,

$$\begin{aligned}\kappa_{tot} &= \frac{1}{2}\rho v^2\left[\left(\frac{NA}{A_r}\right)^2 A_r L_r + NAL + \left(\frac{A}{A_p}\right)^2 NA_p L_p\right] \\ &= \frac{1}{2}\rho LAv^2\left[N^2\left(\frac{A}{A_r}\right)\left(\frac{L_r}{L}\right) + N + N\left(\frac{A}{A_p}\right)\left(\frac{L_p}{L}\right)\right] \\ &= \frac{1}{2}\rho LASv^2\end{aligned} \tag{C.4-3d}$$

where S is a geometric shape factor defined by,

$$S = \left[N^2\left(\frac{A}{A_r}\right)\left(\frac{L_r}{L}\right) + N + N\left(\frac{A}{A_p}\right)\left(\frac{L_p}{L}\right)\right] \tag{C.4-4}$$

The time derivation of $\kappa_{tot}$ required in Equation C.4-1 becomes,

$$\frac{d\kappa_{tot}}{dt} = \rho LASv\dot{v} \tag{C.4-5}$$

**Potential Energy**

In evaluating this term, the notation shown in Figure C.3-1 is used. It is seen that the lowest liquid level reached in the RPV is taken to be at z=0. The potential energy of the fluid is obtained by an integration of displacement times volume above this level for both the RPV and GDCS pool, or,

$$\begin{aligned}\phi_{tot} &= \rho g \int_0^V z\,dV \\ &= \rho g A_r \int_0^{K+H-h_r} z\,dz + \rho g N A_p \int_0^{K+H+h_p} z\,dz \\ &= \frac{1}{2}\rho g A_r z^2 \Big|_0^{K+H-h_r} + \frac{1}{2}\rho g N A_p z^2 \Big|_0^{K+H+h_p} \\ &= \frac{1}{2}\rho g A_r\left[(K+H-h_r)^2 - 0\right] + \frac{1}{2}\rho g N A_p\left[(K+H+h_p)^2 - 0\right] \\ &= \frac{1}{2}\rho g A_r\left[(K+H)^2 - 2(K+H)h_r + h_r^2\right] \\ &\quad + \frac{1}{2}\rho g N A_p\left[(K+H)^2 + 2(K+H)h_p + h_p^2\right]\end{aligned} \tag{C.4-6}$$

The time derivative of this term becomes,

$$\begin{aligned}\frac{d\phi_{tot}}{dt} &= \frac{1}{2}\rho g A_r\left[0 - 2(K+H)\dot{h}_r + 2h_r\dot{h}_r\right] \\ &\quad + \frac{1}{2}\rho g N A_p\left[0 + 2(K+H)\dot{h}_p + 2h_p\dot{h}_p\right]\end{aligned} \tag{C.4-7}$$

where $\dot{h}_r = \frac{dh_r}{dt} = v_r$ and $\dot{h}_p = \frac{dh_p}{dt} = v_p$

Equation C.4-7a is simplified and written in terms of quantities for the drain line by using mass conservation given by Equation C.4-3a plus the fact that the volumes displaced in the RPV, drain line, and GDCS pools are the same such that,

$$A_r h_r = NAh = NA_p h_p \tag{C.4-8a}$$

$$h_p = h\frac{NA}{NA_p} = h\frac{A}{A_p} \tag{C.4-8b}$$

and

$$h_r = h\frac{NA}{A_r} \tag{C.4-8c}$$

Using these and Equation C.4-3 in Equation C.4-7 gives,

$$\frac{d\phi_{tot}}{dt} = \frac{1}{2}\rho g\left[-2(K+H)A_r v_r + 2A_r h\frac{NA}{A_r} v\frac{NA}{A_r} + 2(K+H)NA_p v_p + 2NA_p h\frac{A}{A_p} v\frac{A}{A_p}\right] \tag{C.4-8d}$$

This simplifies to,

$$\begin{aligned}\frac{d\phi_{tot}}{dt} &= \frac{1}{2}\rho g\left[2hv\frac{(NA)^2}{A_r} + 2hv\frac{NA^2}{A_p}\right] \\ &= \rho g N^2 A^2 hv\left[\frac{1}{A_r} + \frac{1}{NA_p}\right] \\ &= \rho g N^2\frac{A^2}{A}hv\end{aligned} \tag{C.4-9}$$

where the free surface parameter is defined by,

$$A = \left[\frac{1}{A_r} = \frac{1}{NA_p}\right] \tag{C.4-10}$$

**Mechanical Work**

The mechanical work term in Equation C.4-1 is also evaluated using the notation in Figure C.3-1. Mechanical work performed by the system on its surroundings is defined as force times velocity in the direction of the force and is stated as follows:

$$W = P_p NA_p v_p - P_r A_r v_r \tag{C.4-11a}$$

Equation C.4-3 is used to express W in terms of quantities applicable to the drain line to give

$$\begin{aligned}W &= P_p NAv - P_r NAv \\ &= \left(P_p - P_r\right)NAv\end{aligned} \tag{C.4-11b}$$

**Friction Loss**

The friction loss term E in Equation C.4-3 accounts for damping or flow resistance in the system. Only the drain line loss needs to be considered because v is much greater than either of $v_r$ and $v_p$. The friction loss term consists of two terms. One of these is caused by viscous dissipation within the fluid contained in the drain line and the other from wall friction and form losses in the pipe. The wall friction/form loss term is by far the largest term but the viscous dissipation term is included for completeness. In evaluating the viscous dissipation term, a parabolic velocity profile was used for simplicity and because the viscous term is comparatively small for any assumed profile, which gives

$$v_r = 2v\left[1-\left(\frac{r}{R}\right)^2\right] \tag{C.4-12}$$

The viscous dissipation term is given by,

$$E_v = -N\int_0^L -\int_0^R \tau\frac{dv_r}{dr}2\pi r\,dr\,d\ell \tag{C.4-13}$$

where,

$$\tau = -\mu\frac{dv_r}{dr} \tag{C.4-14}$$

The integration in Equation C.4-13 is carried out to give,

$$E_v = \frac{8\mu NALv^2}{R^2} \tag{C.4-15}$$

The much more significant wall friction/form loss term is evaluated using the force acting on the fluid times the average velocity. The force acting on the drain line fluid is,

$$\Delta PNA = \sum\left(\frac{f\ell_i}{D_i}+k_i\right)\left(\frac{A_i}{A}\right)^2\frac{1}{2}\rho v^2 NA = \frac{1}{2}F\rho v^2 NA \tag{C.4-16}$$

where the line loss coefficient is given by,

$$F = \sum\left(\frac{f_i\ell_i}{D_i}+k_i\right)\left(\frac{A_i}{A}\right)^2 \tag{C.4-17}$$

which is the familiar summation of wall friction and form loss for each line segment of area $A_i$ and length $\ell_i$ and friction factor $f_i$. The work performed on the fluid by the friction is then,

$$E_f = \Delta P N A v = \frac{1}{2} F \rho v^2 N A v = \frac{1}{2} F \rho N A v^3 \qquad \text{(C.4-18)}$$

The total friction loss is then,

$$E = E_v + E_f = \frac{8 \mu N A L v^2}{R^2} + \frac{1}{2} F \rho N A v^3 \qquad \text{(C.4-19a)}$$

Substituting Equations C.4-5, C.4-9, C.4-11b and C.4-19a into Equation C.4-1 gives the equation of motion for the fluid as,

$$\rho L A S v \dot{v} + \rho g \frac{N^2 A^2}{A'} h v = -\left(P_p - P_r\right) N A v - \frac{8 \mu N A L v^2}{R^2} - \frac{1}{2} F \rho N A v^3 \qquad \text{(C.4-19b)}$$

Simplification gives,

$$\rho L A' S \ddot{h} + \left[ \frac{8 \mu N A' L}{R^2} + \frac{1}{2} F \rho N A' |v| \right] \dot{h} + \rho g N^2 A h = \left(P_r - P_p\right) N A' \qquad \text{(C.4-20)}$$

where,

$$\ddot{h} = \frac{dv}{dt} = \frac{d^2 h}{dt^2}$$

$$\dot{h} = v = \frac{dh}{dt} \qquad \text{(C.4-21)}$$

and h = fluid displacement in the drain line.

Note that displacements in the RPV and GDCS pools are obtained from h and area ratios as specified by Equation C.4-8. Note also that the absolute value of v in the damping factor has been used to render this factor always positive. The equation of motion given by Equation C.4-20 is simplified and rewritten in a form similar to that used in classical vibration theory ([1], p. 51) as follows:

$$m \ddot{h} + c \dot{h} + k h = f(t) \qquad \text{(C.4-22)}$$

where

| | | |
|---|---|---|
| m | = | $\rho LA'S$ = mass factor |
| c | = | $8\mu NA'L/R^2 + F\rho NA'\|v\|/2$ = damping factor |
| k | = | $\rho g N^2 A$ = stiffness factor |
| f(t) | = | forcing function = $(P_r - P_p)NA'$ for step change in pressure (C.4-23) |

### C.4.3 Solution Summary

It is noted that Equation C.4-22 is non-linear because the damping factor contains the velocity $v = \dot{h}$. It has not been possible to obtain an exact solution to the equation of motion for this problem as formulated. Accordingly, a simplifying assumption was made so that the essential characteristics of the system could be studied without resorting to numerical solution techniques except for confirmation of the approach. The assumption was made that an average absolute value of velocity v denoted by $v_a$ be used. The value of $v_a$ was taken as the average of the sum of absolute minimum and the absolute maximum values divided by two attained by v during a transient. The validity of this assumption was checked by numerically integrating Equation C.4-22, as explained in Subsection C.5.4.

#### C.4.3.1 General Solutions

The general solution to the homogeneous part of Equation C.4-22, which now has constant coefficients, depends on the relative values of the coefficients. A possible solution to Equation C.4-22 is of the form,

$$h = e^{st} \tag{C.4-24}$$

where the possible values of s are given by,

$$s_{1,2} = -\frac{c}{2m} \pm \sqrt{\left(\frac{c}{2m}\right)^2 - \frac{k}{m}} \tag{C.4-25}$$

The form of the solution depends on the value of the terms under the square root sign which in turn depends largely on the geometrical configuration of the system. The characteristics of the three possible solutions are described for each case in the following.

**Overdamped System**

In this case $\left(\frac{c}{2m}\right)^2 > \frac{k}{m}$ and the general solution to the homogeneous part of Equation C.4-22 is

$$h = C_1 e^{s_1 t} + C_2 e^{s_2 t} \tag{C.4-26}$$

where the coefficients are obtained from the specified boundary conditions.

**Critically Damped System**

In this $\left(\frac{c}{2m}\right)^2 = \frac{k}{m}$ and $s_1 = s_2 = s = -c/2m$. The solution is

$$h = C_1 e^{s_1 t} + C_2 e^{s_2 t} \tag{C.4-27}$$

The drain line radius for which the system is critically damped can be calculated explicitly from the expression $\left(\frac{c}{2m}\right)^2 = \frac{k}{m}$ by substituting the value for c, m, and k from Equation C.4-22 and neglecting the viscous dissipation term in the damping factor which has been verified to be very small relative to the friction loss term. This yields for the critical line radius,

$$R_c = \frac{Fv_s}{4LS}\sqrt{\frac{LSA'}{g\pi}} = \frac{Fv_s}{4}\sqrt{\frac{A'}{g\pi LS}} \tag{C.4-28}$$

**Underdamped System**

In this case $\left(\frac{c}{2m}\right)^2 < \frac{k}{m}$ and the radical of the square root term in Equation C.4-25 is negative. The values of s in Equation C.4-25 then become,

$$\begin{aligned} s_1 &= p + iq \\ s_2 &= p - iq \end{aligned} \tag{C.4-29}$$

where,

$$\begin{aligned} p &= -\frac{c}{2m} \\ q &= \sqrt{\left|\left(\frac{2}{2m}\right)^2 - \frac{k}{m}\right|} \\ i &= \sqrt{-1} \end{aligned} \tag{C.4-30}$$

The general solution is for this case

$$h = e^{pt}\left(C_1 \sin qt + C_2 \cos qt\right) \tag{C.4-31}$$

### C.4.3.2 Particular Solutions

Two different forcing functions f(t) were considered. In the first, a step change in RPV pressure occurring at time zero was used as described in the derivation of the equation of motion. In equation form, this forcing function is written as

$$f(t) = (P_r - P_p)NA' \tag{C.4-32a}$$

The second forcing function considered was a sinusoidal or harmonic function with an amplitude equal to that of the step change function above. In equation form this is written as,

$$f(t) = (P_r - P_p)NA' \sin \omega t \tag{C.4-32b}$$

where $\omega$ is the forcing function angular frequency in rad/s.

The particular solution for the step change forcing functions is obtained by substitution of Equation C.4-32a times a constant into Equation C.4-22,

$$h_{pa} = (P_r - P_p)NA'/k \tag{C.4-33}$$

The particular solution for the sinusoidal forcing function is more involved and was obtained from Thomson ([1], p.53) as,

$$h_{pa} = (P_r - P_p)NA' \sin(\omega t - \varphi) \Big/ \sqrt{\left(k - m\omega^2\right)^2 + (c\omega)^2} \tag{C.4-34a}$$

where phase angle $\varphi$ is obtained from,

$$\tan \varphi = (c\omega / k) \Big/ \left(1 - \frac{m\omega^2}{k}\right) \tag{C.4-34b}$$

### C.4.3.3 Parameter Definitions

Several parameters describing the system behavior are defined in the following. First, the natural angular frequency of the fluid system in radians/second is defined as ([1], p. 4).

$$\omega_n = \sqrt{\frac{k}{m}} \tag{C.4-35a}$$

when k and m are given by Equation C.4-23. Note that the natural angular system frequency is a function of the system geometry only (the fluid density cancels out). Second, the natural frequency in cycles/second of the system is simply,

$$f_n = \omega_n/2\pi \tag{C.4-35b}$$

Third, the natural system time period in seconds/cycle is given by,

$$\tau_n = 1/f_n = 2\pi/\omega_n \tag{C.4-35c}$$

Fourth, the critical damping factor $c_c$ is calculated by setting the radical in Equation C.4-25 equal to zero,

$$\left(\frac{c}{2m}\right)^2 = \frac{k}{m}$$

which gives,

$$c_c = 2\sqrt{km} = 2m\omega_n \tag{C.4-35d}$$

The damping ratio is defined as,

$$\xi = c/c_c \tag{C.4-35e}$$

Finally, the magnification factor, which is a measure of amplification of the forcing function magnitude that can be expected, is given as a function of the forcing function to system natural angular frequency ratio and the damping ratio by ([1], p.53)

$$\frac{X}{X_0} = \frac{1}{\sqrt{\left[1-(\omega/\omega_n)^2\right]^2 + \left[2\xi(\omega-\omega_n)\right]^2}} \tag{C.4-35f}$$

where $X_0$ is the zero frequency or step function displacement being the same as the particular solution for the step change forcing function given by Equation C.4-33.

### C.4.3.4 Initial Conditions

The constants $C_1$ and $C_2$ in the three general solutions given by Equations C.4-26, C.4-27 and C.4-31, together with a particular solution given by Equations C.4-32a and C.4-32b, are evaluated with specified displacement h and velocity $\dot{h}$ at time equal zero. The algebra becomes simpler if $h = \dot{h} = 0$ at $t = 0$ is used, although other initial condition can be used. A non-zero initial displacement condition would simply change the location of the zero point on the ordinate axis and would not affect the general characterics of the system. The solutions for the system step change response are given first for the three cases with the zero initial conditions.

**Overdamped Case**

For the displacement and velocity in the drain line, the solutions are

$$h = C_1 e^{s_1 t} + C_2 e^{s_2 t} + \left(P_r - P_p\right) NA'/k \tag{C.4-36a}$$

and,

$$\dot{h} = s_1 C_1 e^{s_1 t} + s_2 C_2 e^{s_2 t} \tag{C.4-36b}$$

where

$$C_1 = \frac{A'}{\rho g NA}\left(P_r - P_p\right) \Big/ \left(\frac{s_1}{s_2} - 1\right)$$
$$C_2 = -\frac{s_1}{s_2} C_1 \tag{C.4-36c}$$

The general behavior of the fluid displacement in the system when subjected to a step change in pressure is illustrated in Figure C.4.4-1. The system responds slowly and the static displacement is not reached for a long time. There are no level oscillations in an overdamped system. Note that Equation C.4-36a gives the displacement in the drain or connecting line. Level displacements in the RPV and GDCS pools are characteristically the same only smaller in magnitude, since they are obtained from Equation C.4-36a by multiplying by the corresponding area ratios as prescribed by Equations C.4-8.

**Critically Damped Case**

The drain line displacement and velocity are,

$$h = C_1 e^{st} + C_2 t e^{st} + NA'\left(P_r - P_p\right)/k \tag{C.4-37a}$$

and,

$$\dot{h} = \left(sC_1 + C_2\right) e^{st} + sC_2 t e^{st} \tag{C.4-37b}$$

where,

$$C_1 = -\frac{A'}{\rho g NA}\left(P_r - P_p\right)$$
$$C_2 = -sC_1 \tag{C.4-37c}$$

The general response of the line fluid displacement is given in Figure C.4.4-2. The displacement approaches a steady value corresponding to the imposed pressure difference relative quickly but there are no oscillations for a critically damped system.

**Underdamped Case**

The drain line displacement and velocity are

$$h = e^{pt}\left[C_1 \sin qt + C_2 \cos qt\right] + NA'\left(P_r - P_p\right)/k \qquad \text{(C.4-38a)}$$

$$\dot{h} = pe^{pt}\left[C_1 \sin qt + C_2 \cos qt\right] + e^{pt}\left[qC_1 \cos qt - qC_2 \sin qt\right] \qquad \text{(C.4-38b)}$$

where

$$C_2 = -NA\left(P_r - P_p\right)/k$$

$$C_1 = -\frac{p}{q}C_2 \qquad \text{(C.4-38c)}$$

The general response of the line fluid displacement is given in Figure C.4.4-3 as an illustration of the oscillatory behavior that occurs for the underdamped case. The amplitude of the oscillations decreases in accordance with the exponential multiplier in Equation C.4-38a, and the period of the oscillations is that of the natural period, which is about 160s as explained in the next section.

The complete solution with the sinusoidal forcing function and overdamped system given by Equations C.4-26 and C.4-34a is

$$h = C_1 e^{s_1 t} + C_2 e^{s_2 t} + \left(P_r - P_p\right)NA' \sin\left(\omega t - \varphi\right) \Big/ \sqrt{\left(k - m\omega^2\right)^2 + \left(c\omega\right)^2}$$

$$h = C_1 e^{s_1 t} + C_2 e^{s_2 t} + B \sin\left(\omega t - \varphi\right) \qquad \text{(C.4-39a)}$$

where,

$$B = \left(P_r - P_p\right)NA' \Big/ \sqrt{\left(k - m\omega^2\right)^2 + \left(c\omega\right)^2} \qquad \text{(C.4-39b)}$$

The corresponding velocity is,

$$\dot{h} = s_1 C_1 e^{s_1 t} + s_2 C_2 e^{s_2 t} + \omega B \cos\left(\omega t - \varphi\right) \qquad \text{(C.4-39c)}$$

The constants $C_1$ and $C_2$ become, when applying the zero displacement and zero velocity boundary conditions,

$$C_1 = \frac{s_2 B}{s_1 - s_2} \sin(-\varphi) - \frac{\omega B}{s_1 - s_2} \cos(-\varphi) \qquad \text{(C.4-40a)}$$

$$C_2 = -\frac{s_2 B}{s_1 - s_2} \sin(-\varphi) + \frac{\omega B}{s_1 - s_2} \cos(-\varphi) - B \sin(-\varphi) \qquad \text{(C.4-40b)}$$

where the phase angle $\omega$ is given by Equation C.4-34b.

The constants are not given for the critically damped and underdamped cases because the system under consideration is overdamped (as illustrated later) and also because the forcing function dominates following one to two natural cycle time periods.

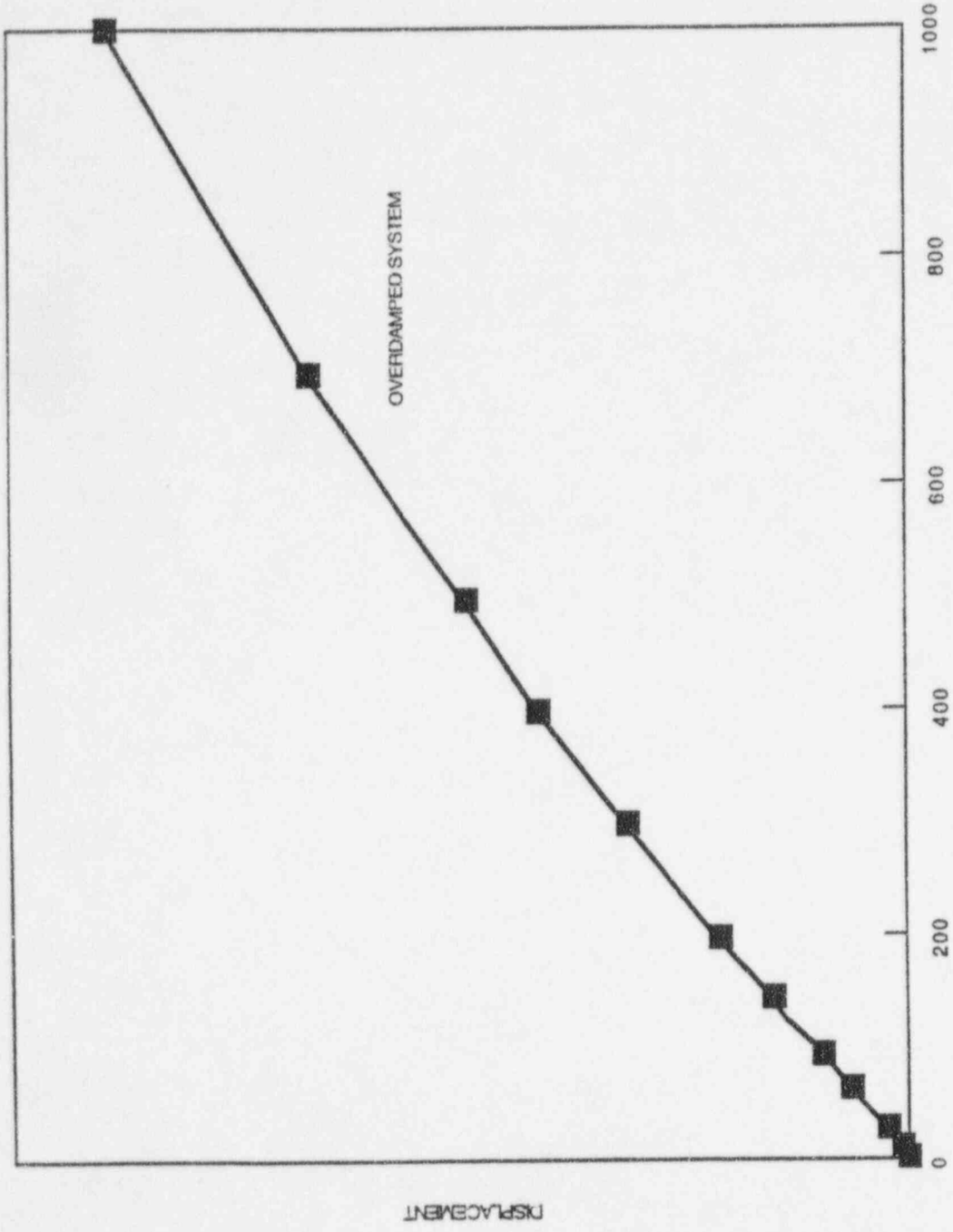


Figure C.4.4-1. Fluid Displacement in Connecting Pipe for Overdamped Damped System

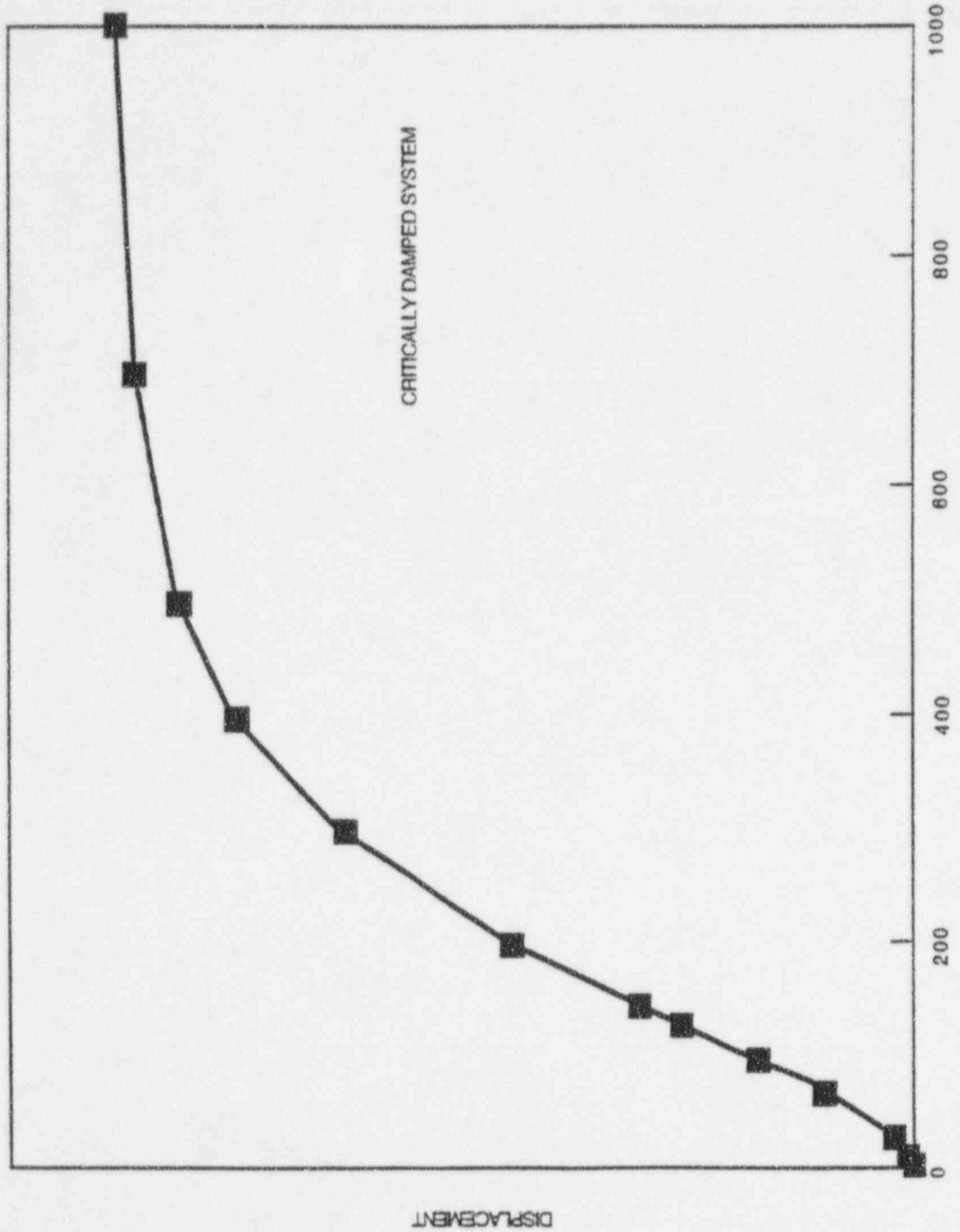


Figure C.4.4-2. Fluid Displacement in Connecting Pipe for Critically Damped System

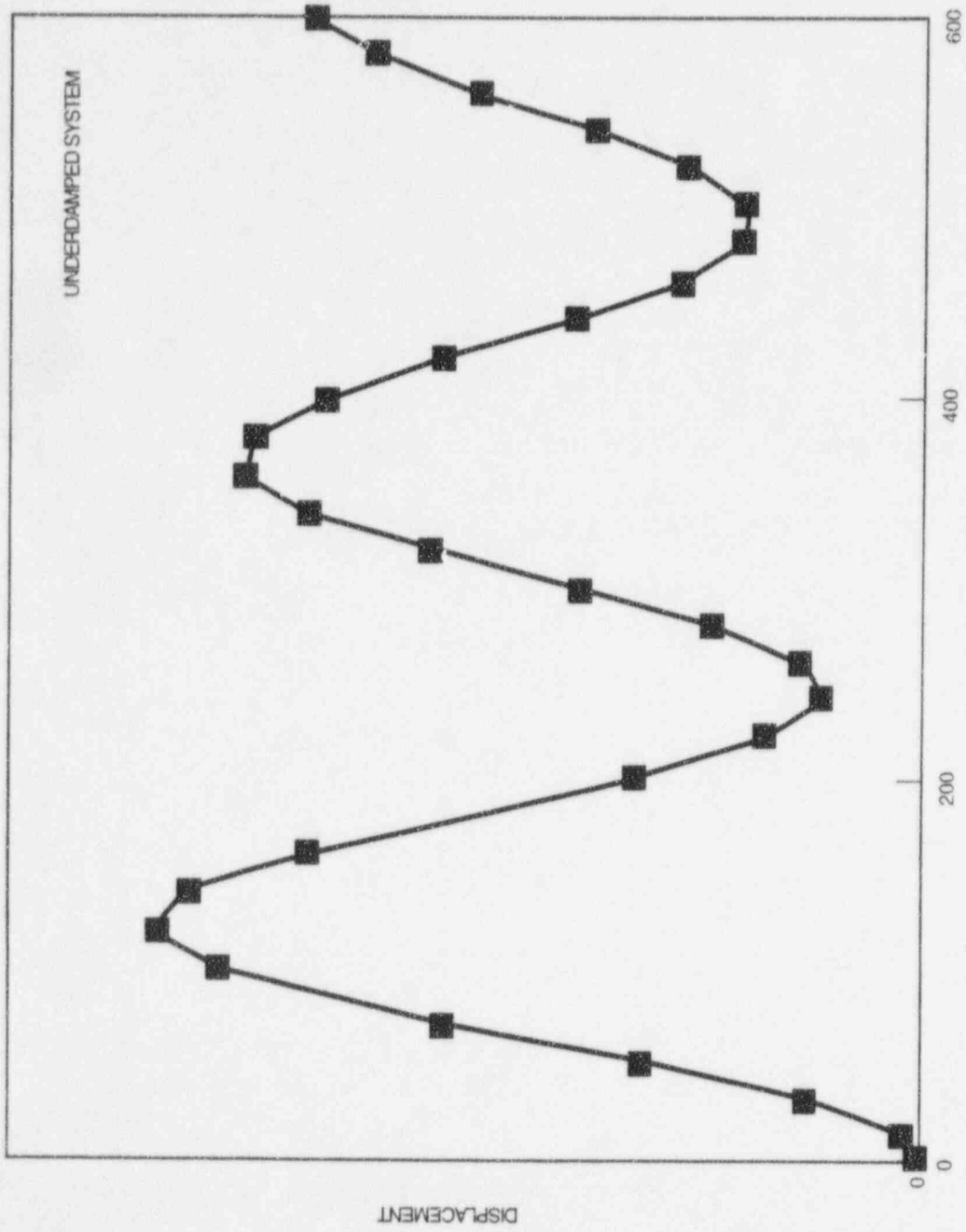


Figure C.4.4-3. Fluid Displacement in Connecting Pipe for Underdamped System

## C.5 Analysis Results

In this section an overview of the evaluation cases considered in this study is given followed by the major results. The results of a parametric evaluation of the uncertainties introduced by simplifying assumption are also given. Finally, a comparison of analytical solutions made possible by utilizing a constant damping coefficient and the corresponding solution obtained by numerical integration of the complete equation of motion is made.

### C.5.1 Evaluation Cases

The two basic geometric situations considered in the study where liquid level movements or oscillations might be possible are those pictured schematically in Figures C.3-1 and C.3-2.

### C.5.2 Application to RPV/GDCS Pool System

Results are provided for the step change and forced harmonic boundary conditions in separate subsections in the following.

#### C.5.2.1 Step Change Results

#### C.5.2.2 Forced Harmonic Results

### C.5.3 Application to RPV/SP System

#### C.5.3.1 Step Change Results

#### C.5.3.2 Forced Harmonic Results

### C.5.4 Parametric Evaluation of Uncertainties

### C.5.5 Comparison of Analytical and Numerical Results

#### C.5.5.1 Comparison of Step Change Results

#### C.5.5.2 Comparison for Harmonic Results

## C.6 Scaling Parameters

## C.7 Conclusions

The following conclusions are offered as a result of this study:

- A methodology was developed for evaluating the fundamental characteristics and dynamics of liquid masses connected by pipe lines.
- The RPV/GDCS pool and RPV/SP systems are significantly overdamped and stable for input pressure differences greater than about 0.5m head equivalent and become more stable for higher inputs.
- Small pressure difference changes of less than 0.3m head equivalent may result in small amplitude and slow level oscillations.
- A fundamental characteristic of these systems is that the relatively small diameter connecting drain lines act to decouple the liquid masses and to damp-out free oscillations.

- Natural cycle times for these systems are relatively long and varied by a factor of about three for the range of geometric parameters studied.
- The liquid level amplitude resulting from a harmonic forcing function input is lower than that of the step forcing function input because of a less than unity magnification factor when the step forcing function magnitude is greater than about 0.3m head.
- The magnification factor is less than unity even with a forcing function input frequency equal to that of the system's natural frequency (i.e., at resonance) and input magnitude greater than 0.3m head. The magnification factor decreases with larger magnitude inputs.
- RPV liquid level rate of change is very slow (~0.005 m/s maximum) for the reference pressure change input of 0.75m head equivalent.
- Nondimensionalization of the equation of motion revealed that the only nondimensional group governing the level movements is the damping ratio for the connecting line.

## C.8 References

[1] *Vibration Theory and Applications*, Thomson, W.T., Prentice-Hall, Inc., Englewood Cliffs, N.J., 1965.

[2] *Transport Phenomena*, Bird, R.B., W.E. Steward and E.N. Lightfoot, John Wiley and Sons, Inc., New York, London, Sydney, 1960.